Alma Mater Studiorum – Università di Bologna

DOTTORATO DI RICERCA IN

Ingegneria Civile, Ambientale e dei Materiali

Ciclo XXVIII

Settore Concorsuale di afferenza: 08/B3

Settore Scientifico disciplinare: ICAR/09

TITOLO TESI

Advanced Minor Destructive Testing for the Assessment of Existing Masonry

Presentata da: Diego Marastoni

Coordinatore Dottorato	**Relatore**
Alberto Lamberti	**Andrea Benedetti**
	Correlatore
	Luca Pelà

Esame finale anno 2016

Summary

Acknowledgments

Abstract

The mechanical characterisation of material components in existing masonry structures has been the topic of several research studies. Most of them are currently focusing on mortar, the most difficult material component to be characterised, trying to evaluate its behaviour. To achieve this aim, a good option is performing minor-destructive testing (MDT) such as the in-situ penetrometric tests or the extraction of samples to be tested in the laboratory. This thesis focuses on MDT for the mechanical characterisation of historical mortars. In the first part, a novel in-situ MDT technique is investigated, based on the field vane shear test for soils. The instrumentation consists in a four-winged pin (X-Drill) and a torque wrench. The testing procedure consists in inserting the pin in a mortar joint and applying a torque to the pin through the dynamometric key. The dynamometric key records the magnitude of the torque while the pin brings the material to failure. This research presents the results of an experimental campaign based on the comparison between standard tests and X-Drill measurements on different types of mortars. The interpretation of the test, based on the analysis of the local stress evaluated on the failure surface, provides a possible correlation between the measured torque and the compressive strength of the material.

After the X-Drill development, the thesis focuses on the extraction of samples to be tested in laboratory. The in-situ core drilling of existing masonry is a convenient sampling technique since it does not induce excessive damage to the historical structure and it allows a direct estimation of the mechanical properties by testing the extracted specimens in the laboratory. Brazilian tests can be carried out on cores including a diametral mortar joint with a defined inclination with respect to its original horizontal

position. A new integrated methodology is developed for the comprehensive mechanical characterisation of historical mortar based on different types of experimental tests results. This task is carried out by means of a large set of experiments performed ex-novo on lime mortar masonry walls built in the laboratory. The processing of the results from Brazilian tests on cores with inclined diametral joint is complemented with the application of the double punch tests on mortar joints that may be also extracted through core drilling. The proposed experimental methodology is then compared with the results obtained from standard tests performed on the same materials, such as compression tests, flexural tests and shear tests on triplets.

Finally, the parameters obtained are used as input parameters for 2D and 3D numerical analyses based on the Continuum Damage Mechanics constitutive model. This model allows to represent the material mechanical degradation through a single scalar parameter, which depends on the fracture energy dissipated during the failure process. The comparison between the experimental results and the numerical analyses confirm the good prediction capacity of the proposed techniques.

Keywords: Minor-Destructive Tests, Penetrometric Tests, Historical Masonry Assessment, Lime Mortar, In-Situ Sampling, Double Punch Test, Mohr-Coulomb Theory, Shear Strength, Failure Envelope, Nonlinear Analyses, Fracture Mechanics, Continuum Damage Model.

Sommario

La caratterizzazione meccanica dei materiali che compongono strutture in muratura è stato l'oggetto di numerosi studi di ricerca. La maggior parte di questi è incentrata sulle malte, essendo il materiale più difficile da caratterizzare, cercando di stimarne il comportamento meccanico. Per raggiungere questo obiettivo, una buona opzione pare essere quella di utilizzare test moderatamente distruttivi (MDT), come prove penetrometriche o estrazione di campioni da testare in laboratorio.

Questo lavoro è focalizzato sulle tecniche MDT per la caratterizzazione meccanica di murature storiche. Nella prima parte viene studiata una nuova tecnica MDT in-situ basata sul Field Vane Test per i terreni. La strumentazione, infatti, consiste in un chiodo alettato (chiamato X-Drill) e una chiave torsiometrica. La procedura di test consiste nell'inserire il chiodo in un letto di malta e successivamente nell'applicare un momento torcente mediante una chiave dinamometrica. Quest'ultima registra il valore massimo di torsione mentre il chiodo porta a rottura il materiale. Si presentano i risultati di una campagna sperimentale basata sul confronto di test di compressione standard con le letture di prove X-Drill eseguite su campioni di malta di proprietà differenti. La calibrazione è stata basata sull'analisi delle tensioni locali sulla superficie di rottura, ottenendo una possibile correlazione tra momento massimo misurato e resistenza a compressione del materiale.

Successivamente, la ricerca si è concentrata sull'estrazione di piccoli campioni da testare in laboratorio. Il carotaggio di campioni in situ eseguito su murature esistenti può essere una tecnica conveniente, dal momento che non produce lesioni eccessive sulla struttura e permette una stima diretta delle proprietà meccaniche. La prova

Brasiliana può essere eseguita su carote che includano un giunto di malta diametrale, ponendo quest'ultimo inclinato rispetto alla direzione orizzontale. Viene proposta una tecnica integrata di caratterizzazione meccanica per le malte storiche che si basa sull'analisi e confronto di diversi tipi di prove sperimentali. Questa metodologia è stata sviluppata con l'ausilio di una campagna prove eseguita ex-novo in laboratorio su elementi in muratura con malta di calce idraulica. L'utilizzo combinato della prova Brasiliana su carote con giunto di malta inclinato e delle prove a punzonamento su lastrine di giunto di malta estratte dal muro ha consentito di stimare un dominio di rottura come inviluppo degli stati tensionali corrispondenti a ciascuna prova. I risultati sono poi stati confrontati con quelli ottenuti da prove standard di compressione, flessione e taglio su triplette.

Infine, i parametri ottenuti dall'elaborazione sono stati utilizzati per la realizzazione di analisi numeriche su modelli agli elementi finiti 2D e 3D con leggi costitutive basate sulla meccanica del danno continuo. Tali leggi permettono di rappresentare il degrado del materiale attraverso un unico parametro scalare, il quale dipende dall'energia dissipata durante la frattura. Il confronto tra risultati sperimentali e numerici ha confermato la bontà del modello proposto per la caratterizzazione delle malte storiche.

Parole chiave: Prove Limitatamente Distruttive, Prove Penetrometriche, Vulnerabilità Murature Storiche, Malta di Calce, Campionamento In-Situ, Double Punch Test, Teoria Mohr-Coulomb, Resistenza Taglio, Inviluppo Rottura, Analisi Non-Lineari, Meccanica della Frattura, Modello Danno Continuo.

Chapter 1. Introduction

The assessment of historical buildings has become a fundamental topic in the conservation of the architectural heritage, especially in the last decades where relevant catastrophic events have threatened many important structures. The evaluation of the structural health and the identification of possible vulnerabilities in those facilities shall allow the preservation of the cultural heritage value that they represent.

The conservation of the architectural heritage requires a multidisciplinary approach involving a variety of professionals and organisations. For this reason, in 2003 the International Council on Monuments and Sites produced a document of recommendations (ISCARSAH 2003a; ISCARSAH 2003b) to assist the professional figures involved in historical masonry assessment and facilitate the communications between them.

The current approach for the historical building assessment can be defined "Knowledge-Based Assessment" and requires information about the original structural conception, its construction techniques, the possible damages or modifications occurred in the building life and finally on the present state. As reported in the aforementioned document (ISCARSAH 2003a), the diagnoses are based on historical qualitative and quantitative approaches; the qualitative approach is mainly based on direct observation of the structural damage and material degradation as well as historical and archaeological research. On the contrary, the quantitative approach is mainly based on material and structural tests, monitoring and structural analyses. Concerning the latter one, data and information should first be processed approximately, to establish a more comprehensive plan of activities in proportion to the real problems of the structures. In some cases, it is

convenient to organise the material characterisation in stages, beginning with simple techniques and eventually integrating them with more sophisticated methodologies.

Non-destructive tests should be preferred to those that may involve any alteration to the structure. However, those kinds of tests often do not provide the required reliability concerning the investigated material's results. In this case, it should be necessary to assess the benefit to be obtained by opening up the structure in terms of reduced structural intervention against the loss of culturally significant material (a cost-benefit analysis). For this reason, minor-destructive tests are increasingly used for the assessment of existing structures, providing more reliable results than non-destructive tests while maintaining a limited damage on the investigated part.

Masonry is one of the most common materials in European heritage buildings. The building technique of masonry structures is mostly the same since centuries ago, consisting in superposing blocks or raw stones and, eventually, filling the joints by using mortar. The heterogeneous nature of the material introduce even more uncertainty on its mechanical behaviour, since the structural element capacity depends on the complex interaction of the units and mortar joints. Masonry structures are generally composed of materials characterised by very low tensile strength and that may easily show cracking or separation between elements. Nevertheless, these signs are not necessarily an indication of danger as masonry structures are intended to work mainly in compression.

The preliminary analysis of masonry requires the identification of the characteristics of the constituent materials: the units (stones or bricks) and the type of mortar (cement, lime, etc.). It is also necessary to know how the elements are bonded (dry joints, mortar joints etc.) and the way in which they are geometrically related to each other. Different kinds of tests may be used to ascertain the composition of the wall.

Focusing on the Italian territory, where the earlier European societies have settled and developed important technologies for the building construction, masonry structures have to deal with the seismic hazard. The latest important seismic events occurred in the Italian territory, such as Umbria-Marche in 1997, L'Aquila 2009 and Emilia-Romagna 2012, caused huge damages on lots of historical masonry buildings. Italian governance faced with these casualties introducing the approach proposed by ICOMOS in the current Standard (D.M. 14/01/2008 2008).

Figure 1.1 Effect of earthquake on masonry structures: Basilica of Saint Francis in Assisi, Italy in 1997 (a), Prefecture Palace in L'Aquila, Italy in 2009 (b) and Clock Tower in Finale Emilia, Italy in 2012 (c).

Figure 1.1a,b,c show some collapses occurred during the aforementioned events as evidences of the real losses in case of high magnitude earthquakes. As clearly noticeable in these pictures, one of the principal causes of collapse is the complete disruption of the mortar, leading to disconnection of the units and consequent loss of the wall bearing capacity. Furthermore, masonry structures are often characterised by local mechanisms of failure, such as those involving vaults and roofs (Figure 1.1a and Figure 1.1b) or separation among structural parts (Figure 1.1c).

Nowadays, a significant effort is carried out to understand better the existing materials' behaviour by means of mechanical tests performed in-situ. A more precise knowledge about the cracking or failure phenomena in the element investigated could help in safeguarding the cultural heritage and allows developing more reliable models for the assessment of buildings.

1.1.   Aims and Objectives of the Thesis

The main aim of this thesis is to provide a reliable methodology for experimental characterisation of historical masonry. The work was developed following two main stages:

- development of a novel MDT for the in-situ mechanical characterisation of mortar;
- comparison between some novel non-standard MDT techniques based on laboratory testing of extracted material (i.e. Brazilian Test on cored samples with inclined mortar joint and Double Punch Test of mortar joints) and available standard

approaches (i.e. compression, flexural test of mortar prisms and shear tests of masonry triplets).

According to the ICOMOS Guidelines (ISCARSAH 2003b), it is preferable to plan the characterisation of materials of existing masonry structures in stages, processing firstly the outcomes of simple tests that could provide a first impression on the structural health. Secondly, the information retrieved from the first stage can help to choose further and more comprehensive experimental methodologies, such as those including MDT.

According to the aforementioned Guidelines, the first part of the present research provides a new technology for quick in-situ evaluation of the mechanical properties of historical mortar. The proposed technique, called X-Drill penetrometer, reveals to be a promising methodology of investigation, since the instrumentation is quite cheap and the test is simple as for the execution and the interpretation of the results.

The second stage of the research investigates non-standard techniques as an alternative to standard tests that usually cannot be performed on historical masonry. The direct comparison between standard and non-standard techniques is carried out considering historical-like materials reproduced in the laboratory according to the traditional construction practice.

The experimental setup for Brazilian Test on core samples with inclined mortar joint is enhanced compared to previous works available in the literature. The introduction of linear variable differential transformers (LVDTs) placed parallel to the joints allows to measure the relative displacement of the two halves of the specimens and thus to derive important mechanical parameters. Moreover, the combination of different non-standard tests provides a new integrated methodology for a better interpretation and a more robust prediction of the materials' mechanical parameters.

The outcomes of the interpretation can be used as input parameters for numerical analyses, based on advanced constitutive models, such as Continuum Damage Mechanics ones, that can give further information on the nonlinear behaviour of the resisting element.

1.2.   Outline of the Thesis

This thesis consists in six Chapters.

Chapter 1 provides the introduction and the objectives of the research.

Chapter 2 presents a brief overview on the current masonry standards in the European Union both for new masonry constructions and for the historical masonry assessment. A state-of-the-art of available experimental and numerical techniques currently used for existing masonry assessment is also included.

Chapter 3 presents the development of a novel MDT instrumentation. The X-Drill is based on the field vane test used for soils, consisting in a four-winged pin inserted in the material. A torque is then applied to the pin through a dynamometric key, which records the maximum value at failure. The calibration of the instrument was carried out in laboratory using a large set of mortar specimens with different compressive strengths. The analysis of local stresses on the material led to a linear correlation between the maximum torque measured and the compressive strength of the mortar. The proposed interpretation method returned a high prediction capacity on the mortar strength.

Chapter 4 presents a large experimental campaign carried out on specimens extracted from masonry walls reproduced in the laboratory using historical-like materials. The experimental campaign included also standard specimens prepared following the current standards for compression, flexural and shear tests. The extraction was carried out using a novel dry coring technique instead of water-cooled coring, in order to collect less disturbed specimens. Once the core samples were extracted, the walls were dismantled to obtain mortar joint specimens to be tested through DPT. These two tests can be performed in real experimental campaigns on existing structures, while the standard tests are hardly applicable since the samples extracted are not prismatic and regular. The core samples were subject to Brazilian Test with inclined mortar joint (BT), which induces a composite state of stress on the mortar joint. The test was enhanced by introducing LVDTs on both circular faces in order to measure the relative displacement of the bricks shaping the joint. This solution provided information about elastic, strength and nonlinear properties of mortar. The outcomes of BT and DPT were combined using a 3D representation of the state of stress (i.e. Mohr's Circles), allowing defining a more precise estimation of failure envelope. The resulting compressive, tensile and shear strengths obtained by the failure envelope were compared with the standard tests performed, confirming the good agreement of the results.

Chapter 5 validates the experimental results presented in the previous Chapter 4 by means of 2D and 3D FE analyses based on a Continuum Damage Mechanics constitutive model. In particular, the samples tested were modelled using micro-models (i.e. units and mortar were defined separately as a heterogeneous model) with the parameters obtained by the integrated interpretation.

Chapter 6 presents an extended summary, the main contributions of this work and the conclusions that can be derived from this study. Suggestions for future work are also pointed out.

Chapter 2. State-of-the-art of experimental and numerical analysis of masonry

This Chapter presents a critical review of the state-of-the-art on experimental and numerical approaches for the analysis of existing masonry.

The available experimental approaches can be classified into Destructive Tests (DT), Minor Destructive Tests (MDT) and Non-Destructive Tests (NDT), depending on the procedures adopted during the testing operations.

The available numerical approaches can be classified depending on the type of analysis performed (i.e. linear/nonlinear and static/dynamic), on the modelling scale (i.e. macro, micro or multi-scale) and on the constitutive law assumed (i.e. elasticity, plasticity or damage mechanics).

2.1. State-of-the-art of the experimental characterisation of masonry

The current European Standard for new masonry construction is the Eurocode 6 (EN 1996-1-1:2005 2005). The first part of the standard reports the minimum requests in terms of material quality, such as composition, durability and mechanical properties.

Concerning mortar, the material used must agree with the EN 998-2:2010 (EN 998-2:2010 2010) which contains all the information about the preparation procedures, the proportions of sand, binder and water and the durability requirements. The binder used in the mortar can be either cement (EN 197-1:2011 2011) or hydraulic lime (EN 459-1:2010 2010). EN 1015-1:1999 (EN 1015-1:1999 2007) reports the necessary analyses

to be performed on the granulometry of sand by means of sieves, granting a well graded dimensions of the grain sizes. Other information about durability, water absorption and void contents is reported in the following parts of EN 1015.

Regarding the mechanical properties, the EN 998-2:2010 (EN 998-2:2010 2010) reports a list of standards for the mechanical characterisation of mortars. The ordinary tests such as three-point bending and compression tests are described in EN 1015-11:1999 (EN 1015-11:2007 2007), which defines the curing time, the dimensions of the specimens and the loading increment ratio necessary to perform a correct test.
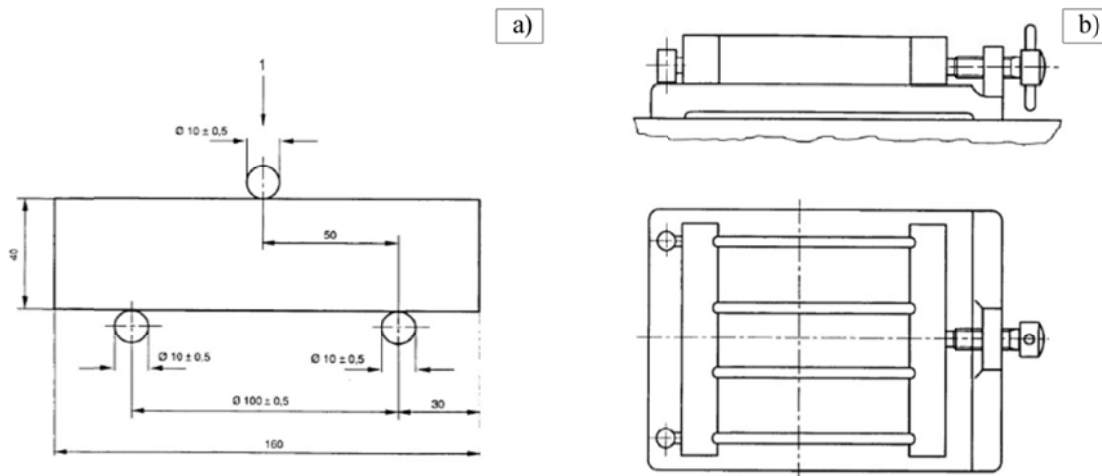
Figure 2.1 Instructions for mortar: testing setup (a) and moulding (b) (EN 1015-11:2007 2007).

The units used in masonry construction are classified according to different standards, depending on their nature. The most used units are clay bricks and natural stones. Clay units composition and their standardised dimensions are described in EN 771-1:2011 (EN 771-1:2011 2011), while their mechanical characterisation is reported in EN 772-1:2011 (EN 772-1:2011 2011). The same subdivision is made for the natural stone units, where their classification is summarised in EN 771-6:2011 (EN 771-6:2011 2011) and their testing procedures in EN 772-6:2011 (EN 772-6:2011 2011).

Once the mechanical properties are identified, Eurocode 6 provides empirical expressions in order to evaluate the homogenised mechanical properties of masonry starting from those of the components. Some examples of empirical relations are reported in Equation 2.1a,b for the estimation of the characteristic value of the masonry compressive strength f_k and its Young's modulus E.

$$f_k = K \cdot f_{cb}^{0.65} \cdot f_{cm}^{0.25}; \quad E = 1000 \cdot f_k \qquad\qquad (2.1a,b)$$

Where K is a constant dependent on the masonry units used, f_{cb} and f_{cm} are respectively compressive strength of units and mortar.

The shear behaviour of masonry can be estimated through specific tests described in EN 1052-3:2002 (EN 1052-3:2002 2002), which provides the procedures to be followed in order to obtain the initial shear strength. Such parameter allows to define the failure envelope in terms of $\sigma - \tau$ stresses (i.e. Mohr-Coulomb), considering the possible crack formation as a two-dimensional interface failure.

In the specific case of the evaluation of existing masonry, the experimental procedures contained in the aforementioned standards appear inappropriate, since the constituent materials usually do not comply with the minimum requirements of composition or material strength. Moreover, the dimensions of the specimens required by the standards are hardly obtainable from an existing structural element. For this reason, it is necessary to define novel reliable methodologies for the accurate mechanical characterisation of masonry components in existing structures.

The Italian Cultural Heritage is composed mainly of historical masonry buildings, largely diversified in materials and construction techniques. Due to the high seismic hazard of the Italian territory, the national governance had to introduce further instructions and rules for the prevention and the restoration of the historical building. These rules were collected firstly in the Italian Standard (D.M. 14/01/2008 2008) in 2008, and then extended to its Instructions (Circolare 02/02/2009 n. 617 2009).

Italian Standards provide a precise schedule to be followed in order to obtain the requested level of knowledge of the investigated building, based on the European Recommendations for the safeguard of the Cultural Heritage buildings (ISCARSAH 2003a; ISCARSAH 2003b). Firstly, it is necessary to retrieve the documentation about the structure realisation, such as original design projects, historical information about restoration interventions, structural alterations or relevant damages. All these information can contribute to the identification of the structural system and to the estimation of the loads acting on the resisting structure. Secondly, it is necessary to plan a survey to find possible incongruences between the original project and the current condition of the building. Once the global resisting system is identified, it is finally necessary to proceed with the material characterisation by performing experimental tests.

The Instructions of Italian Standard (Circolare 02/02/2009 n. 617 2009) provide a table containing reference values of mechanical parameters for different types of masonry. The proposed reference values refer to masonry realised with weak mortar, thick joints and no transversal interconnection between eventual multiple layers. If the masonry investigated presents some kind of reinforcement or is in better condition than in the reference condition, it is possible to use some correction factors to increase the mechanical properties. For limited and adequate levels of knowledge (named as LC1 and LC2), the parameters assumed for the vulnerability analysis of the structure must comply with the range provided by the former table. Possible higher results obtained by experimental tests can be used only to increase the parameters that in any case have to fall within the range provided. If the number of tests performed is sufficiently large (exhaustive tests), it is possible to assume an accurate level of knowledge (i.e. LC3) allowing using directly the results of the experimental tests. The aforementioned standard reports the type of tests to be performed in order to consider the requested knowledge level. For example, if the level of knowledge LC3 is needed, Destructive Tests (DT) or Minor-Destructive Tests (MDT) are required. Non-Destructive Tests (NDT) are allowed as complementary tests, reducing the amount of DTs or MDTs. In fact, the Instructions to the Italian Standard (Circolare 02/02/2009 n. 617 2009) suggest that MDTs and DTs can be replaced for a total amount of 50% with NDTs by tripling the number of the tests removed.

Recent studies (Borri et al. 2011; Galli et al. 2014) showed that the Instruction to the Italian Standard provides conservative values, suggesting that operating in an accurate level of knowledge could lead to more reliable results and could significantly reduce the restoration interventions.

In addition to the National Standard, Italian Regions can provide further regulations to describe more in detail the assessment of historical masonry. As an example, the Tuscan "Regional Program VSM" (VSM Regione Toscana 2003) provides a complete characterisation of the masonry typologies that can be encountered on the territory, organised as an abacus with a standardised classification (see Figure 2.2).

Figure 2.2 Example of the abacus for the masonry textures by the Tuscany Region (VSM Regione Toscana 2003).

2.1.1. Destructive Testing (DT)

DT consists mainly of testing either mid or large-size structural elements until bringing them to failure in order to define their mechanical behaviour. These methods lead to a complete characterisation of the material, since the investigated element is tested until its ultimate capacity. However, such techniques are highly invasive since they bring the investigated structural elements to failure and require a consequential substitution of the damaged part. In common practice, this approach is feasible in structures destined to complete demolition or partial demolition and subsequent reconstruction of some parts.

An useful DT is the diagonal compression test (Brignola et al. 2008; Corradi et al. 2003), in which a masonry structural member is isolated from the surrounding structure. The outer part of the investigated portion is demolished to allow the insertion of hydraulic jacks, which provide a controlled compression. The test can be either performed for compressive strength (if the compression is given perpendicular respect

to the joints) or for the evaluation of composite compression-shear actions (if the compression is given in diagonal direction).
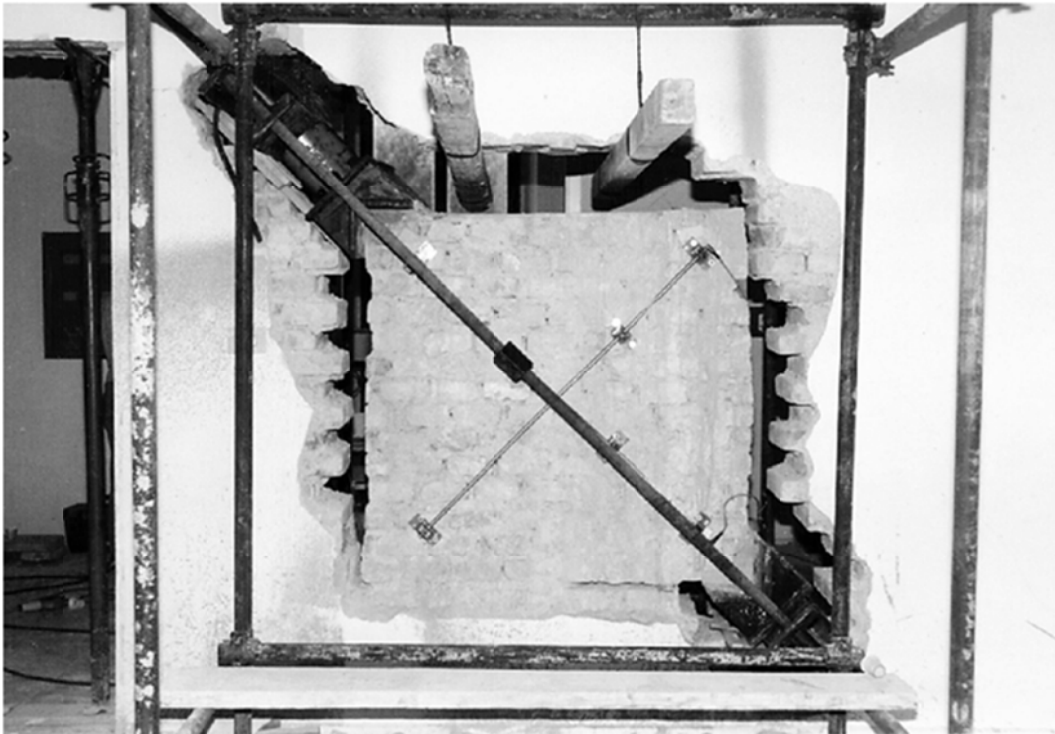
Figure 2.3 Diagonal compression test performed in-situ (Corradi et al. 2003).

Figure 2.3 shows the experimental setup of the in-situ diagonal compression test (Corradi et al. 2003). It requires an almost square-shaped part of the panel subjected to load, thus the angle of application of the load is fixed at 45°. Other studies (Page 1981; Milosevic et al. 2012) extended the investigation to all the possible inclinations, reproducing the test in the laboratory. The studies showed the biaxial anisotropy of masonry due to the different position of the mortar courses (see Figure 2.4).
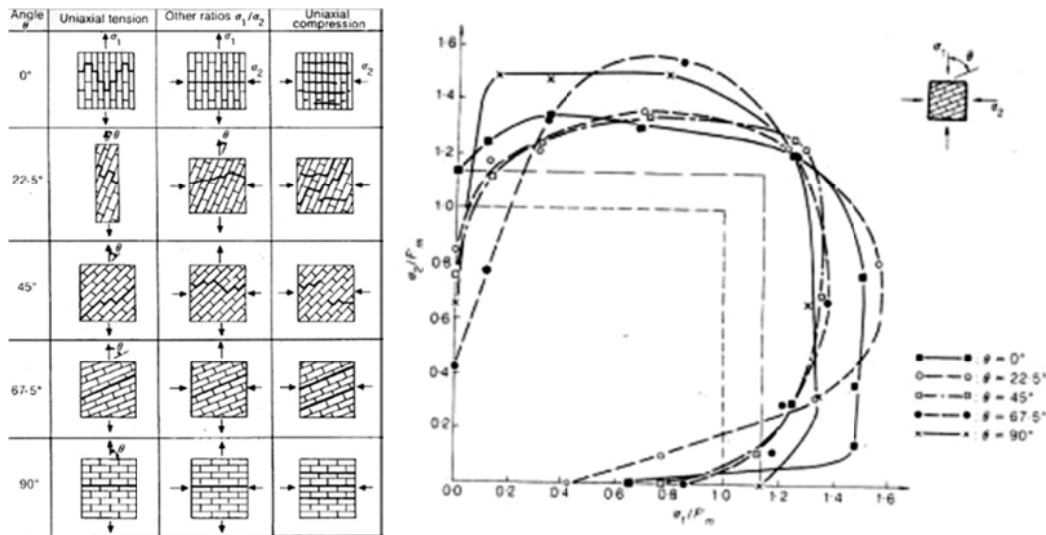
Figure 2.4 Biaxial behaviour of mortar subjected to diagonal compression at different inclinations (Page 1981)

A comprehensive research project (NIKER Project 2010b) was carried out to define a general strategy for the material characterisation of existing masonry. The specimens used were prepared in laboratory following the common masonry typologies (Figure 2.5) composed mainly by natural stones, fired-clay bricks or mudbricks connected each other by different kind of binders (earth, lime, gypsum or cement mortars).

Figure 2.5 Overview of materials used in NIKER (NIKER Project 2011)

The single materials were characterised using the available standard tests to obtain information concerning compressive and tensile strength, Young's modulus and composition. The tests on the structural members were performed using different techniques for in-plane or out-of-plane loading scenarios, performing static tests on massive wall specimens and in-plane cyclic shear tests (see Figure 2.6a).
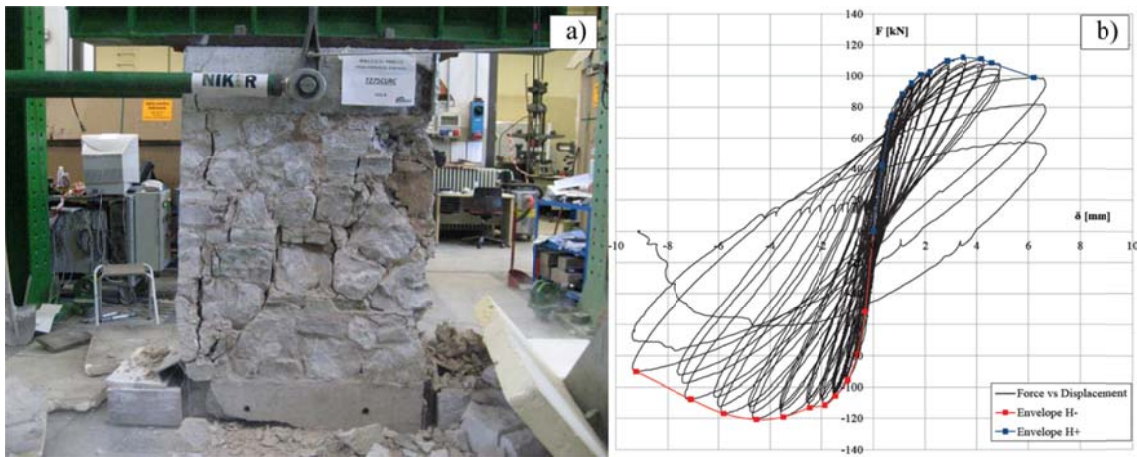
Figure 2.6 Cyclic test on stone masonry panel: specimen after failure (a) and hysteretic loops (b) (NIKER Project 2011).

As an example, the cyclic tests performed on massive wall specimens showed the characteristic softening behaviour of masonry elements. In fact, the envelope of the hysteretic loops shown in Figure 2.6b and the reducing slopes of the unloading curves indicate the degradation of the mechanical properties at each cycle due to material cracking.

Despite the high reliability of the results obtained by DT, the experimental setup is very expensive since it requires large and complex instrumentations especially for on-site applications (see Figure 2.3). In addition, by isolating the element to investigate, the stability of the global structure might be compromised, thus a support frame is usually needed to avoid compromising the vertical load-bearing system.

2.1.2. Minor-Destructive Testing (MDT)

Different techniques were developed in order to reduce costs, risks and damage occurrences. MDT is based on mechanical tests performed on a small portion of the structural element. It produces limited damage that usually does not require any immediate structural replacement. This solution reduces the costs in terms of instrumentation and time, but it introduces more uncertainties derived from the local representativeness of the test. In fact, by reducing the investigated area the results appear rather scattered, being historical masonry a heterogeneous material.

Commonly used MDTs to be performed on masonry structures are the single flat jack test to determine the stress level on a vertical panel (ASTM C1196 1991) and the double

flat jack to estimate the Young's modulus and the compressive strength of masonry (ASTM C1197 1991). The test procedure starts by measuring the distances between at least three couples of marker-points placed either over and below the investigated area in case of the single flat jack, or inside the investigated area in case of the double flat jack. Then, either a single mortar joint or two joints have to be cut by means of a circular saw, allowing the jacks to be inserted (Figure 2.7a). Just after the cut is made, it is necessary to measure the dislocation of the marker-points due to the removal of material. This technique is an application of the stress releasing method, which provides information on the elastic properties of the material by removing a part of it. In case of single flat jack test, the oil is pumped into the jack and gradually until the initial distance between the marker-points is recovered (Figure 2.7b).
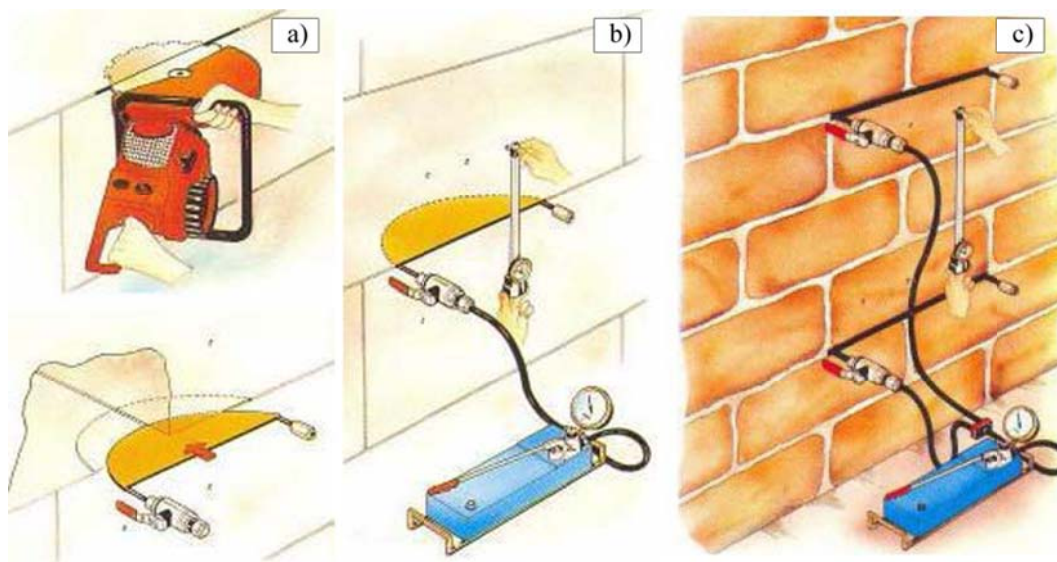
Figure 2.7 Flat Jack Test: cut and insertion of the jack (a), Single Flat Jack Test (b) and Double Flat Jack Test (c)

Concerning the double flat jack test, the oil is pumped until the material between the jacks is brought to failure (Figure 2.7c). The loading during the test is carried out in different stages, increasing the pressure of the oil at each step and then holding it to redistribute the stresses on the material. The measurement of local deformation in the internal part at the jacks is carried out by means of gauges. These instruments can be positioned either vertically or horizontally respect to the mortar joints. The procedure must be repeated at each loading step. The information obtained allows defining the stress-deformation curve, necessary to have an estimation of the Young's modulus of the composite material and its Poisson's ratio.

These tests are widely used in mechanical characterisation of existing masonry and they provide useful information about the material investigated. Binda used the double flat jack test (see Figure 2.8a) for the mechanical characterisation of the remains of the Cathedral of Noto (Binda et al. 2003; Binda et al. 1999; Binda & Tiraboschi 1999), showing good results in the evaluation of the deformability of the materials. The loading-unloading cycles showed the characteristic decay of the elastic properties at each cycle and the softening behaviour of the material (Figure 2.8b).
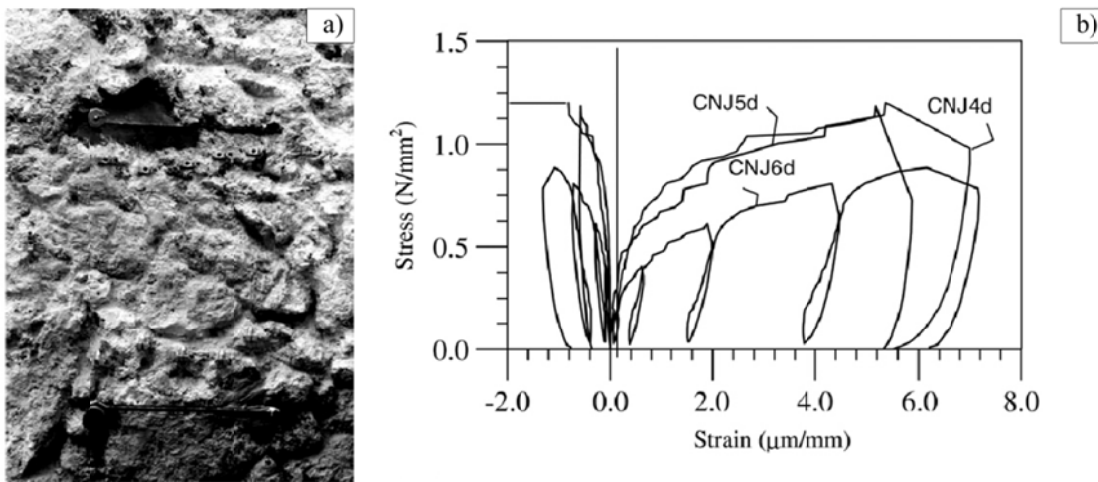
Figure 2.8 Double Flat Jack Test: prospect of the masonry investigated (a) and plot of the results for lateral and vertical strains vs. vertical stress (b) (Binda et al. 2003).

A complementary method to the single flat jack for the evaluation of the elastic properties was presented by Lombillo (Lombillo et al. 2010) as an application of the hole-drilling test for isotropic linear-elastic materials (ASTM E837 2008). The procedure consists in adapting a normalized experimental procedure for the quantification of the residual stresses for a heterogeneous material such as masonry. The proposed method allows the deduction, by means of a suitable mathematical process, of the principal stresses (σ_{max} and σ_{min}), and their direction (β), basing on three deformations (ε_1, ε_2 and ε_3) registered in three directions. The experimental procedure is very complex and consists of several steps that have all a strong influence in the results. Instead of using three strain gauges as proposed in the relative standard (ASTM E837 2008), for the analysis of masonry it is preferable to use a large number of strain gauges (Figure 2.9a) in order to reduce possible experimental bias. The deduction of the stresses from the deformations registered in the strain gauges is strongly influenced by some constants that correlate the deformations caught in the strain gauges. These

constants can be obtained in a theoretical way depending on few dimensional parameters, such as Young's modulus and Poisson's ratio, or experimentally by means of a test based on the realisation of a wall of similar quality to the material tested in situ (Figure 2.9b).

Figure 2.9 Hole-drilling technique: detail of the gauge positioning (a) and test execution in the laboratory for the calibration of the analytic method (b) (Lombillo et al. 2010).

An interesting alternative technique for minor-destructive testing is the extraction of samples to be subject to destructive testing in the laboratory. The sampling procedure must inflict the lowest possible damage to the historical structure. The technique adopted is very important, since the specimens must be as undamaged as possible to be representative of the in-situ material. The extraction of mortar samples from the joints of a wall is difficult, since the material is brittle and usually crumbles as soon as it is removed from the original location. The sampling of wall portions, to evaluate the properties of the composite material, is almost impossible for existing historical structures. The common sampling technique is by means of core drilling performed horizontal and perpendicular to the face of a structural member, like a wall. Different types of specimens can be extracted from the existing wall, such as specimens containing one diametral mortar joint or multiple joints (Figure 2.10).

Figure 2.10 Cylindrical specimens extracted by core-drilling: single and three joint specimens (a) and two joint specimens (b)

Benedetti and co-workers (Benedetti et al. 2008) focused on single-joint specimens, deriving the strength envelope of historical mortars by testing 70 to 110 mm masonry cores extracted from an existing building. Different Brazilian tests were carried out with variable inclinations of the diametral mortar joint respect to the horizontal (Pelà et al. 2012; Benedetti & Pelà 2012). The mortar joint could be subject to different combinations of shear-compression stresses by varying the joint inclination, for instance from 45º to 60º. This method takes the most advantage from this kind of specimen, since much more information can be obtained than in Brazilian tests executed maintaining the same inclination of the mortar joint, e.g. 45º (Braga et al. 1992; Filardi et al. 1996; Benedetti et al. 2008). Besides that, the sampling technique is effective since the mortar joint keeps confined by two bricks, allowing the extraction of rather undisturbed mortar specimens.

In other recent studies (Pelà et al. 2012; Marastoni et al. 2016; Pelà et al. 2015) the cylindrical samples were tested with the diametral mortar joint inclined with respect to its original horizontal position in the wall (Figure 2.11a). Such special testing set-up induces to the mortar in the joint a stress state of simultaneous normal compression and tangential shear (Figure 2.11b). Different combinations of shear-compression stresses can be applied to the mortar joint by varying the diametral joint inclination.
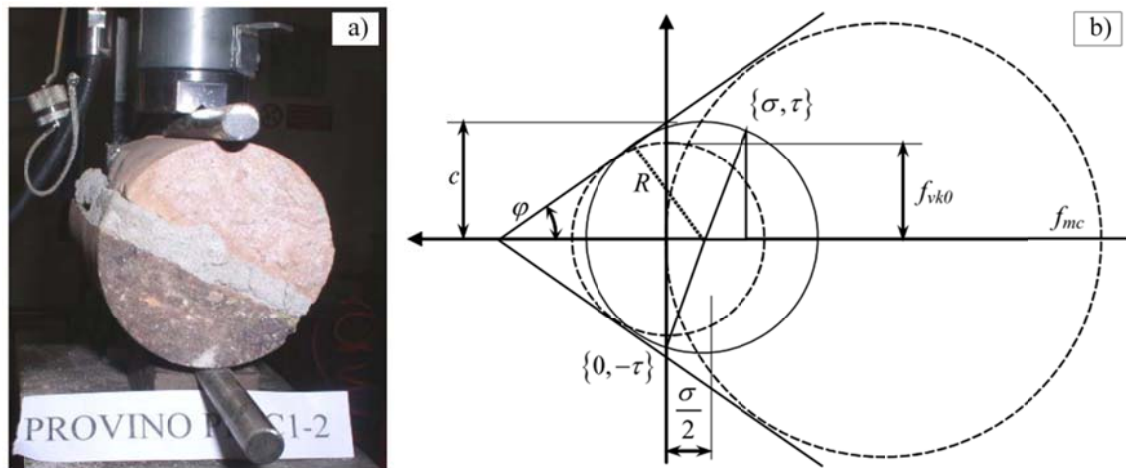
Figure 2.11 Brazilian Test on cored sample with diametral joint rotated respect to the horizontal (a) and its interpretation (b) (Benedetti et al. 2008).

This last improvement of the experimental technique led to the derivation of more information from the tests than in previous studies (Braga et al. 1992; Filardi et al. 1996), where the Brazilian tests were carried out with a fixed inclination of the mortar joint of 45°. In these studies from the nineties, the authors were mostly interested in obtaining a relationship between the shear strength of the joint and those of medium (triplets) and big (walls) assemblages of cement mortar masonry.

All the aforementioned studies about Brazilian tests on cores with inclined diametral joint showed that the mode of failure of the specimen is strongly dependent on the type and strength of mortar. In case of low-strength lime mortar, the failure was characterised in most cases by a fracture crossing the mortar joint at the core's centre and involving the upper and lower brick-mortar interfaces at the sample extremities (combined sometimes with detachment of a small brick wedge close to the load), see Figure 2.12a. This mode of failure was called "parasymmetric" or "centrally symmetric" (Pelà et al. 2015) and it was observed in experimental programs carried out with low-strength mortars performed firstly by Braga (Braga et al. 1992) with lime-cement mortar characterised by a compressive strength range between 1.8 MPa and 2.5 MPa. A recent study carried out by Pelà (Pelà et al. 2015) showed the same outcomes of the aforementioned one using lime mortar with compressive strength of 1.9 MPa. These ranges of strength values are actually representative of the behaviour of typical low-strength historical mortars. For higher strength mortars, different types of failure were observed. Other authors (Mazzotti et al. 2014) report failures resulting from either splitting of the core or pure shear sliding along the brick-mortar interface (Figure

2.12b), with a cement-lime mortar with higher strength of 7.8 MPa, that could be hardly considered representative of a low-strength historical mortar. Similar results were observed in previous study (Braga et al. 1992), showing an almost vertical crack, splitting the bricks parallel to the load direction (Figure 2.12c), for a high-strength cement mortar.
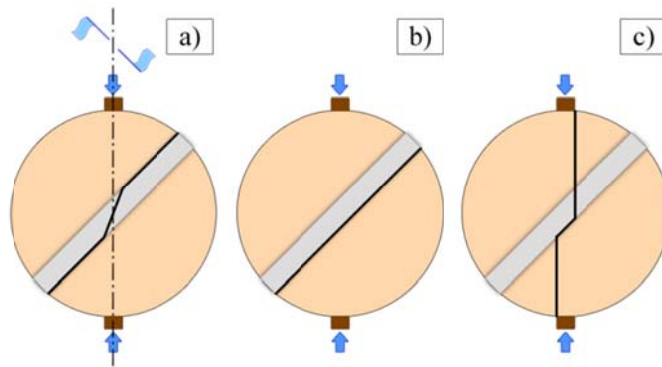
Figure 2.12 Modes of failure observed in Brazilian tests on cores with inclined diametral joint: a) "parasymmetric" or "central symmetric" fracture (Pelà et al. 2015) for low-strength mortars; b) shear sliding along the brick-mortar interface (Mazzotti et al. 2014) and c) splitting failure (Mazzotti et al. 2014; Braga et al. 1992) for higher strength mortars.

Another interesting testing technique on masonry cylindrical specimens is that proposed by the UIC 778-3 recommendations of the International Union of Railways (UIC 1995). Compression tests are performed on masonry cylinders with 150 mm diameter loaded on the lateral surface. The cylinder is centred in the middle of a vertical joint, so that the test is performed in the same direction in which the load is expected to act. The lateral surfaces are regularised by means of mortar caps between the sample and the steel loading plates as shown in Figure 2.13.
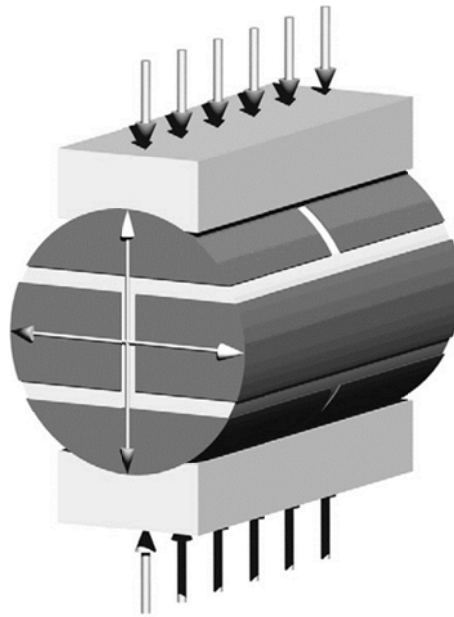
Figure 2.13 Setup of the compression of three joint cored specimen (Brencich & Sabia 2008).

The UIC 778-3 recommendations suggest that a minimum of three samples should be tested for each type of brickwork, but six should preferably be used if available. The method was used by Brencich and co-workers to evaluate the compression strength of clay brick masonry (Brencich et al. 2004; Brencich & Sterpi 2006; Bilello et al. 2007). The sampling technique is considered as minor destructive, since only a small portion of the structure is affected by the extraction, while the specimen is sufficiently complex to represent the interaction among units, horizontal and vertical mortar joints.

A research about the mechanical characterisation of existing mortar was published by Henzel and Karl (Henzel & Karl 1987) on the Double Punch Test on mortar joint specimens extracted from an existing wall. This work is widely used for the evaluation of existing mortar strength, since it provides reliable information on the material investigated. Due to the particular shape of the specimens, several studies enriched this technique to evaluate the influence of the thickness of the specimens (Drdácký 2011; Pelà et al. 2012; Sassoni et al. 2014). These studies showed a strong dependency on the slenderness ratio of the specimens on the maximum load (see Figure 2.14a).
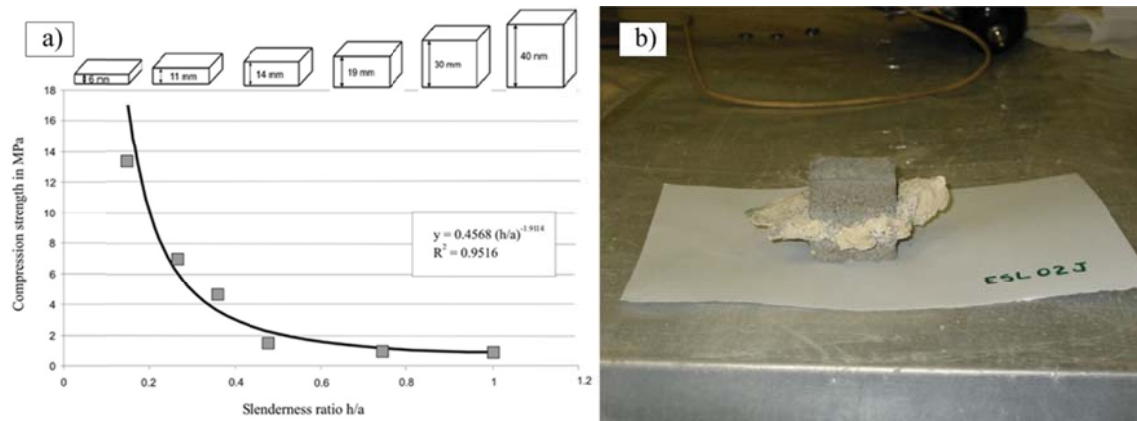
Figure 2.14 Influence of the slenderness of the specimens on the maximum load (Drdácký 2011) (a) and capping for irregular specimens of mortar (Válek & Veiga 2005) (b).

Other studies investigated on the influence of possible irregularities of the loading surfaces on the results obtained from the DPT. The solution provided by these works is to ensure the planarity of the loading area by means of caps. Some authors (Sassoni et al. 2014) compared the outcomes of DPTs performed using different capping materials with non-capped specimens. In addition, Válek (Válek & Veiga 2005) compared regularised cut specimens with non-standard ones capped with mortar designed to be stronger than the extracted samples (Figure 2.14b). Both reported similar results, assessing that capping on non-regular specimens has a strong influence on the results of the DPT, but using properly arrangements can reduce the scattering around the results.

Another type of in-situ tests classified between NDT and MDT is the penetrometric technique, since the entity of damage caused at the structure is minimal. However, these tests must be performed directly on the material to investigate, requiring the removal of eventual plaster or coating surfaces. These tests are usually an adjusted version of standard tests for other materials (mainly concrete) useful to estimate the compressive strength by performing micro-destructive analysis. The most common penetrometer is the Windsor Probe, initially designed for hardened concrete investigation as the US codes assess (ASTM C803 2010). The instrumentation consists in a gun loaded with a standard explosive cartridge or a spring-based system with a defined energy amount. The latter approach is more appropriate for testing low strength mortars, since the former is more appropriate for cement based ones. After shooting at the investigation surface, a metal pin is forced to penetrate in the material. The penetration depth is inversely proportional to the compressive strength of the concrete (Figure 2.15a).

Gucci's penetrometer (PNT-G) is a different system for the in situ investigation of existing mortar (Gucci & Barsotti 1997). The instrument is composed of a portable driller connected to an electronic apparatus that measure the energy necessary to drill a fixed depth (Figure 2.15b).

Figure 2.15 Penetrometric techniques: Windsor Probe (a) and Gucci's Penetrometer (PNT-G) (b)

Other researchers developed different types of penetrometers, like Liberatore (Liberatore et al. 2001) or Felicetti (Felicetti & Gattesco 2006), taking inspiration from the dynamic penetrometric test for soils (SPT, Standard Penetration Test). The number of blows needed by the probe to penetrate for a standard depth is correlated to the density of the material and, by using a proper empirical formulation, to its compressive strength. In order to have a constant impact energy on each blow, the percussion is provided by an internal spring-based impact mechanism (Figure 2.16a) or by means of a standard sclerometer (Figure 2.16b).
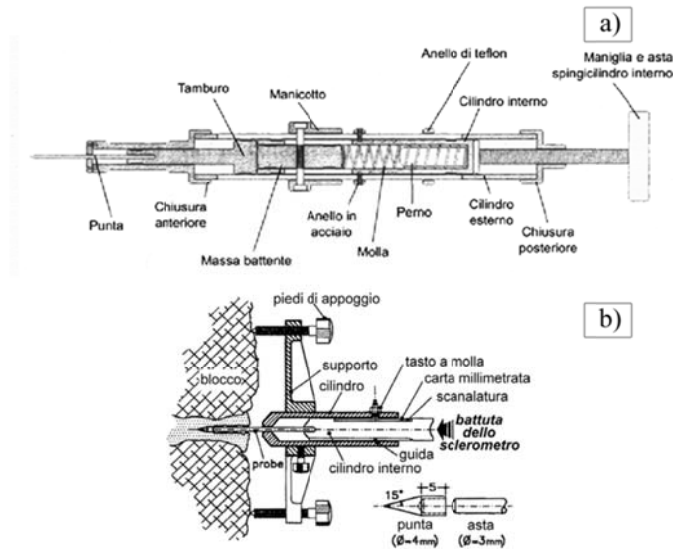
Figure 2.16 Penetrometric techniques: Liberatore's (Liberatore et al. 2001) (a) and Felicetti's

Penetrometers (Felicetti & Gattesco 2006) (b)

Sclerometric test is also well-known as NDT for concrete, based on the rebound effect of a mass hitting the material surface (EN 12504-1:2009 2009). After measuring the rebound height of the mass, which is directly correlated to its superficial hardness, it is possible to estimate the compressive strength. Since the operating principle is based on the rebound effect on the material to investigate, usually it is necessary to remove parts of plaster or coating,

Using a similar principle, Van Der Klugt (Van Der Klugt 1991) developed a sclerometric pendulum, and the rebound index is expressed as the maximum angle of rebound of the mass (Figure 2.17).

Figure 2.17 Pendulum sclerometer developed by Van Der Klugt (Van Der Klugt 1991)

2.1.3. Non-Destructive Testing (NDT)

With the introduction of new technologies in the structural health monitoring of existing masonry structures, several NDT techniques were developed to obtain information on the structure without damaging it. Most of them are based on the propagation of sonic and electromagnetic waves in the material.

The sonic method refers to the transmission and reflection of mechanical stress waves through a medium at sonic frequencies (McCann & Forde 2001). The five most commonly used sonic methods are:

- Sonic transmission method.
- Sonic/seismic tomography.
- Sonic/seismic reflection method.
- Sonic resonance method.

Sonic transmission method involves the passing of a compressional wave at frequencies between 500 Hz and 10 kHz through the element under investigation. Transmission of the wave is initiated by the impact of the force hammer, and reception is performed by an accelerometer which can be positioned directly opposite the emitter (Figure 2.21a).

In some cases, it is not possible to place the receiver directly opposite to the emitter. Thus a semi-direct (Figure 2.21b) or indirect (Figure 2.21c) configuration of the probes can be performed. The results are adjusted through empirical rules provided by authors and recommendations (ACI Committee 228 2004; Yaman et al. 2001). The resulting wave velocity is an average of the local velocity along the path and it is not possible to establish the position and the extent of any possible material discontinuity.
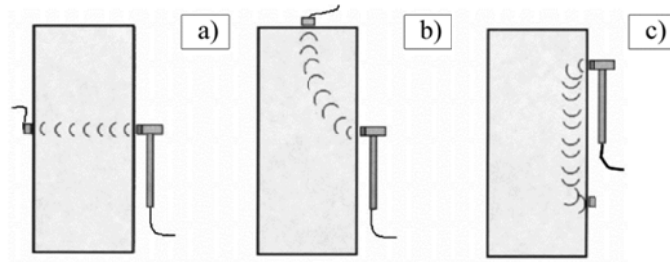
Figure 2.18 Transmission modes for sonic wave tests: direct (a), semi-direct (b), indirect (c) (McCann & Forde 2001).

Sonic tomography represents an improvement in the sonic transmission test method (Saisi et al. 2000). Tests are performed along paths that are not perpendicular to the wall surfaces. A dense net of ray-paths thus crosses the wall of the structure or the masonry section, where each one refers to a specific travel time between the sonic source and receiver through the structure. These values of travel time can be used to compute a three-dimensional reconstruction of the velocity distribution across the selected cross-section (see Figure 2.19) so that local variations in velocity can be identified and correlated with zones of weakness or different material layers in the internal fabric of the structure. It is usual to assume a linear structural response in the application of the tomographic method.
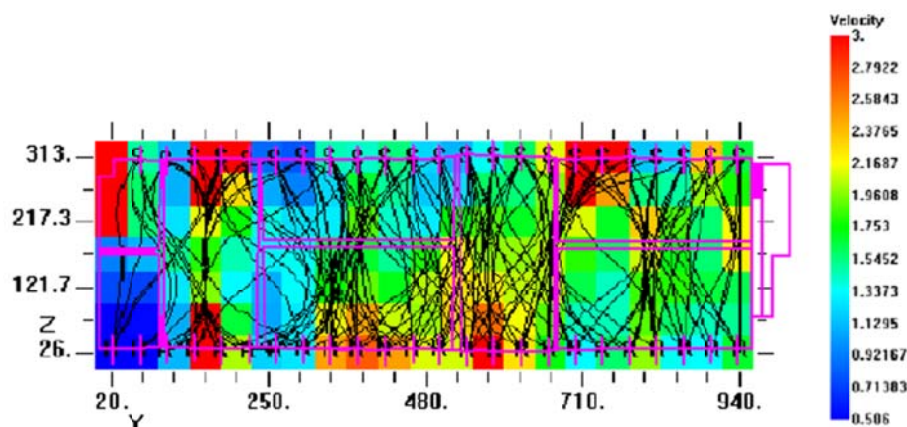
Figure 2.19 Example of tomography compared to the wall texture (Colla 2009).

In the sonic reflection method both the emitter and receiver of the sonic wave are placed on the same face of the masonry (as for indirect transmission shown in Figure 2.18c), but the stress wave recorded is the direct stress wave reflected from any discontinuity interface of the element investigated. The velocity calculated from the rear wall or face of a structure is a measure of the local velocities along the path.

The problems that can be investigated by reflection methods are:

- Internal dimensions and shape of the masonry element.
- Type and properties of fill.
- Voiding within the fill material.
- Cracks and voids within the internal fabric of the structure.

Seismic waves, which are also generated by an impact source, are commonly referred to NDT applications and propagate at frequencies in the range from 100 Hz to 1 kHz. The range of frequencies refers both to seismic and sonic waves, thus in practice the terms are often interchanged. Despite its advantages, the sonic reflection method is not recommended since the resolution achievable with the low frequency energy is poor and it is often difficult to distinguish reflections from surface waves and refracted arrivals (McCann & Forde 2001).

The most recent development of sonic and ultrasonic methods is known as the "Impact–Echo" test method (McCann & Forde 2001; Colla 2003), which was originally developed to measure concrete thickness and integrity from one surface. The method is performed on a point-by-point basis by using a small-instrumented impulse hammer to hit the surface of the material investigated at a given location. An accelerometer mounted adjacent to the impact location records the reflected energy, as reported in Figure 2.20.
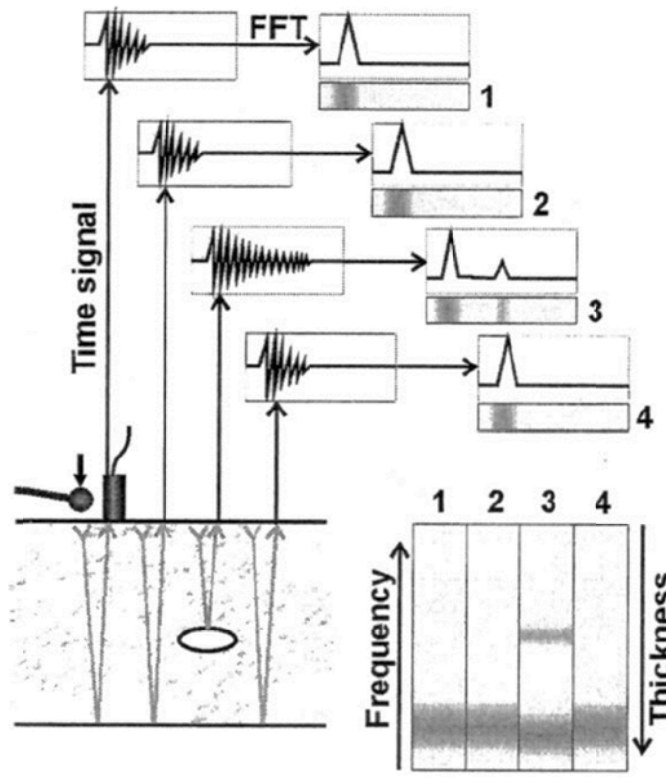
Figure 2.20 "Impact-Echo" principles scheme (Colla 2003)

Since reflected signals are more easily identified in the frequency domain, the received energy recorded in the time domain is passed to a signal analyser for frequency domain analysis using a fast Fourier transform (FFT). A transfer or frequency response function (FRF) is then calculated for the impulse generated and resonant frequency peaks in the transfer function or frequency spectrum record indicate reflections or echoes of the wave energy. These peaks allow identifying the position of the discontinuity interfaces, which can be either the outer surface of the material or internal defects. A simplified and "primitive" application of the "Impact-Echo" method was used for several years to detect voids presence behind plaster due to its eventual detachment from the wall. In this case, the wall was tapped with a lightweight hammer and the sound associated with a hidden cavity or defect produced a significant change in frequency. The method is rapid to use since the human ear is extremely sensitive to the change in the resonant frequency.

It is worth mentioning that ultrasonic methods are not feasible in masonry due to its high attenuation characteristics and numerous boundaries resulting in scattering of both incident and reflected waves. The ultrasonic methods, generated by a piezoelectric

transducer at frequencies above 20 kHz, are more suitable for detection of flaws in metal castings or for non-destructive testing of concrete.

Some attempts were made for identifying material properties and locating specific defects of single components such as units (Figure 2.21a) or mortar samples (Figure 2.21b) (Gabrielli & Colla 2014).
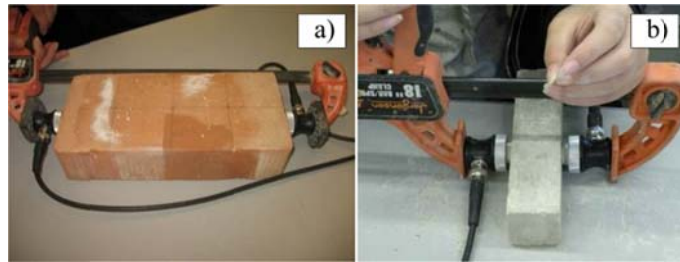
Figure 2.21 Ultrasonic tests performed on brick unit (a) and mortar specimen (b) (Gabrielli & Colla 2014)

Impulse radar uses the same instrumentation as for Ground Penetrating Radar (GPR) (McCann et al. 1988) but usually deploys higher frequency antenna above 1 GHz, allowing to increase the resolution reducing the penetrating capacity to the depth of the element to investigate. On each variation of mechanical properties of the material encountered by the wave, part of it is reflected and captured from the receiver probe. The principle of radar technique is reported graphically in Figure 2.22a.
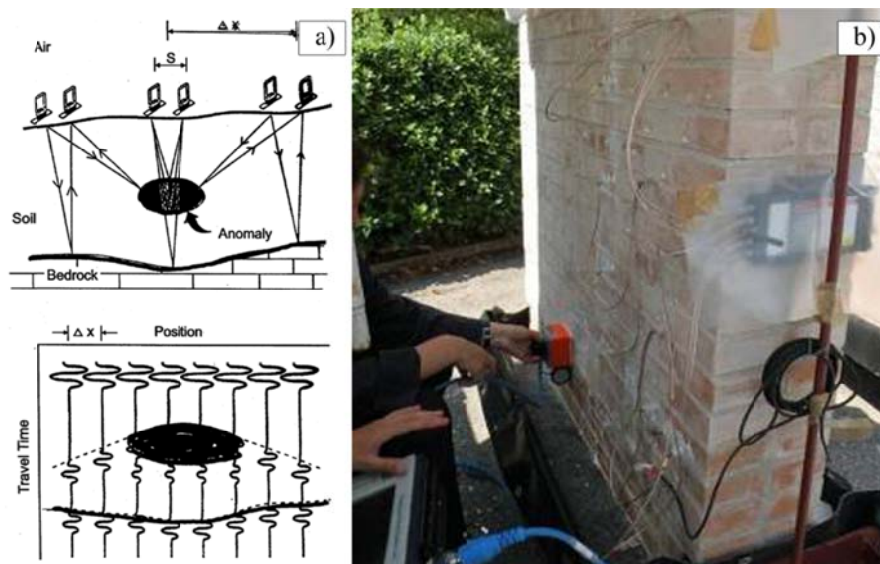
Figure 2.22 Radar principles (McCann & Forde 2001) (a) and its application on masonry element (Colla et al. 2011) (b).

Infrared thermography is based on the conversion of the thermal radiation into the visible spectrum by means of specific infrared sensors. It was observed that masonry structures characterised by voids (such as chimney or niches), discontinuities (enclosed openings) or damages emit differing amounts of infra-red radiation (Colla et al. 2008), even with presence of plaster. This phenomenon is due to different thermal inertia of the materials or cavities producing a different radiation. In Figure 2.23 it is noticeable the presence of cracks connecting the openings at the first floor.

Figure 2.23 Thermography overview of a building façade (Colla et al. 2008).

Moreover, moisture concentration can be easily identified, allowing finding eventual infiltration of water that can provide further damages on the structure. Figure 2.23 reports dark areas related to higher moisture content of the wall due to rainwater from the roof. This method has proved to be most effective as a reconnaissance tool for the rapid assessment of large buildings.

In general, NDT techniques are more suitable for a qualitative survey, allowing retrieving general information on the structure health and providing only few parameters for the mechanical characterisation. For this reason the current standards and recommendations for historical structure assessment (D.M. 14/01/2008 2008; Circolare 02/02/2009 n. 617 2009; ISCARSAH 2003b) suggest to use NDTs as complementary tests to major destructive ones, providing useful information to plan an appropriate experimental campaign of mechanical tests on the building object of investigation.

2.2.   State-of-the-art of the numerical analysis of masonry

Once the mechanical characterisation of the material is achieved, it is necessary to analyse the structural system through numerical models. The masonry assessment can be based on linear and nonlinear analyses both in static and dynamic configurations on finite element models or using local analyses with kinematic approach.

Linear static analysis is the most simple analysis to be performed. The Italian Standard (D.M. 14/01/2008 2008) suggests it only for simple structures. Linear dynamic analysis (i.e. Modal Analysis combined with response spectrum analysis) is widely used in seismic assessment, since it provides further information on the dynamic behaviour of the structure such as influence of modal components on the global behaviour (see Figure 2.24a). The hypothesis of linear materials is however the major limitation to the reliability of these analysis.

Nonlinear static analyses (Pushover) are well-known in the professional practice, and consist in step-by-step analyses increasing the horizontal loading until the collapse. The constitutive model of the elements is nonlinear. The equilibrium can be calculated on the deformed geometry at each step, thus including also the nonlinear geometric effects. The results give information about the ultimate capacity of the structure, considering the nonlinear behaviour in the resisting elements (see Figure 2.24b and Figure 2.24c).

Nonlinear dynamic analysis (Time-History) considers all the nonlinear properties of the materials subjected to a time-dependent action that usually is defined by accelerograms. This analysis is the most expensive in terms of computational costs, since it is based on the integration of motion equations for each degree of freedom. For this reason, Time-History analyses are limited to special case-studies (Figure 2.24) and are not so widely used in practice-oriented works.
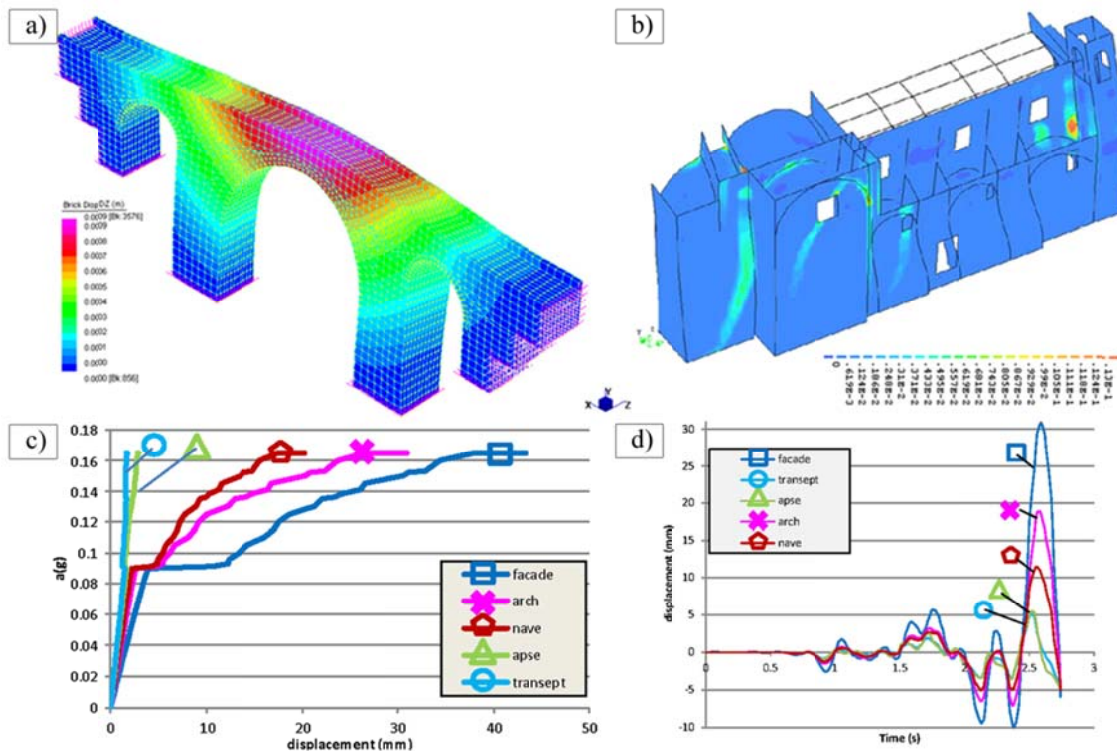
Figure 2.24 Vibrational mode for S. Marcello Pistoiese Bridge in Lizzano (Italy) (Pelà et al. 2009) (a) and nonlinear model of San Marco church in L'Aquila (Italy) (Endo et al. 2015) (b): Pushover capacity curves (c) and Time-History analysis results (d).

Local analyses are usually performed on structural parts, in which the cracking process produces the separation from the structure leading to the formation of local mechanisms. These analyses are based on limit-analysis principles, considering the element as a rigid body whose failure is determined by a lack of equilibrium. This type of analyses is used for safeguarding the eventual overturning of facades (Figure 2.25a), large portion of walls under thrusting roofs (Figure 2.25b), etc.
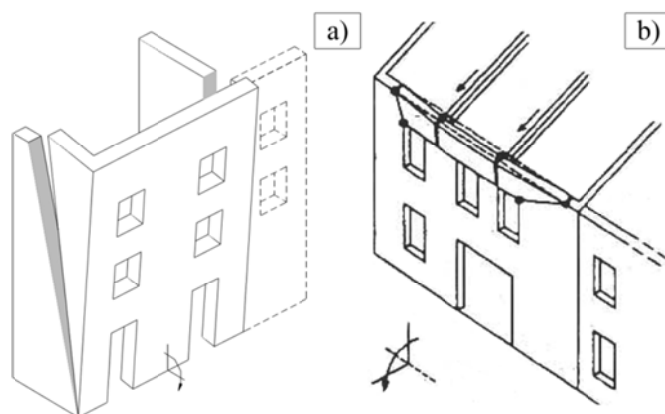
Figure 2.25 Local failure of masonry based on limit analysis: overturning of facade (a) and of portion of wall under thrusting roof (b) (NIKER Project 2010a).

2.2.1. FE modelling for masonry assessment
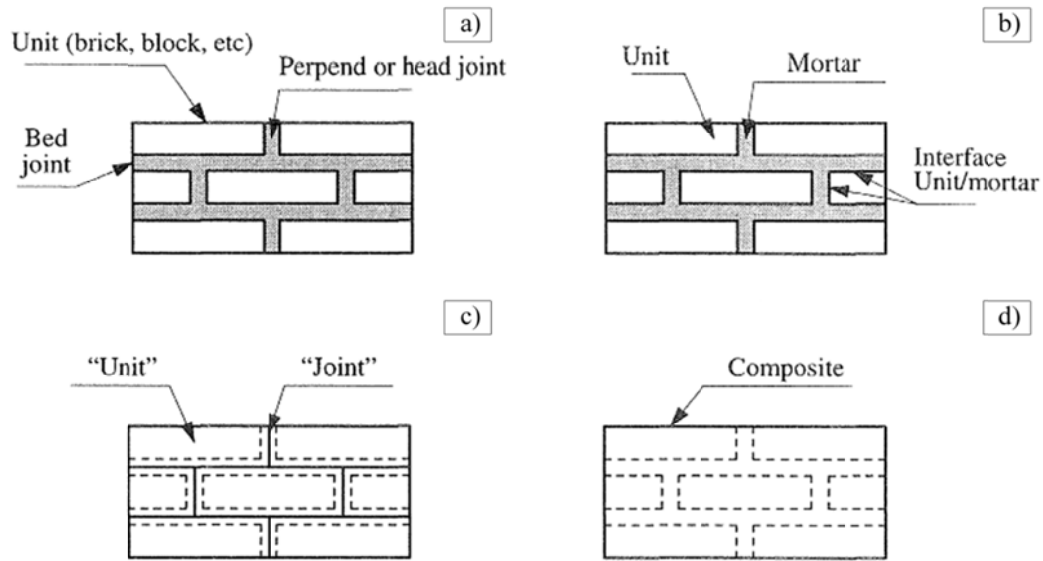
Figure 2.26 Modelling strategies for masonry structures: (a) masonry sample; (b) detailed micro-modelling; (c) simplified micro-modelling; (d) macro-modelling (Lourenço et al. 1995).

Several modelling approaches are currently available to deal with the analysis of masonry structures (Roca et al. 2010). The different approaches use different theories, resulting in different levels of complexity and cost.

Masonry texture (Figure 2.26a) can be represented with its heterogeneous nature by representing all the materials as a continuous mesh comprehensive of discontinuous mortar-units interfaces. This approach is commonly known as micro-modelling (Figure 2.26b) and leads to a definitely precise description of the material, allowing considering eventual crack or slips between units and joints by means of discontinuous interfaces (see Figure 2.27a,b,c).
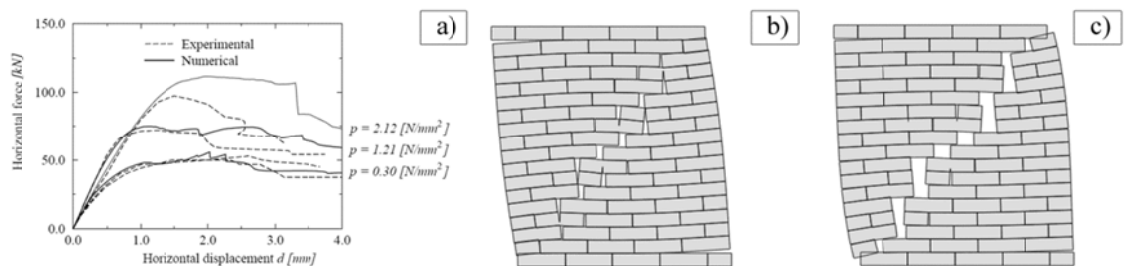
Figure 2.27 Micro-modelling of masonry shear walls (Lourenço 1996): load displacement diagrams (a); deformed mesh at peak load (b); deformed mesh at collapse (c).

The primary aim of micro-modelling technique is to represent closely the masonry material from the knowledge of the properties of each constituent and the interfaces. The necessary experimental data has to be obtained from laboratory tests in the constituents and small masonry samples. Despite the advantages, the detailed micro modelling requires a large number of parameters and the high number of degrees of freedom making it hardly suitable for large models. However, this technique is widely used for the modelling of isolated masonry elements, allowing understanding accurately the local behaviour at the level of constituents.

This drawback is partially solved by means of simplified micro-models (Gambarotta & Lagomarsino 1997; Lotfi & Shing 1994), where the description of the solid components is made by continuous mesh with elastic properties, while the behaviour of the mortar joints and unit-mortar interfaces is lumped into the discontinuous elements (Figure 2.26c). Masonry is thus considered as a set of elastic blocks bonded by potential fracture/slip lines at the joints. Further improvements can consider even the potential crack internally to the units. Nevertheless, the simplified strategy still requires a strong effort in terms of computational costs, making the analysis of complex structures hard to manage.

In large and practice-oriented analyses, the knowledge of the interaction between units and mortar can be neglected in the analysis of the global structural behaviour. In these cases, a continuum material (i.e. macro-modelling) shall be more suitable (Figure 2.26d). Macro modelling is largely diffuse for the global analysis of structures, but the mechanical properties of the homogenised material are difficult to be determined. The anisotropic behaviour of masonry can be considered using specific models. Available models were provided by Pelà (Pelà 2009; Pelà et al. 2011a; Pelà et al. 2013)and Lourenço (Lourenço et al. 1995). The first one is based on establishing a one-to-one mapping relationship between the behaviour of an anisotropic real material and that of an isotropic fictitious one. This general formulation allows adjusting an arbitrary isotropic criterion to the particular behaviour of the orthotropic material. The orthotropic elastic and inelastic behaviours can be modelled in such a way that very different mechanical responses can be predicted along the material axes (see Figure 2.28). This model showed its predictive capacity both for linear and nonlinear analyses of homogenised macro-models.
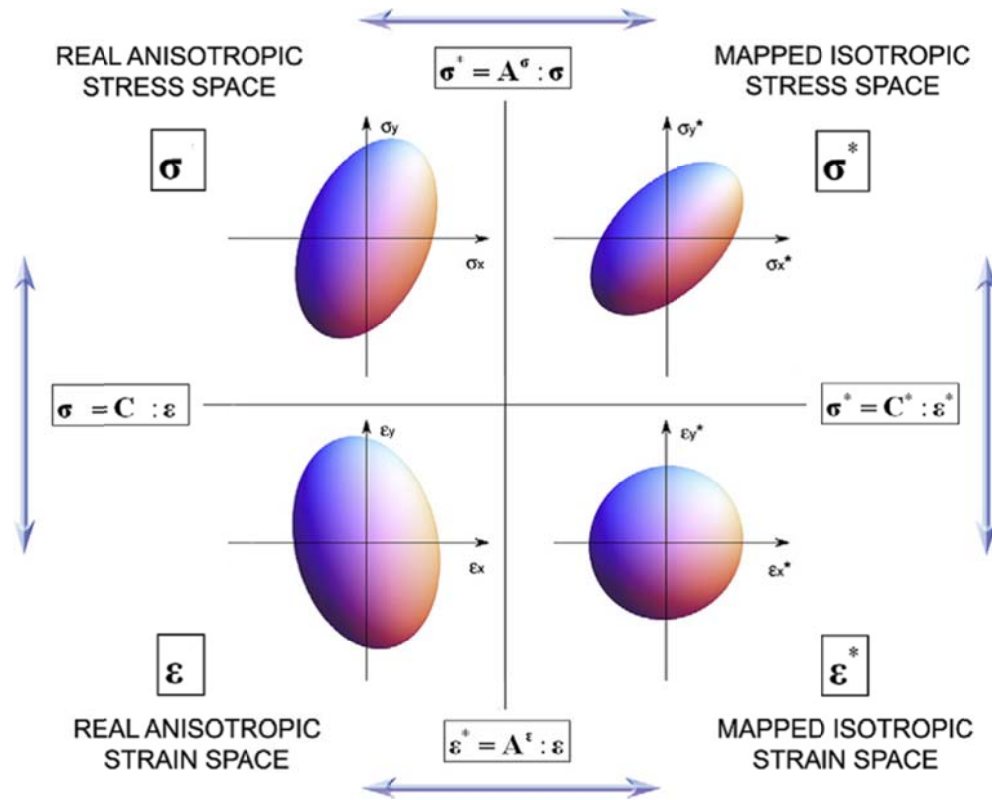
Figure 2.28 Stress and strain mapping developed by Pelà et al. (Pelà et al. 2011a)

Lourenço (Lourenço et al. 1995) developed an anisotropic model that combines the advantages of modern plasticity concepts with a powerful representation of anisotropic material behaviour, including different hardening or softening behaviour along each principal stress direction. The proposed yield surface was based on Rankine-type criterion in tension and Hill-type criterion in compression (Figure 2.29).
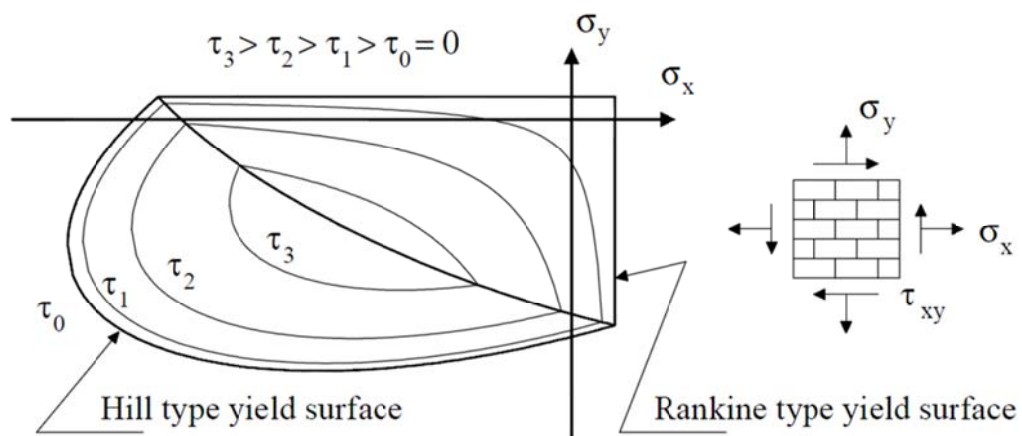
Figure 2.29 Lourenço yield surface (Lourenço et al. 1995).

Concerning macro modelling, it is difficult to consider the influence of internal phenomena on the macroscopic properties, such as strain localisations or stresses redistribution among the microstructure, especially when strain localisations lead to complex dissipation mechanisms at the structural level. On the contrary, micro-model simulation contains all the aforementioned information directly explicated. This method provides the best accuracy in taking into account the microstructure influence on the structural behaviour. However, when applied to large-scale analyses, the computational cost and the geometric construction of the micro-model become hard to manage.

Mid-way between micro modelling and macro modelling there are multi-scale models, which represent a very popular approach used nowadays for the detailed analysis of single structural members (Petracca et al. 2016). These methods take into account, to different extents and in different ways, all the relevant length scales of the structural problem. These modelling techniques are based on Computational Homogenization Method (CHM) (Petracca et al. 2016; Quinteros et al. 2012; Zucchini & Lourenço 2002; Zucchini & Lourenço 2009). The micro-structural features are not physically represented in the structural model but they are obtained from a representative sample of the microstructure called representative volume element (RVE) which is associated to each integration point of the macroscopic mesh (Figure 2.30). The RVE is then used to obtain a homogenized response to the macroscopic strain field, retrieving the homogenised constitutive behaviour from the micro-model assumptions.
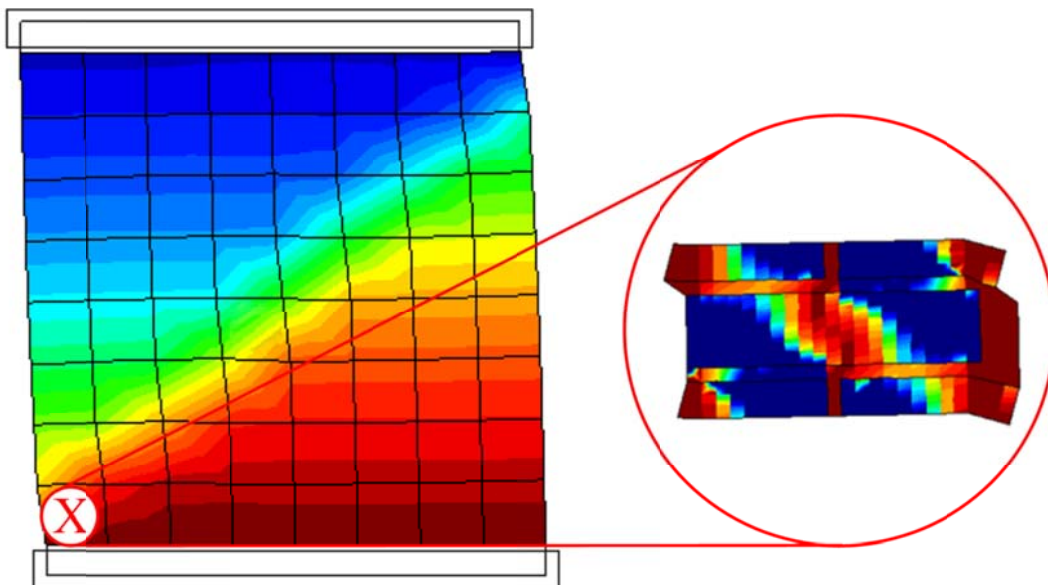

Figure 2.30 Multi-scale model application: structural macro-scale and representative volume element at the micro-scale (Petracca et al. 2016).

2.2.2. Constitutive models for masonry assessment

The most common nonlinear constitutive models for masonry are based on either plasticity theory or continuum damage mechanics. Plasticity theory considers the development of non-reversible strains in the nonlinear range. The theory of plasticity is a constitutive law purposely designed for metals (Chen & Han 1988). However, it can also be used for quasi-brittle materials, such as concrete or masonry, loaded in triaxial compression and shear-compression problems where inelastic non-recoverable strains are observed. The incapability of the theory to reproduce the elastic stiffness degradation of quasi-brittle materials subjected mainly to tension cannot be accepted for cyclic loading. In this case, the continuum damage theory applied to smeared cracking models is more appropriate. In fact, continuum damage theory (Kachanov 1986) does not comply non-reversible deformations, but when the maximum load is reached the elastic properties of the material decrease.

An example of loading and unloading phases for both Plasticity and Damage models is reported in Figure 2.31a,b.
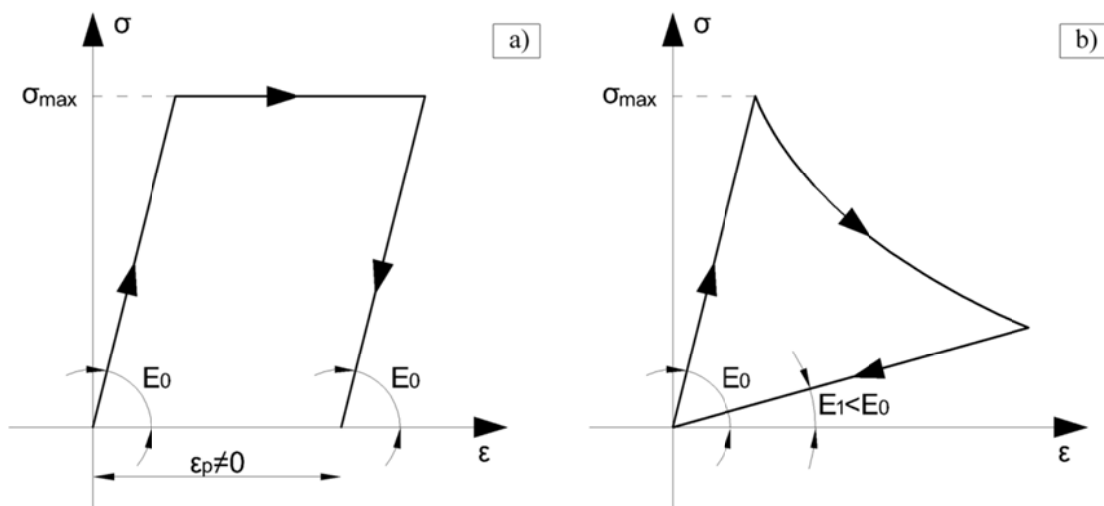
Figure 2.31 Comparison of loading-unloading in plastic models (a) and damage models (b).

Different development of the continuum damage theory led to the definition of new constitutive models. The basic development considers an isotropic damage behaviour (Simo & Ju 1987), where the elastic properties of the materials are governed by a single scalar quantity named d, non-dependent on the type of stresses at the failure. The damage scalar is related to a softening function dependent on the fracture energy of the

system. The same behaviour is applied to compressive, tensile and shear state of stresses, reducing the possibility to define different behaviour on each failure mechanism. Moreover, the possible damage occurred for a tensile action influences in the same magnitude the compressive behaviour of the material, which is a strong approximation for brittle materials. In fact, the formation of cracks consequently to tensile state of stress has only a small influence on the compressive behaviour of the brittle materials. For this reason this model was enriched (Mazars 1986; Pelà et al. 2011a) defining two different scalar damage indexes referred to two different conditions: d^+ for more brittle tensile stress states and d^- for compressive stress states. The evolution of each damage variable is defined by proper softening/hardening functions, dependent on the fracture energy under tensile or compressive conditions.
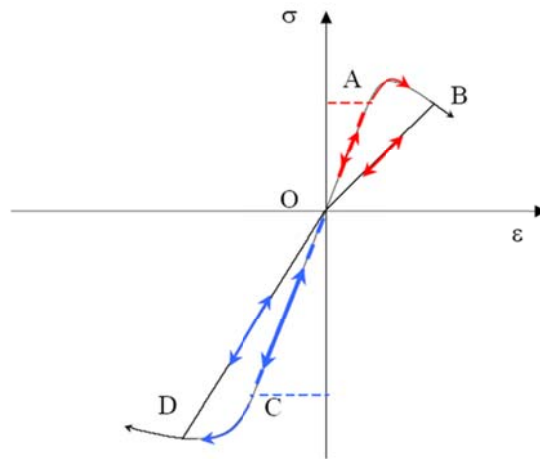
Figure 2.32 Unilateral effect under cyclic load paths (Pelà 2009).

The real behaviour of quasi-brittle materials like masonry are evidently midway between the two ideal models given by plasticity and damage mechanics theory, as it is clearly visible in Figure 2.6b.

Sophisticated constitutive models (Faria et al. 1998; Lubliner et al. 1989) were developed to take into account both the plastic and damage behaviours. The combination of degradation of stiffness (provided by the continuum damage theory) with the capability to represent non-reversible strains (provided by the plasticity theory) allowed obtaining a more representative model for cyclic behaviour of brittle materials, as shown in Figure 2.33. The aforementioned plastic-damage models were mainly applied to the analysis of concrete structures.
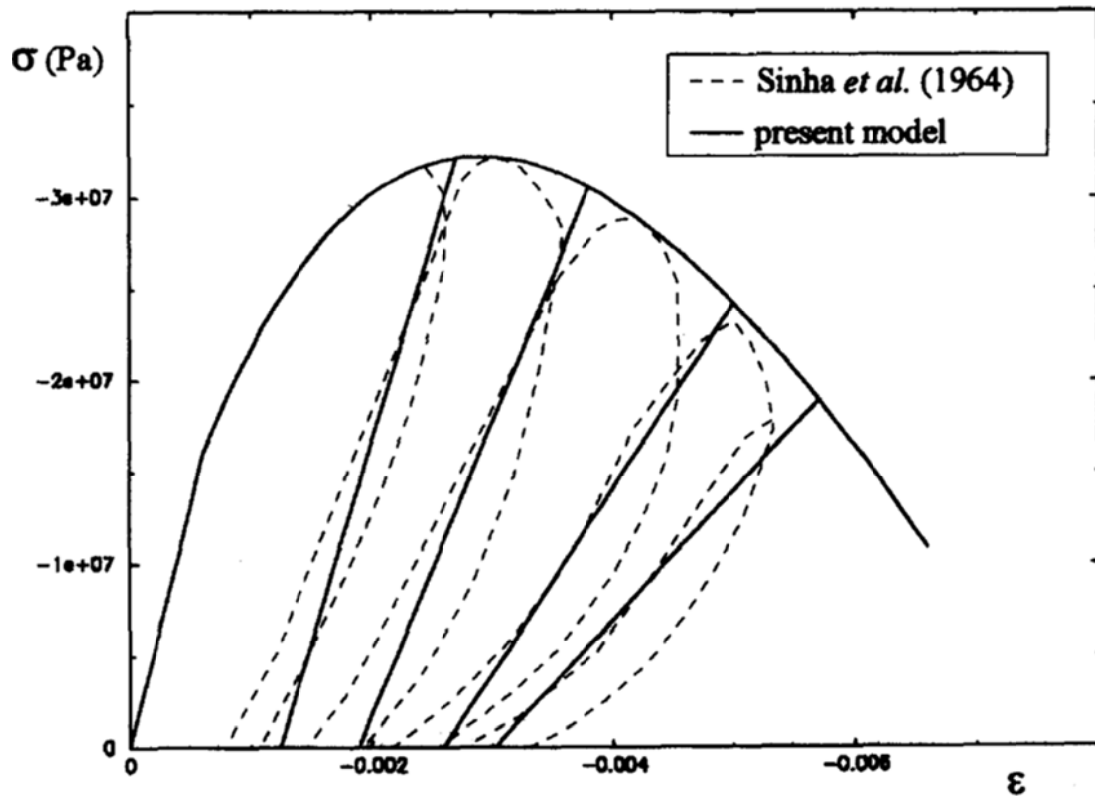
Figure 2.33 Application of Faria's model (Faria et al. 1998) to concrete cyclic compressive tests (Sinha et al. 1964).

Recent studies (Roca et al. 2013; Pelà et al. 2011b; Saloustros et al. 2014a; Saloustros et al. 2014b) used the continuum damage models for the evaluation of existing masonry structures. The numerical models included only a representative part of the structure (Saloustros et al. 2014a), like in the evaluation of the current damage and deformation of the Church of the Poblet Monastery (Figure 2.34a,b) and of the Cathedral of Mallorca (Roca et al. 2013; Pelà et al. 2014; Roca et al. 2012) (Figure 2.34c,d).
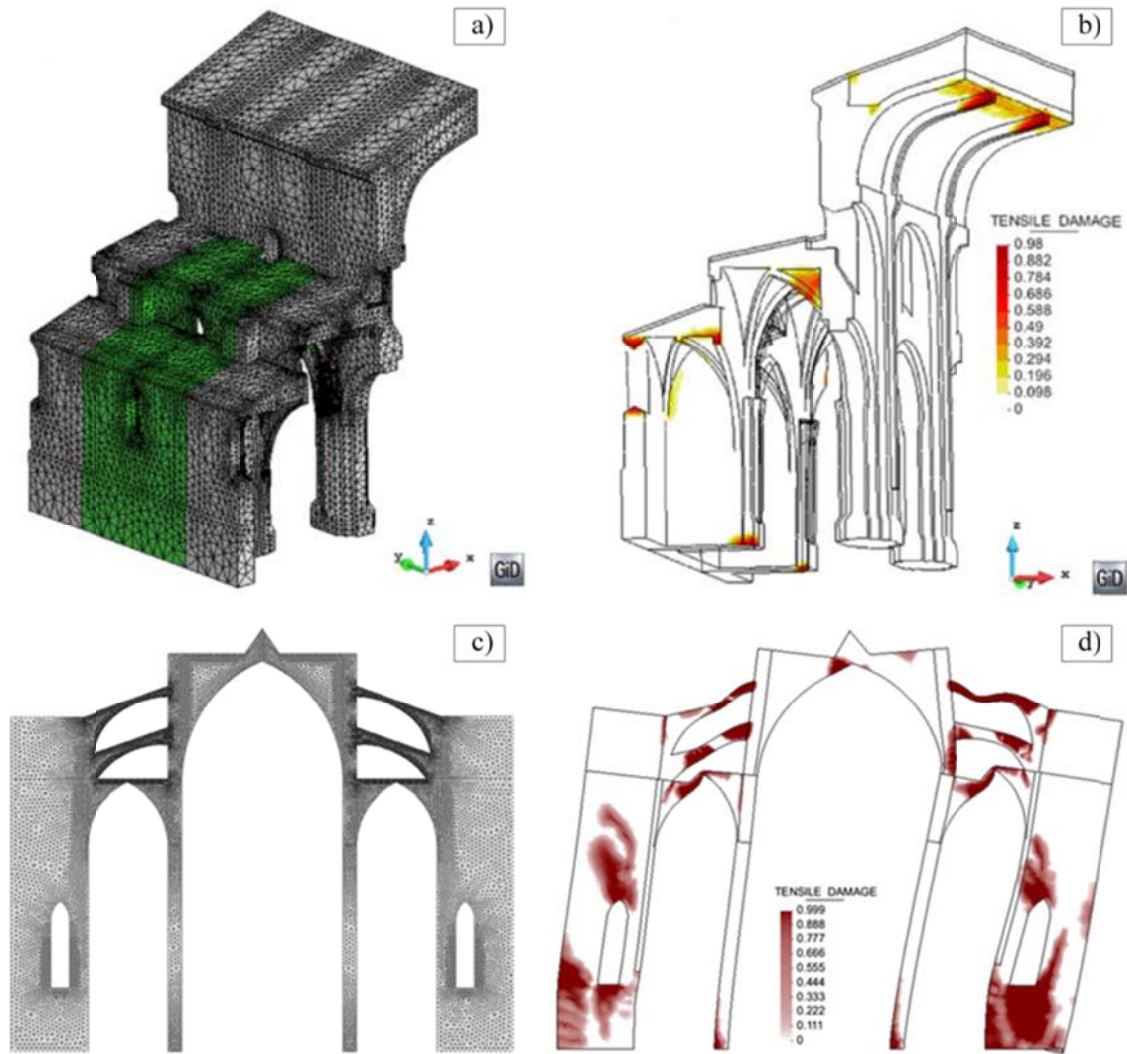
Figure 2.34 Example of nonlinear analyses with continuum damage models: Church of the Poblet Monastery (a) with its damage relative to the demolition of the southern aisle (b) (Saloustros et al. 2014a) and Mallorca Cathedral (c) with its damage due to seismic analysis (d) (Roca et al. 2013).

Complex models require a large number of parameters that are often very difficult to be estimated. For this reason, this work is focused mainly on simpler approaches, such as the isotropic continuum damage model, for a better control of the input data in the analyses performed to validate the experimental tests.

Chapter 3.   A novel penetrometer for in-situ Minor Destructive Testing

This Chapter presents the proposal of a novel penetrometer for the in-situ MDT of existing and historical mortars.

Following a geotechnical approach, a revisited version of the field vane test (Richards 1988) was developed and called X-Drill (Christiansen 2011). It consists of a four-winged pin made of stainless steel, having an external diameter of 10 mm.
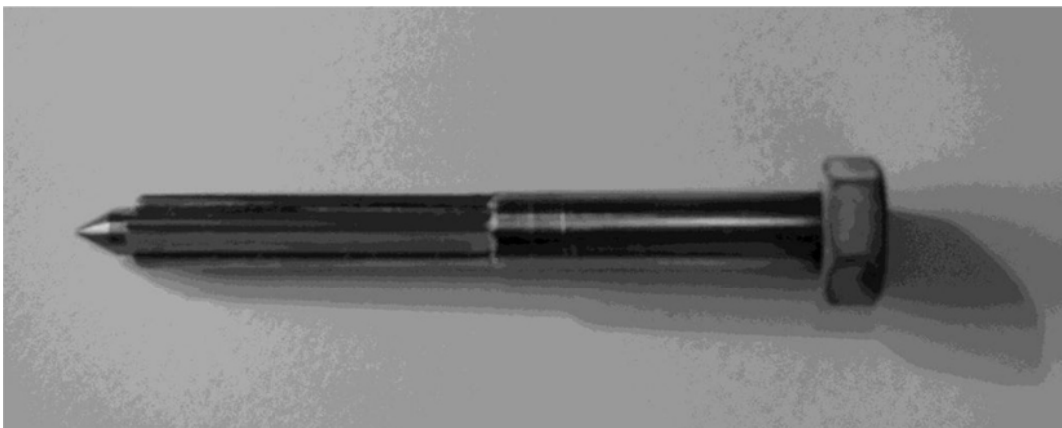
Figure 3.1 First version of the X-Drill (Christiansen 2011)

Firstly, a 6 mm diameter pilot hole is drilled in order to allow the pin introduction into the mortar joint, with a minimum crushing of the surrounding material close to the instrument's wings. The test is performed by using an analogical torque-meter, measuring the maximum torque moment under fracture.

Figure 3.2 First version of the X-Drill during the test (Christiansen 2011)

This research presents an enhanced version of the X-Drill that was developed on purpose for historical mortars. The proposed technique was calibrated by means of a large set of mortar specimens built in the laboratory. The comparison between X-Drill measurements and standard tests conducted on different types of mortars provides preliminary results for the calibration of the MDT technique.

3.1.   Geometry of the New Penetrometer

The novel version of X-Drill is obtained from a steel bolt class 8.8, which was chosen for its high performances and, at the same time, for its large availability. The bolt was shaped using a metal lathe tool and it is composed by three parts: a cubic head of 15 mm side, to which the dynamometric key is connected; a 40 mm long cylindrical body having a diameter of 6.5 mm; a winged end with four wings of 1 mm height. The length of the winged part is L_w=15 mm. A conic tip is provided on the back to ease the penetration of the X-Drill into the material. The novel X-Drill proposed for mortars is shown in Figure 3.3.
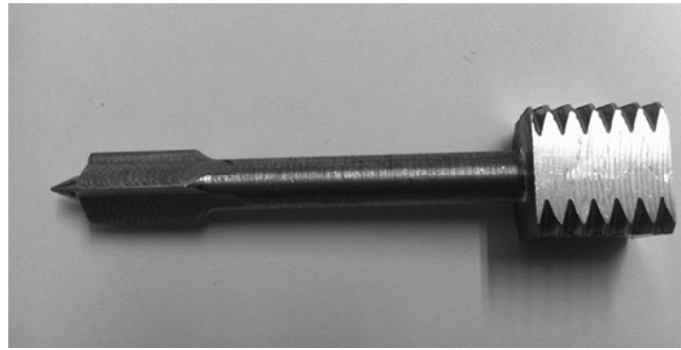
Figure 3.3 Novel X-Drill proposed for mortars

The original version of the X-Drill was designed to be hammered into the pilot hole at a variable depth in a range between 15 to 20 mm, measured by the operator at each test (Christiansen 2011). This procedure introduced L_w as a further variable affected by measurement bias. On the contrary, the novel version of the X-Drill proposed in this research sets a fixed penetration depth of L_w=15 mm.

Another improvement proposed in this research with respect to the previous version is the reduction of the diameter, allowing a deeper penetration of the pin for a better investigation of the inner material. This is an important choice dealing with existing masonry, where the external surfaces are subjected to environmental deterioration and could lead to an erroneous estimation of the material properties. At the same time, a reduced diameter for the pin reduces the area of the investigated zone preserving the integrity of a larger part of the mortar joint. Figure 3.4 shows the geometry improvements described above.
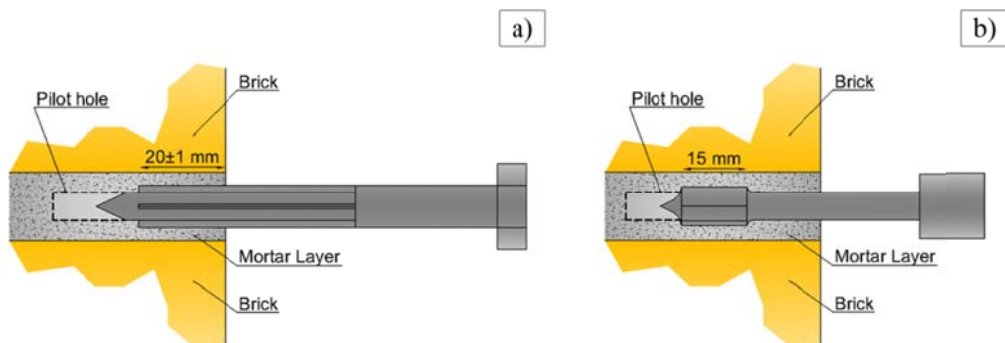
Figure 3.4 Longitudinal section of the X-Drill in first version (a) and novel one (b)

The instrument is coupled with a torque wrench, allowing measuring the maximum torque necessary to bring the material to failure. The torque wrench used in this research is equipped with an analogic display able to measure moments between 0-30 Nm with a precision of ±0.5 Nm. Figure 3.5 shows the blue pointer measuring the instantaneous value of torque, dragging the red one forward. After the failure is reached and the torque starts to decrease, the red pointer is fixed at the maximum position, allowing the operator to read the maximum torque reached.

Figure 3.5 Analogic torque wrench used in this research

3.2.   Theoretical Interpretative Model

The X-Drill test was normally interpreted up till now by using empirical correlations of experimental data in terms of torque vs. compressive strength (Christiansen 2011). This research presents a possible theoretical interpretation of the test based on the stress state of the material at the failure moment.

The mortar during the test is loaded by shear stresses along the fracture surface, identified by a cylindrical shape shown in Figure 3.6.
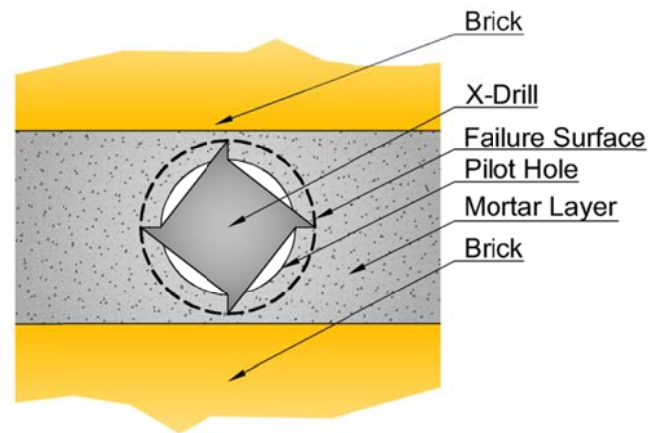
Figure 3.6 Transversal section of the X-Drill inserted in the mortar joint

The wings of the pin, inserted into the mortar, induce also compression to mortar, resulting in a composite state of stress of shear and compression.

The torque applied to the X-Drill section is therefore totally balanced by the tangential stresses τ along the failure surface, considering a constant stress distribution. However, in reality the contact between the investigated material and the instrument produces a friction effect, biasing the torque reading of a certain quantity M_0, called initial torque. Taking into account this phenomenon the correct equilibrium condition is expressed by Equation 3.1:

$$\tau = \frac{2 \cdot (M_v - M_0)}{\pi \cdot D_e^2 \cdot L_w} \tag{3.1}$$

where M_v is the torque measured by the dynamometric key, D_e is the diameter of the failure surface, L_w is the wings' length. The outer equilibrium statement is represented in Figure 3.7a.

The equilibrium condition can be defined making reference to a quarter of the instrument section, due to its radial symmetry. The first hypothesis considers constant tangential stresses along the failure surface, as calculated in Equation 3.1. The torque M_v is produced by four distributions of normal stress σ_1, located at the contact area between the mortar and the instrument's wings (Figure 3.7b)
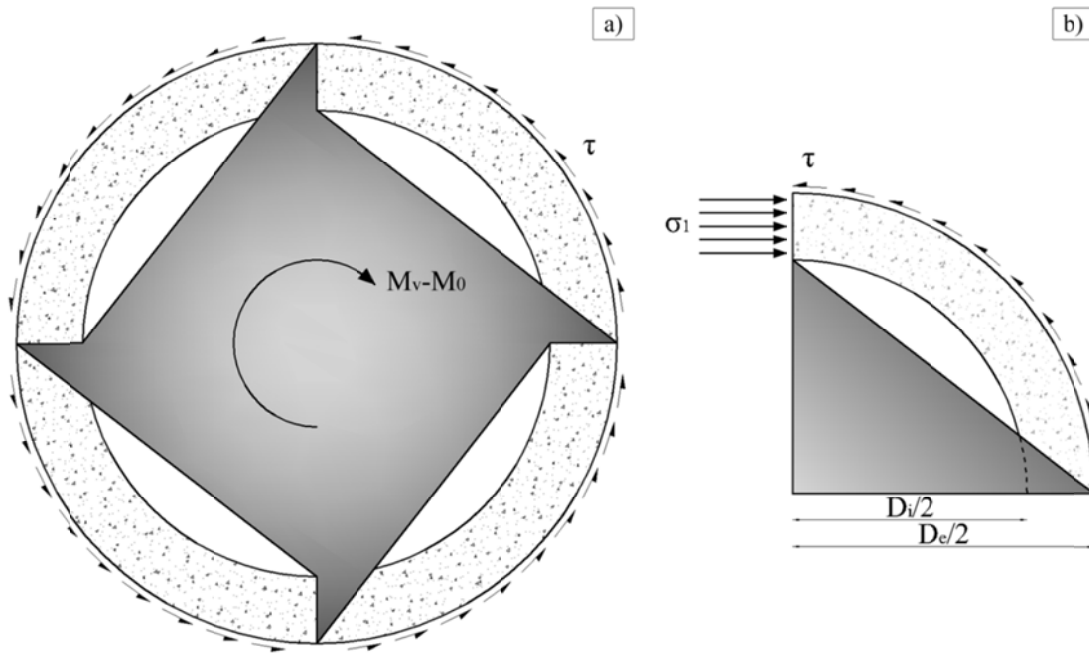
Figure 3.7 Cross-section equilibrium on the hypothetical failure surface of the X-Drill (a) and reference quarter stress distribution (b)

In order to evaluate the magnitude of the constant normal stress σ_1 it is necessary to analyse the rotational equilibrium. The relevant equilibrium condition is defined in Equation 3.2:

$$\sigma_1 = \frac{\pi \cdot D_e^2}{D_e^2 - D_i^2} \cdot \tau \tag{3.2}$$

where D_i is the diameter of the pilot hole.

The radial confinement component σ_2, perpendicular to τ, is calculated with the Hilsdorf's Theory (Hilsdorf 1969) reported in Equation 3.3 considering a plane stress condition, allowing the material to expand in longitudinal direction granted by the pilot hole.

$$\sigma_2 = \frac{v_m - \rho_E \cdot v_s}{1 + \rho_E \cdot \rho_h} \cdot \sigma_1 \tag{3.3}$$

where ρ_E is the Young's modulus ratio calculated as the mortar's modulus E_m divided by the steel one E_s, ρ_h the thickness ratio calculated as the mortar's thickness h_m divided by the steel part dimension, and v_m and v_s are respectively the Poisson's ratio of mortar and steel.

Being the steel Young's modulus more than two order of magnitude than the common mortar one, the radial expansion of the mortar in the contact zone is almost prevented. Analytically this consideration means that the stiffness ratio in Equation 3.3 can be assumed as $\rho_E \rightarrow 0$. Thus, the normal stress in radial direction σ_2 can be estimated approximately as reported in Equation 3.4:

$$\sigma_2 \cong \nu_m \cdot \sigma_1 \tag{3.4}$$

The state of stress defined by Equations 3.1, 3.2, 3.4 must be represented as a Mohr's circle in the σ-τ plane, as shown in Figure 3.8.
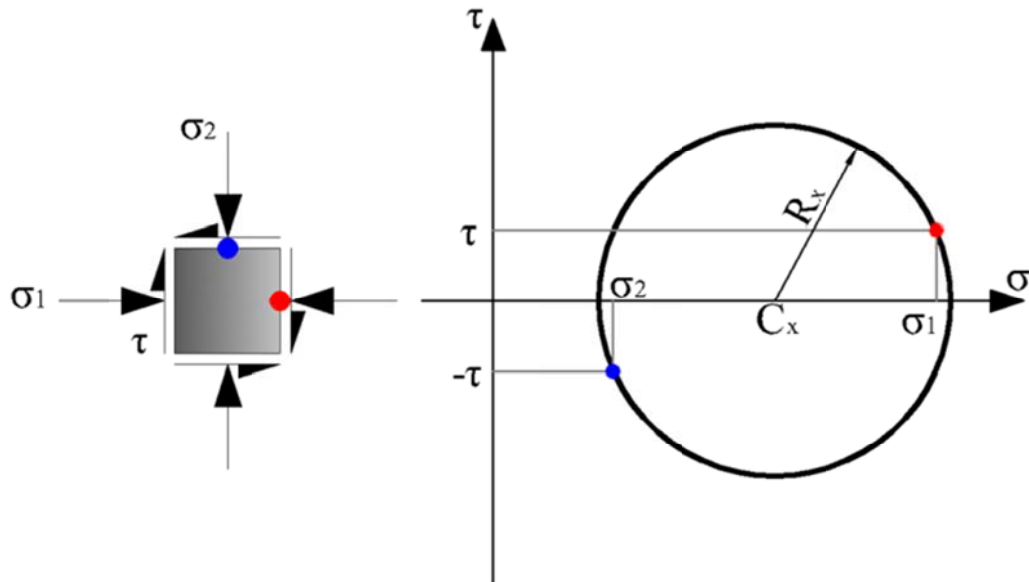
Figure 3.8 Mohr's circle for mortar's state of stress under plane stress condition.

Figure 3.8 shows the construction of the Mohr's circle relative to the assumed state of stress of the mortar. C_x and R_x are respectively the circle's centre and its radius, calculated by Equations 3.5a,b:

$$C_x = \frac{\sigma_1 + \sigma_2}{2}; \quad R_x = \sqrt{\tau^2 + \left(\frac{\sigma_1 - \sigma_2}{2}\right)^2} \tag{3.5a,b}$$

Using simple geometric relations between the aforementioned parameters and the Mohr-Coulomb theory, it is possible to estimate the cohesion c as a function of the friction angle φ, as reported in Equation 3.6:

$$c = \frac{R_x - C_x \cdot \sin(\varphi)}{\cos(\varphi)} \qquad\qquad (3.6)$$

Considering the Mohr-Coulomb criterion the tensile and compressive strengths can be obtained by the Equations 3.7a,b:

$$f_t = \frac{2 \cdot c \cdot \cos(\varphi)}{1 + \sin(\varphi)}; \quad f_c = \frac{2 \cdot c \cdot \cos(\varphi)}{1 - \sin(\varphi)} \qquad\qquad (3.7a,b)$$

where f_t and f_c are respectively the tensile and compressive strength of the mortar.

Brittle materials are characterised by different tension and compression strengths. Previous studies (Benedetti & Pelà 2012; Benedetti et al. 2008) assessed that the ratio between tensile and compressive strengths in historical mortars may be approximately equal to its Poisson's ratio, usually in the range of v_m=0.20÷0.30. Thus, it is possible to obtain an approximated relationship between the Poisson's modulus and the friction angle of the mortar, as reported in Equations 3.8.

$$\varphi = \arcsin\left(\frac{1 - f_t/f_c}{1 + f_t/f_c}\right) \cong \arcsin\left(\frac{1 - v_m}{1 + v_m}\right) \qquad\qquad (3.8)$$

Using standard Poisson's values for the mortar such as v_m=0.25, the resulting friction angle is φ=36.87°, in line with recent studies about the evaluation of Mohr-Coulomb parameters for this kind of material (Marastoni et al. 2016; Pelà et al. 2012; Pelà et al. 2015; Binda et al. 1994).

3.3.   Experimental Campaign

An experimental campaign was carried out to validate the theoretical interpretation of the X-Drill proposed in the previous section. Firstly a large set of standard specimens was designed to ensure a wide range of mortar compressive strength. Secondly, each specimen was tested using the X-Drill and then crushed in standard compression test, in order to define a direct correlation between the two measurements.

3.3.1. Materials

Seven different mixtures of mortar were realized using different proportions of fine river sand, cement, hydraulic lime and water. The components adopted for the mixture are summarized below:

- Moderately Natural Hydraulic Lime NHL 3.5;
- Portland Cement 32.5 R;
- Fine river sand $0 \div 2$ mm.

The proportions between the components were studied according to the Italian Standard (D.M. 14/01/2008 2008), introducing few modifications in order to obtain a sufficient wide range of final compressive strengths. The exact mass quantities for each mixture are reported in Table 3.1.

Table 3.1 Mortar mixtures adopted in the reference campaign

Mixture	Hydraulic Lime [kg]	Cement [kg]	Sand [kg]	Water [kg]	Total [kg]
A1	5.0	0.0	15.0	3.0	23.0
A2	2.0	3.0	16.0	2.5	23.5
A3	4.0	1.1	16.0	3.0	24.1
A4	3.5	2.5	15.0	2.7	23.7
B2	3.4	0.0	18.0	3.0	24.4
B3	1.5	2.5	14.9	2.5	21.4
B4	1.0	1.5	18.0	2.5	23.0

Mixtures "A" were obtained by using a water/binder weight ratio of approximatively $0.5 \div 0.6$, reproducing a standard historical mortar. Mixtures "B" were prepared in order to have a lower strength, so the water/binder ratio was set around 1.0, i.e. reducing the binder quantity.

3.3.2. Preparation of specimens

Three specimens for each mortar mixture were casted, using PVC moulds with nominal dimensions $150 \times 150 \times 150$ mm^3 (Figure 3.9). The samples were stored for 28 days in a climatic chamber (20°C and 98% RH) according to the Italian Standards (D.M. 14/01/2008 2008).

After the curing period, two pilot holes were drilled in the centre of two opposite faces of each specimen. The pilot hole was drilled using a drill press equipped with a 7 mm hardened steel bit, in order to produce an orthogonal perforation as much as possible.

Figure 3.9 shows the specimens after the execution of the holes. The 20 specimens are classified in Table 3.2.

Figure 3.9 Samples after the execution of the pilot holes.

Table 3.2 Mortar specimens' dimensions

Name	a [mm]	b [mm]	c [mm]	Name	a [mm]	b [mm]	c [mm]
A1.1	150	150	149	B2.1	150	150	144
A1.2	150	150	148	B2.2	150	150	145
A1.3	150	150	145	B3.1	150	150	146
A2.1	150	150	150	B3.2	150	150	144
A2.2	150	150	150	B3.3	150	150	115
A2.3	150	150	148	B4.1	150	150	145
A3.1	150	150	148	B4.2	150	150	143
A3.2	150	150	150	B4.3	150	150	148
A3.3	150	150	150				
A4.1	150	150	149				
A4.2	150	150	149				
A4.3	150	150	146				

3.3.3. Test execution

The X-Drill test was performed twice on each sample, i.e. at two opposite faces. The sample was placed on a vertical press under a constant load of 2 kN. Once the sample was blocked, the X-Drill was hammered into the pilot hole until the wings were completely inserted, as shown in Figure 7.

Figure 3.10 Sample ready for the X-Drill test

The torque wrench was then connected to the head of the X-Drill. The test must be performed using caution in twisting the wrench, without giving any transversal force which could spoil the final measurement. Due to the particular shape of the X-Drill, the torque must be applied in the counter-clockwise direction. Table 3.3 reports the results of the X-Drill tests obtained from the two opposite faces of each sample.

Table 3.3 X-Drill tests results

Name	$M_{v,1}$ [Nm]	$M_{v,2}$ [Nm]	Name	$M_{v,1}$ [Nm]	$M_{v,2}$ [Nm]
A1.1	5.0	5.5	B2.1	3.0	2.0
A1.2	5.0	8.0	B2.2	2.0	4.5
A1.3	6.0	4.0	B3.1	12.5	14.0
A2.1	16.5	15.5	B3.2	15.0	14.0
A2.2	20.5	21.0	B3.3	12.0	16.5
A2.3	17.5	20.0	B4.1	6.0	5.0
A3.1	6.5	7.0	B4.2	8.5	7.0
A3.2	6.0	7.0	B4.3	7.5	7.5
A3.3	6.5	7.5			
A4.1	14.5	17.0			
A4.2	17.5	20.0			
A4.3	19.5	17.5			

After the X-Drill tests over the two opposite faces, each specimen was replaced under the vertical press with the damaged faces in contact with the metal plates. The extraction of the X-Drill sometimes pulled out some material, reducing the effective loading area of the compression test. This issue was taken into account by measuring the damaged zone and considering a reduced cross section of the sample in the evaluation of the compressive strength.

The compressive strength obtained from a cubic specimen was reduced to 83% of its original value in order to remove the confinement effect produced by the dimensions ratio, using the Italian Standards for concrete characterisation as reference (D.M. 14/01/2008 2008).

Table 3.4 summarises the effective cross sections of the samples and the results obtained from the compressive test.

Table 3.4 Mortar compression test results

Name	A_n [mm^2]	F_{max} [kN]	f_c [MPa]	Name	A_n [mm^2]	F_{max} [kN]	f_c [MPa]
A1.1	21750	34.3	1.31	B2.1	21000	11.4	0.45
A1.2	21600	37.3	1.43	B2.2	21150	11.7	0.46
A1.3	21150	33.8	1.33	B3.1	21300	138.3	5.39
A2.1	21900	225.6	8.55	B3.2	21000	145.7	5.76
A2.2	21900	229.1	8.68	B3.3	16650	116.7	5.82
A2.3	21600	221.7	8.52	B4.1	21150	46.3	1.82
A3.1	21600	63.3	2.43	B4.2	20850	44.6	1.78
A3.2	21900	63.0	2.39	B4.3	21600	47.1	1.81
A3.3	21900	63.2	2.39				
A4.1	21750	194.2	7.41				
A4.2	21750	201.1	7.67				
A4.3	21300	183.9	7.17				

3.4.   Experimental Calibration of the Instrument

Figure 3.11 shows the relationship between the normalised ultimate torque mv and the experimental compressive strength f_c. The normalised torque is obtained by dividing the torque M_v by the depth L_w of the X-Drill. The values of m_v reported in the figure are the averages between the two normalised torques measured at the opposite faces of each sample. The linear regression of the experimental dataset provides the following empirical equation:

$$f_c = \chi_{exp} \cdot (m_v - m_{0,exp})$$
(3.9)

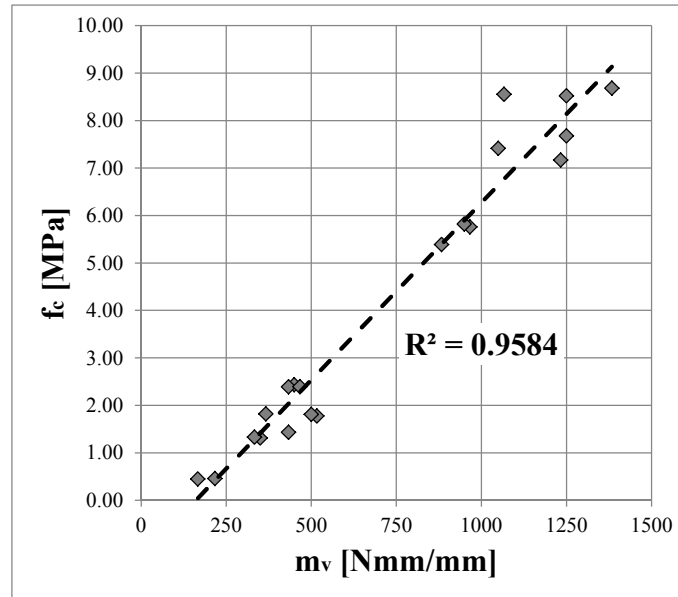with a coefficient of determination of R^2=0.958.

Figure 3.11 Experimental data correlation and linear regression line.

The experimental empirical Equation 3.9 is compared in the following with the interpretation model proposed in Section 3.2. After substituting Equations 3.1-3.6 and Equation 3.8 into Equation 3.7b, the following analytical equation expresses the relationship between f_c and (m_v - m_0):

$$f_c = \chi \cdot (m_v - m_0) \qquad\qquad (3.10)$$

where χ is a correlation factor that is a parameter depending on the mortar's Poisson's modulus v_m and the geometric properties of the X-Drill.

Figure 3.11 indicates a value m_0=161 Nmm/mm. However, the lowest normalised torque measured during the experimental tests was m_v=133 Nmm/mm. This result suggests that the effective value of m_0 is actually smaller than those obtained by the linear regression of experimental results. For this reason, a value of m_0=100 Nmm/mm was considered in the calculations with the analytical prediction model.

The correlation factor χ depends on the assumption of a realistic value for the Poisson's modulus. A sensitivity analysis was carried out to evaluate its influence on the correlation factor. Considering a realistic range of Poisson's modulus of v_m=0.20÷0.30, the χ coefficient assumes values from χ=0.0072 mm^{-2} to χ=0.0059 mm^{-2}, showing a rather low sensitivity. Furthermore, the range of the coefficients of determination in a

range between v_m=0.20÷0.25 is R^2=0.908÷0.940, i.e. very close to that of the linear regression, confirming a good predictive capacity of the model proposed.

Figure 3.12 shows the graphical comparison between the experimental regression line and the interpretation model. For v_m=0.20 (Figure 3.12a) the proposed model gets closer to the experimental regression line for mortars with higher compressive strength. In case of mortars with lower compressive strength, the proposed model slightly overestimates the experimental results. Higher values of the assumed Poisson's ratio (Figure 3.12b,c) provide better agreement for mortars with lower compressive strength, maintaining a conservative prediction for higher ones.
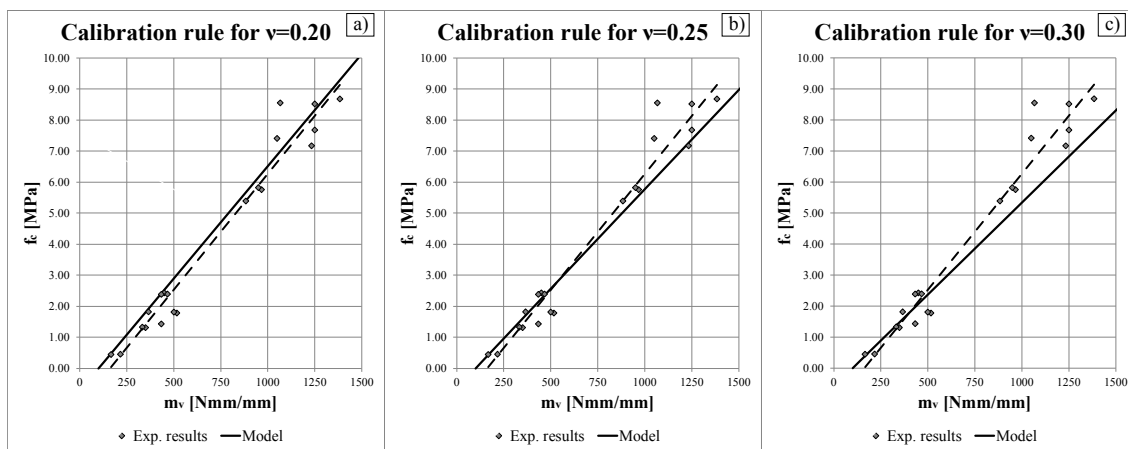

Figure 3.12 Comparison between experimental regression line and the proposed interpretation model depending on the Poisson's modulus: $v_m = 0.20$ (a), $v_m = 0.25$ (b) and $v_m = 0.30$ (c).

It is important to remark that using the assumptions on which it is based the theoretical interpretative model (Section 3.2), the stress level induced in the mortar is very high. Since the test is designed to be performed on existing masonry, the influence of the ordinary loading conditions of the structure can be easily neglected in the interpretation of the X-Drill test results.

As a further confirm of this hypothesis, the first work presented on this instrument (Christiansen 2011) reported also tests performed on the same material at different vertical stress levels. The comparison carried out by Christiansen confirmed that the vertical stress does not influence the X-Drill test results.

Chapter 4. Integrated Laboratory Methodology for Minor Destructive Testing

As for the experimental characterisation of the material components (mortar and units), the current codes only consider tests made on standard specimens, like whole units (EN 1996-1-1:2005 2005; EN 772-1:2011 2011) or prismatic specimens of mortar (EN 772-1:2011 2011) that are mainly intended for new structures.

Concerning the shear behaviour of masonry, the available standards considers only tests performed on specific setups, using two or three units superposed and joined by mortar layers (EN 1052-3:2002 2002). The test is carried out by pre-compressing the specimen orthogonally respect to the mortar layer and exerting a shear state of stress on the mortar by loading one unit while the others are blocked (Figure 4.1a). The bed joints are then subject to a composite state of compression and shear. By varying the magnitude of the pre-compression is possible to determine the failure envelope of the tested samples. The reference standard (EN 1052-3:2002 2002) is based on the Mohr-Coulomb theory to define the failure criterion (Figure 4.1b)., i.e. a two-parameter linear failure envelope.
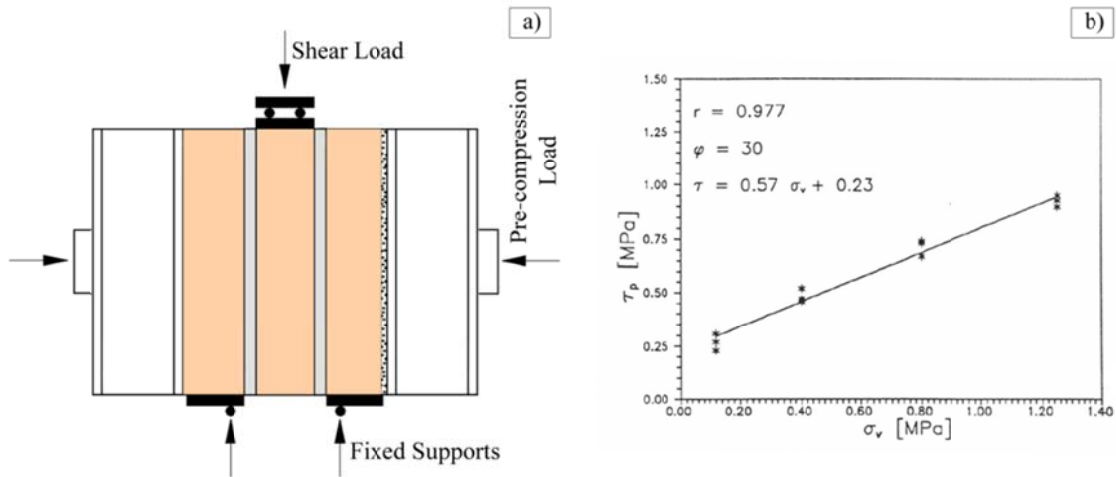
Figure 4.1 Shear test on triplets (EN 1052-3:2002 2002): experimental setup (a) and interpretation of the results (Binda et al. 1994) (b).

Several studies were carried out on the shear test (Binda et al. 1994; Montazerolghaem & Jaeger 2014), using also different setups (Pluijm 1993). This test seems very adequate for the characterisation of masonry, but it is hardly applicable to existing structures since it is almost impossible to extract such samples without damaging the wall. In case of existing masonry structures, it is usually preferable to perform different kinds of tests on extracted specimens. A useful technique to obtain representative specimens from an existing panel is the core drilling (Figure 4.2). Cylindrical samples with variable diameters can be extracted by using different sizes of the core bits.

Figure 4.2 Core drilling during an in-situ experimental campaign

This methodology is appropriate for historical constructions, since samples can be extracted from hidden structural members reducing to the minimum the amount of induced damage.

Recent studies have shown the possibility of core drilling perpendicular to the face of the structural member to extract masonry cylindrical samples to be tested in the laboratory (Pelà et al. 2012; Benedetti & Pelà 2012; Mazzotti et al. 2014; Marastoni et al. 2016). The cores included two circular segments of brick and a diametral mortar joint, with a total diameter of the sample from 70 to 110 mm. In case of the Brazilian tests with 45º inclined joint cores they assumed that the load split into normal and tangential components on the mortar joint. This led to the hypothesis of an infinitesimal thickness of the mortar joint, reducing it to a non-dimensional interface between the bricks.

On the other hand, Benedetti and co-workers (Benedetti et al. 2008) proposed an alternative interpretation of the stress state inside the diametral mortar joint of the cylindrical specimen, by considering the whole mortar layer, instead of reducing it to an interface. In this case, it was possible to introduce into the mechanical interpretation of the test also the mutual interaction between the two circular segments of brick and the mortar in the joint. Such interaction induces a three-dimensional state of stress to the mortar. The graphical interpretation of each test requires the drawing of Mohr's circles representing the complete stress state in the mortar at failure. Most recent experimental studies by the same authors (Pelà et al. 2015; Pelà et al. 2012; Benedetti & Pelà 2012) showed the possibility of carrying out different Brazilian tests by varying the inclination of the diametral mortar joint. In this way, different shear-compression states can be applied to the mortar, corresponding to different Mohr's circles on the Mohr's plane. The Mohr's circles related to the Brazilian tests were complemented with those corresponding to compression tests on the mortar, e.g. using the Double Punch Test (DPT). Finally, all the Mohr's circles representing mortar at failure under different stress conditions were used to derive the Mohr's failure envelope by means of a least square method.

This section presents an experimental program that was intended to reproduce in the laboratory the MDT techniques of in-situ sampling and subsequent laboratory testing of small specimens extracted from historical masonry structural members. At the same time, several specimens were prepared following the relevant standards for the mechanical characterisation (EN 772-1:2011 2011; EN 1052-3:2002 2002; EN 1015-

11:2007 2007) in order to compare the non-standard results with reliable values. Proper material components were chosen in order to reproduce those typically employed in historical masonry with low mechanical properties, i.e. handmade clay bricks and lime mortar. The manufacturing and curing of lime mortar were carefully executed using traditional building techniques in controlled laboratory conditions. Each material component was tested in order to obtain a comprehensive characterisation of its mechanical behaviour. Then, the selected materials were used to build two masonry walls. After the necessary period of curing and hardening to reach a sufficient strength of the material, the extraction of cylindrical samples was carried out by core drilling. A novel dry extraction procedure was adopted, based on an air cooling system, in contrast to common wet core drilling in which water could spoil the lime mortar joints in the samples. Brazilian tests were carried out on 90 mm diameter masonry cores by varying the inclination of the diametral mortar joint with respect to its original horizontal position. DPTs were also executed on mortar joints extracted from the same walls. A comprehensive micromechanical interpretation of the different experimental tests is presented. Finally, an integrated methodology is proposed to obtain a full characterisation of the mechanical properties of mortar, considering the redundant results derived from all the different types of experimental tests executed. The experimental procedures adopted, as well as the theory proposed for the interpretation of the tests, can be considered during the inspection activities on historical masonry structures to evaluate the mechanical properties of the existing mortar.

4.1.   Experimental Campaign

The experimental investigation was carried out at the Laboratory of Technology of Structures and Materials of the Technical University of Catalonia (UPC-BarcelonaTech). In the following, each stage of the experimental program is discussed in detail, paying attention to important issues like the preparation of material samples, the curing conditions, the procedures of extraction and testing.

4.1.1. Materials

Handmade fired-clay solid bricks were used in this experimental program, with nominal dimensions of $305 \times 145 \times 45$ mm^3. The units presented some voids and imperfections, due to their hand-moulded nature.

Cement mortars were used starting from the 20th century and could not be used to represent the behaviour of historical masonry. Lime-cement mortars are often adopted in laboratory experimental programs in order to reduce the curing times compared to a pure-lime mortar, but they usually provide higher strengths that those normally found in historical masonry structures. In this work, a hydraulic lime mortar was employed to obtain a closer representation of an historical material, despite the longer time necessary for its hardening.

The mortar was mixed starting from the raw components. The river sand had $0 \div 2$ mm grain size. The full description of the granulometry is reported in Figure 4.. Natural hydraulic lime (NHL), classified as NHL 3.5 by EN 459-1 (EN 459-1:2010 2010), was utilized. The volume ratio of binder to aggregate was 1:3, a rather typical mix in historical masonry (D.M. 14/01/2008 2008; Circolare 02/02/2009 n. 617 2009).

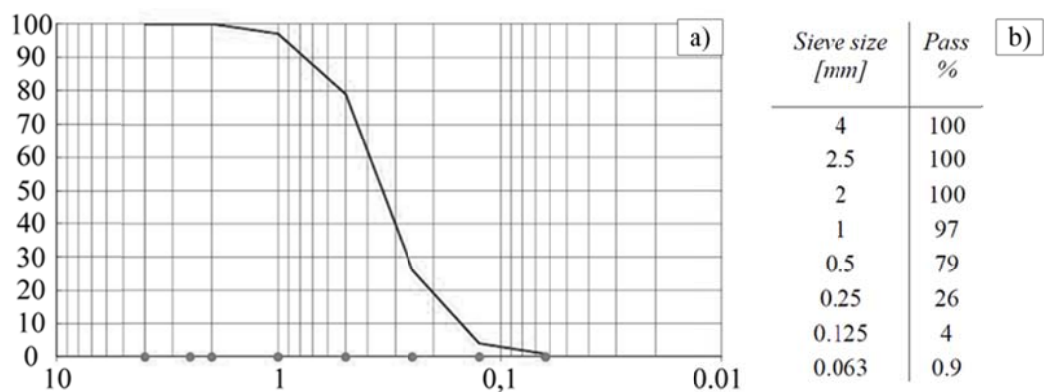| Sieve size [mm]	Pass %
4	100
2.5	100
2	100
1	97
0.5	79
0.25	26
0.125	4
0.063	0.9

Figure 4.3 Sand grain sizes: cumulative curve (a) and granulometry (b).

Once the mortar was prepared, two single-leaf walls were built in stretcher bond with final dimensions $1.6 \times 0.8 \times 0.145$ m^3. The external thickness of the joints was variable from 15 to 20 mm, due to the imperfect faces of the handmade bricks. The wall was built over a steel beam to ease its displacement during the following stages of the experimental campaign. The walls were stored in the laboratory for 60 days, allowing the mortar to harden until reaching a sufficient strength to represent the behaviour of an existing low-strength mortar historical masonry wall.

Standard specimens were prepared during the wall construction in order to obtain a complete mechanical characterisation of the materials used. Concerning bricks, whole units were rectified on the larger faces to be tested in compression (EN 772-1:2011 2011), prismatic specimens were cut from the units to perform flexural and compressive tests (EN 1015-11:2007 2007) and small cylinders were cored from the stretcher face to evaluate Young's modulus (EN 12390-13:2013 2013). On the other hand, mortar specimens were prepared to perform both flexural and compressive strength (EN 1015-11:2007 2007). Finally, nine triplets were prepared to perform shear tests according to the relative standard EN 1052-3:2002 (EN 1052-3:2002 2002).

4.1.2. *Standard Mechanical Characterisation of Materials*

Due to the lack of a specific standard for the evaluation of the tensile strength of bricks, the EN 1015-11:2007 standard for mortars (EN 1015-11:2007 2007) was used as a reference. Eight $40 \times 40 \times 160$ mm^3 prisms were cut (Figure 4.4a) and tested according to a three-point bending setup. Cubic specimens of about $35 \times 35 \times 35$ mm^3 were cut from the bricks and tested (Figure 4.4b). The experimental results of flexural these tests are summarized in Table 4.1.

Since there are no available standards for the laboratory evaluation of the Young's modulus of the brick, the EN 12390-13:2013 (EN 12390-13:2013 2013) for concrete samples was considered as a reference. Cylinders were cored from the header face of the brick with a diameter of 35 mm and length of 75 mm (Figure 4.4d). The upper and lower faces were rectified to make them parallel and then the samples were tested using extensometers to measure the vertical deformation of the central third. After three cycles from 10% to 30% of the failure load, the Young's modulus was determined, as shown in Table 4.1.

Table 4.1 Experimental results for brick specimens.

Flexural strength of brick prismatic specimens		Compressive strength of brick cubic specimens		Young's modulus of cylindrical brick samples	
Sample	f_{fb} [MPa]	Sample	f_{cb} [MPa]	Sample	$E_{10-30\%}$ [MPa]
T1X2	3.81	T1Z1	19.60	Cn2tc	7572
T1X3	3.67	T1Z2	19.50	Cn2'tc	11470
T2X1	3.60	T1Z3	19.10	Cn2"tc3	10335
T2X2	3.52	T2Z1	18.30		
T2X3	3.51	T2Z2	16.60		
T3X1	3.59	T3Z1	17.50		
T3X2	3.88				
T3X3	3.48				
Average	*3.63*	*Average*	*18.40*	*Average*	*9792*
CV	*4%*	*CV*	*6%*	*CV*	*20%*
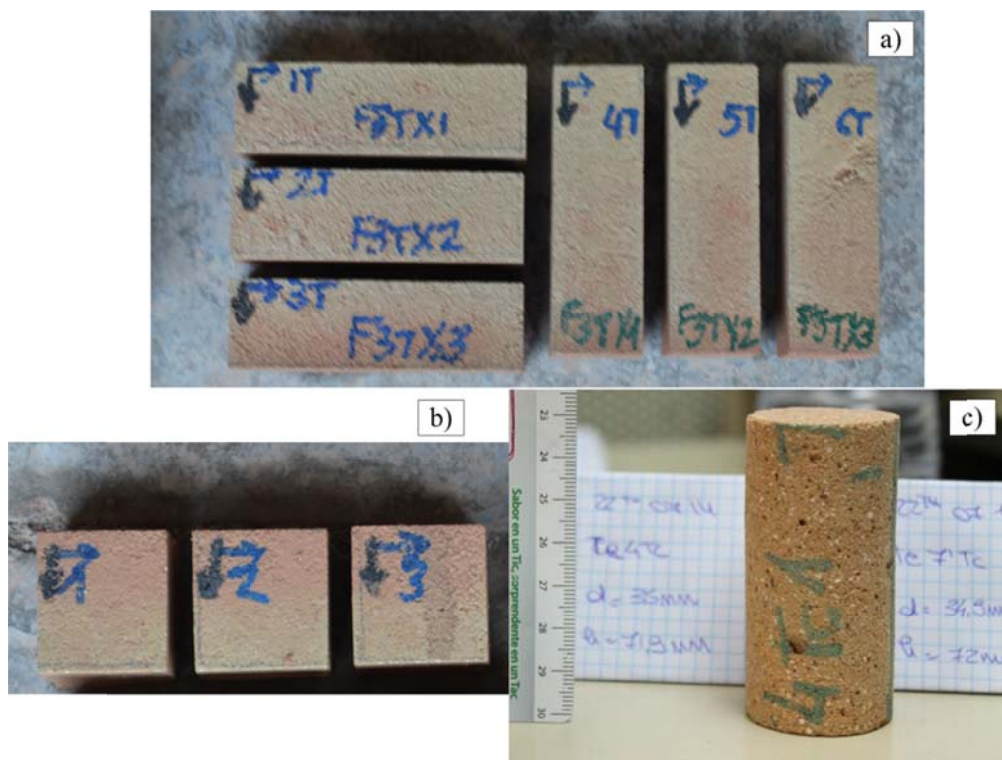
Figure 4.4 Brick specimens: prisms for three-point bending test (a), cubes for compression test (b) and cylindrical sample for Young's modulus evaluation (c).

Similar tests were performed on mortar specimens prepared in metal moulds at the same time of the construction of the walls. Three $40 \times 40 \times 160$ mm^3 prisms (Figure 4.5a) were tested after 270 days after their construction to determine the flexural tensile strength $f_{tm,f}$ according to EN 1015-11:2007 (EN 1015-11:2007 2007). The compression

tests were conducted on the six fragments produced by the flexural tests, following again the EN 1015-11:2007 (EN 1015-11:2007 2007) (Figure 4.5b). The six remaining pieces measured roughly $40 \times 40 \times 80$ mm^3 and were loaded with steel loading platens of 40×40 mm^2. The results are shown in Table 4.2.

Table 4.2 Experimental results for mortar specimens.

Flexure strength of mortar specimens		Compressive strength of mortar specimens	
Sample	$f_{tm,f}$ [MPa]	Sample	f_{cm} [MPa]
NHL_1_F	0.40	NHL_1A_C	2.40
NHL_2_F	0.35	NHL_1B_C	2.50
NHL_3_F	0.36	NHL_2A_C	2.40
		NHL_2B_C	2.14
		NHL_3A_C	2.69
		NHL_3B_C	2.59
Average	*0.37*	*Average*	*2.45*
CV	*7%*	*CV*	*8%*
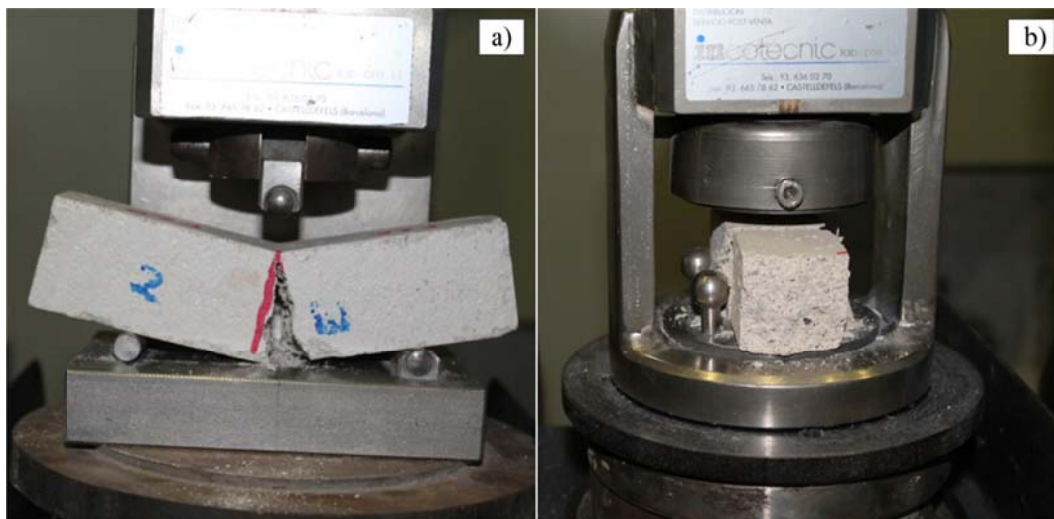
Figure 4.5 Three-point bending test (a) and compression test (b) on mortar prisms.

In order to characterise the shear behaviour of masonry, nine $145 \times 160 \times 305$ mm^3 triplet specimens were built according to the EN 1052-3:2002 (EN 1052-3:2002 2002). The thickness of the mortar layers was variable from 10 to 15 mm due to the imperfections of the units' surfaces. Figure 4.6 shows the experimental setup for the shear test.
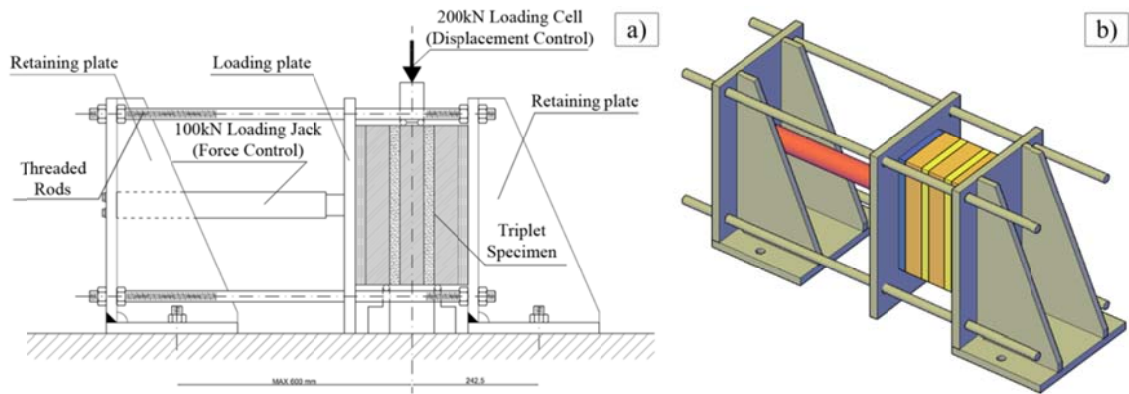
Figure 4.6 Experimental setup for triplet tests carried out in this research (a) and 3D sketch (b).

The tests were carried out following the aforementioned standard (EN 1052-3:2002 2002) placing each specimen on two cylindrical supports (see Figure 4.7a). In this way, the sample is laid vertically, allowing the central unit to move in the vertical direction. The shear force was given by a compression machine equipped with a 200 kN loading cell using a vertical displacement control (7 μm/s). The acquisition rate was set as 10 Hz. To correct the imperfections of the loading surface, a spherical hinge was placed just below the loading jack (see Figure 4.7b).
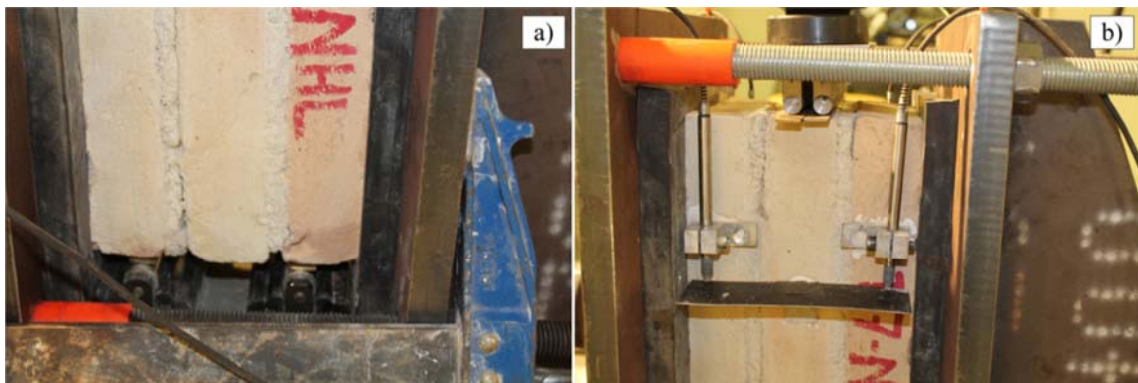
Figure 4.7 Base supports (a) and loading support for triplet specimen (b).

The external plates work as retaining elements fixed to the base of the vertical press. These plates are stiffened by transversal ribs in order to avoid their deformation during the test (see Figure 4.6b). The pre-compression load is given by a 100 kN jack acting on the central plate. This pre-compression loading stage was carried out progressively under force control, using an hydraulic system. The total time employed to reach the desired pre-compression level was 5 minutes. The retaining plates are connected each

other with threaded rods in order to prevent any relative movement of the plates during
the pre-compression stage.

The measurement of the relative displacement of the bricks was carried out by means of
four LVDTs, two on both faces, pasted on the external bricks. The LVDTs were
pointing on a rigid bar connected to the central unit. The instrumentation setup is shown
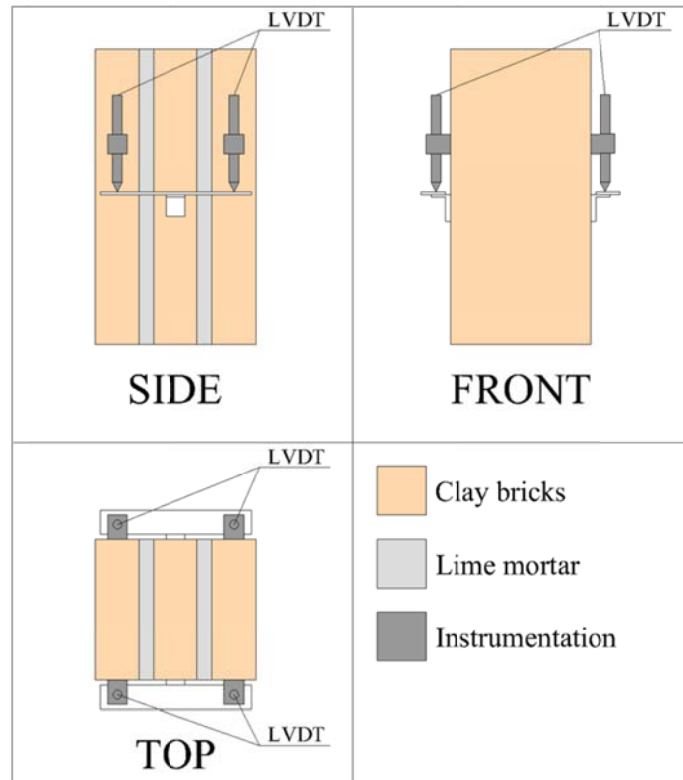in Figure 4.8.

Figure 4.8 Instrumentation setup for triplet tests.

The setup used allowed recording all the stages of the test, consisting of an initial elastic
branch (almost linear), a post-peak degradation due to the formation and propagation of
internal cracks in the mortar layer and an almost constant stage related to a pure sliding
phase on the broken mortar-brick interface. Figure 4.9 reports the experimental curves
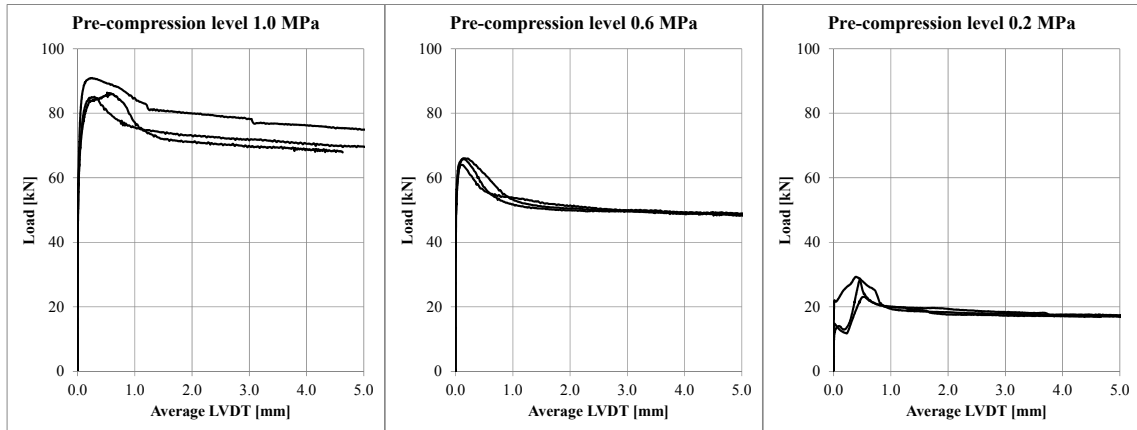obtained by the average measurement of the LVDTs.

Figure 4.9 Triplets tests: load vs. average LVDTs displacement for each step of pre-compression.

The tests were carried out at three pre-compression levels of 0.2 MPa, 0.6 MPa and 1.0 MPa, in agreement with the reference standard (EN 1052-3:2002 2002). The reference standard provides also the methodology for the estimation of the stress distribution over the mortar joint, considering a constant value of normal and tangential stresses as reported in Equations 4.1a,b.

$$\sigma_{max} = \frac{F_H}{A}; \quad \tau_{max} = \frac{F_{max}}{2 \cdot A} \tag{4.1a,b}$$

where F_H is the constant force applied as pre-compression for the joint, A is the area of the mid-section of the mortar joint and F_{max} is the maximum force at failure applied parallel to the joints.

The experimental results derived from the investigated nine specimens are reported in Table 4.3.

Table 4.3 Experimental results of triplet shear tests.

Sample	σ_{max} [MPa]	τ_{max} [MPa]
T1-NHL	0.99	0.98
T10-NHL	0.99	0.96
T13-NHL	0.99	1.03
T3-NHL	0.59	0.75
T7-NHL	0.59	0.72
T12-NHL	0.59	0.75
T2-NHL	0.20	0.33
T5-NHL	0.20	0.26
T11-NHL	0.20	0.33
Average 1.0	*0.99*	*0.99*
CV	*-*	*3%*
Average 0.6	*0.59*	*0.74*
CV	*-*	*2%*
Average 0.2	*0.20*	*0.31*
CV	*-*	*13%*

4.1.3. Extraction of Specimens

The experimental program was carried out in order to reproduce in the laboratory the in-situ sampling and subsequent testing of small specimens extracted from an existing masonry element.

The common specimens which can be extracted are cylindrical specimens and mortar layers for DPT. The mortar specimens can be obtained by extracting a cylindrical specimen including a mortar joint as shown in Figure 4.10a. After having detached carefully the bricks from the mortar (Figure 4.10b), the layers can be cut to be subject to DPT (Henzel & Karl 1987) (see Figure 4.10c).
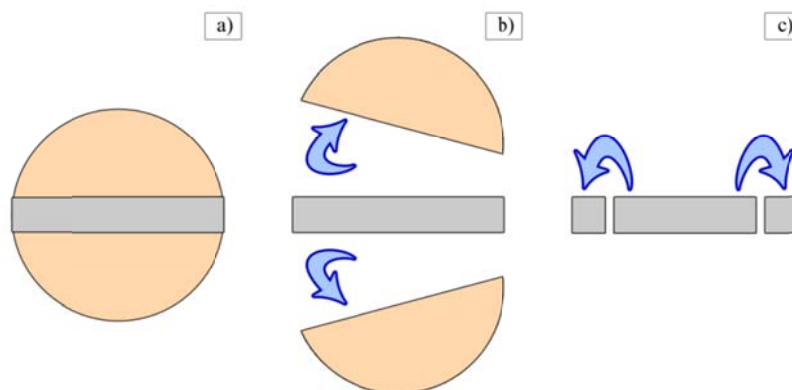

Figure 4.10 Cylindrical specimen extracted (a), removal of the brick parts (b) and cut of the mortar specimens according to (Henzel & Karl 1987) (c).

In this research, the procedure of extracting the mortar layers was slightly different from the aforementioned approach, since the specimens were obtained by dismantling the wall after the core drilling operations.

The extraction of cylindrical specimens from the two walls was carried out 60 days after their construction. The walls were maintained in vertical position during the coring operations (Figure 4.11a). During the movements, a proper confinement was ensured by two horizontal steel profiles, placed below the base and the over the upper edge and connected by four rods tensioned by a small force (Figure 4.11b).

Horizontal core drilling was executed perpendicularly to the face of the walls (Figure 4.11b). A novel procedure was followed in order to avoid spoiling the samples during their extraction. Common core drills, normally adopted for concrete structures, use a water cooling system. This well-known system showed its limitations in previous experimental programs, since water could wash lime mortar joints away (Pelà et al. 2015). In addition, the use of water can be inconvenient in case of sampling activities from the inside of existing historical buildings. For this reason, this research proposes a novel dry extraction procedure, in which air cooling is adopted instead of water cooling, in order to preserve the integrity of the mortar joints. Air cooling is ensured by an aspirator connected to the coring bit. However, during the masonry core drill, the dust might block the sample inside the bit. In fact, the bit usually overheats during drilling, allowing the dust to interpose between itself and the sample. As soon as the core drill stops working and the bit gets colder, its sudden contraction might block the specimen inside. The aspirator continuously removes the dust inside the bit and cools down the system, but sometimes its effect is not sufficient. Therefore, in this study, the masonry was core drilled step by step, making sure that at each small step the dust was removed completely either by the aspirator or by a spray compressor. By using this procedure, a total of 22 intact cores were extracted for this experimental program. In addition, other 30 larger diameter cores were extracted from the walls, without any operational problem, and they were utilized for a different research study.
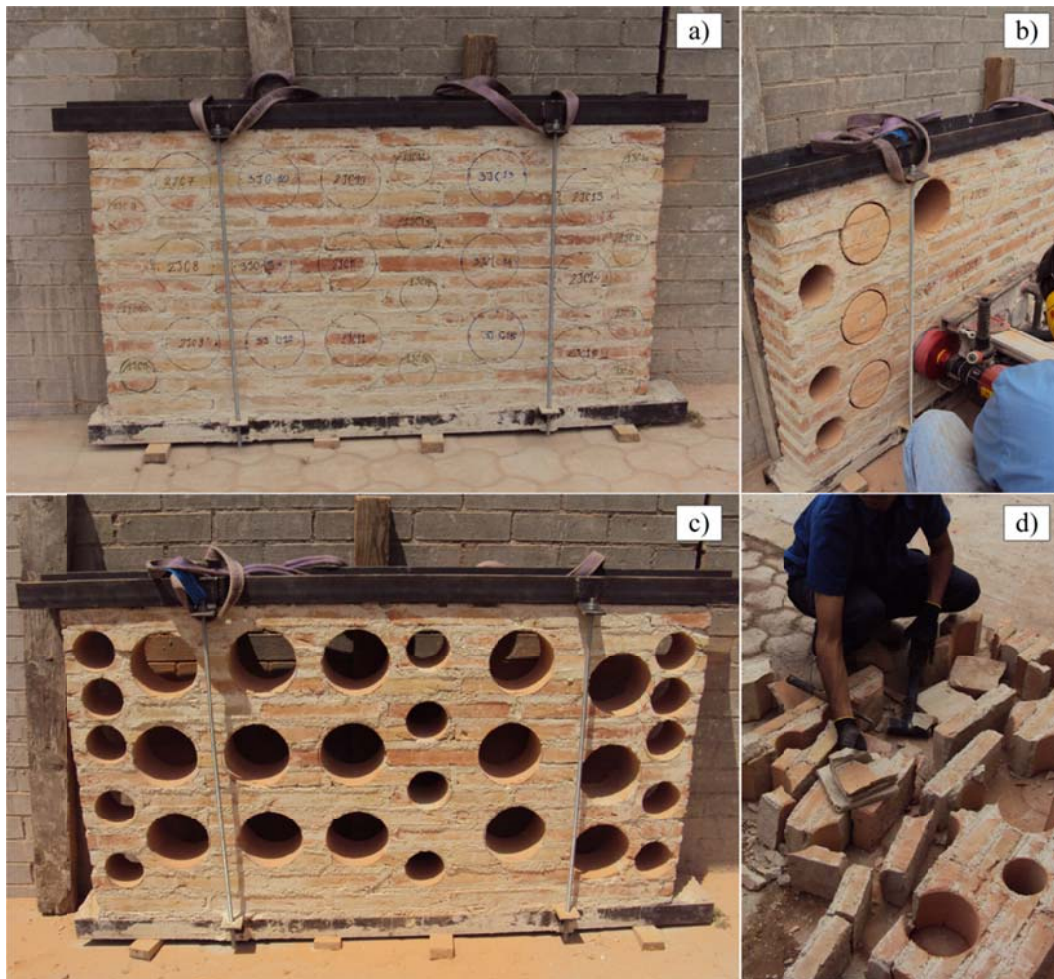
Figure 4.11 Masonry walls before (a), during (b) and after coring (c) and demolition of the wall to retrieve mortar specimens (d).

After the extraction of the core samples, the remains of the two walls shown in Figure 4.11c were dismantled to extract mortar layers. The mortar layers were carefully detached from the bricks using a thin chisel, in order to obtain small mortar samples for the double punch tests (see Figure 4.11d). Every mortar sample was cut to obtain square-shaped specimens, with a side of about 50 mm and variable thickness between 10-20 mm. The thickness of each sample depended on the thickness of the original mortar joint in the wall.

4.2.   Experimental Testing of the Specimens Extracted

This section presents the results from the testing procedures used for the mechanical characterisation of the mortar in the walls. In order to simulate the procedures to be followed during an in-situ experimental campaign, Brazilian Test (BT) of masonry

cores with inclined diametral mortar joint and Double Punch Test (DPT) of mortar layers were performed.

4.2.1. Brazilian Tests on Cores with Inclined Diametral Mortar Joint

The samples that were core drilled from the walls were subject to BTs (Pelà et al. 2015; Pelà et al. 2012; Benedetti & Pelà 2012) after 210 days from the extraction. In this experimental program the specimens were tested with the diametral mortar joint inclined at 45°, 50°, 55° and 60° with respect to the original horizontal direction. A wooden strip was interposed between the metallic plates and the sample in order to distribute uniformly the loading over the irregular lateral surface of the core. All the tests were performed with a high precision compression machine, using a displacement controlled 200 kN load cell. The setup of the test was studied to avoid the separation of the specimen after the failure by placing two soft horizontal supports avoiding in any case spurious confinement effects. The test was conducted under vertical displacement control at a 4 μm/s rate. The relative sliding displacement between the two bricks was measured with high precision LVDTs (range ±1.5 mm, precision ±1.5 μm) at both circular faces (Figure 4.12a and Figure 4.12b). The acquisition frequency was set at 50 Hz due to the high fragility of the failure process.
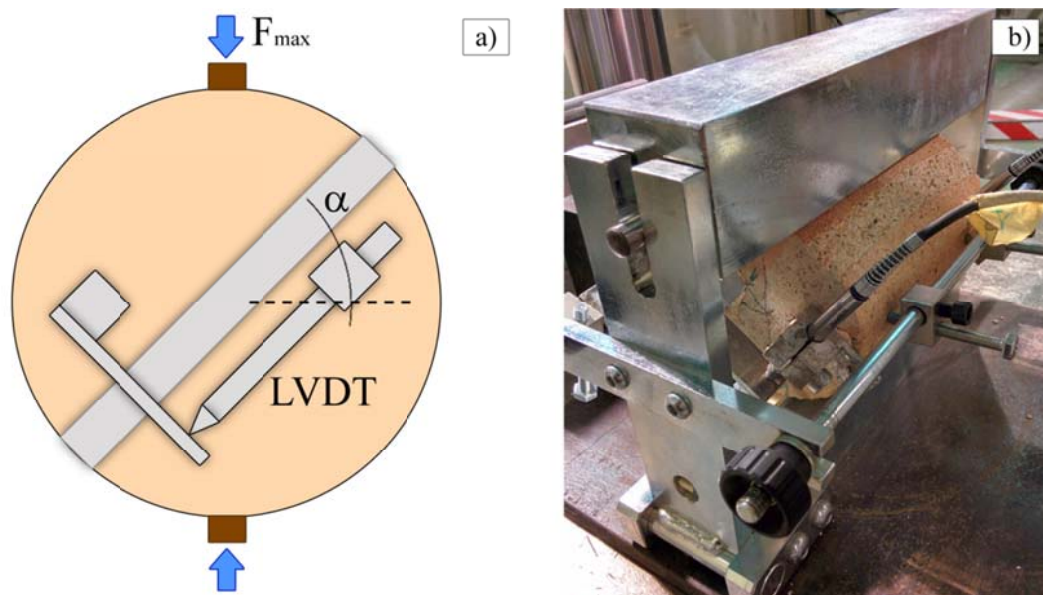

Figure 4.12 Brazilian test on cores with inclined mortar joint: experimental setup (a) and specimen during the test (b).

The diametral mortar layer included between two circular segments of brick is subject to normal compression and tangential shear due to the vertical loading applied during the test. The 14 samples showing the best geometrical regularity after core-drilling were selected for BTs. In most of the specimens analysed in this experimental program, the failure was characterised by a fracture crossing the mortar joint in the centre of the specimen and also interesting the upper and lower unit-mortar interfaces at the extremities (Figure 2.12a). Such kind of failure was called "parasymmetric" or "central symmetric" in a previous study by the authors (Pelà et al. 2015). The observed parasymmetric failures resulted in remarkable agreement with those observed in previous studies on low-strength mortar masonry (Pelà et al. 2015; Pelà et al. 2012; Benedetti & Pelà 2012; Braga et al. 1992; Filardi et al. 1996). The crack sometimes appeared also in the bricks, involving a small wedge under the loading area. Figure 4.13 reports a summary of the crack patterns obtained in all the specimens.
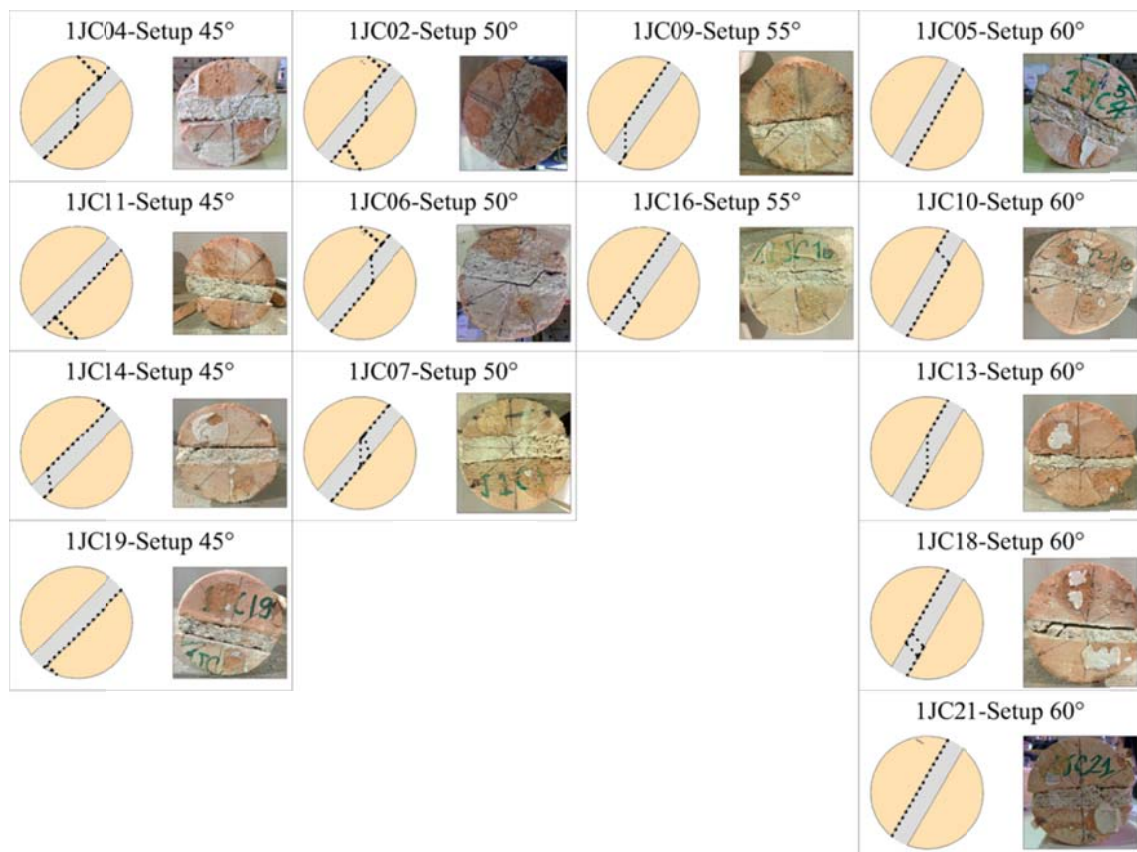
Figure 4.13 Brazilian tests on cores with inclined mortar joint: types of failure in all the core samples.

Figure 4.14 shows the experimental load vs. joint displacement curves obtained from all the BTs. The displacement controlled tests provide more relevant information than the

force controlled ones. Consequently, it was possible to obtain the post-peak softening branch describing the nonlinear behaviour of the material. However, the execution of a displacement controlled BT is a complex task due to the remarkable brittleness of mortar material. Due to the fragile behaviour of the experimental response, it was impossible to record continuously the post-peak phase in all the investigated samples.
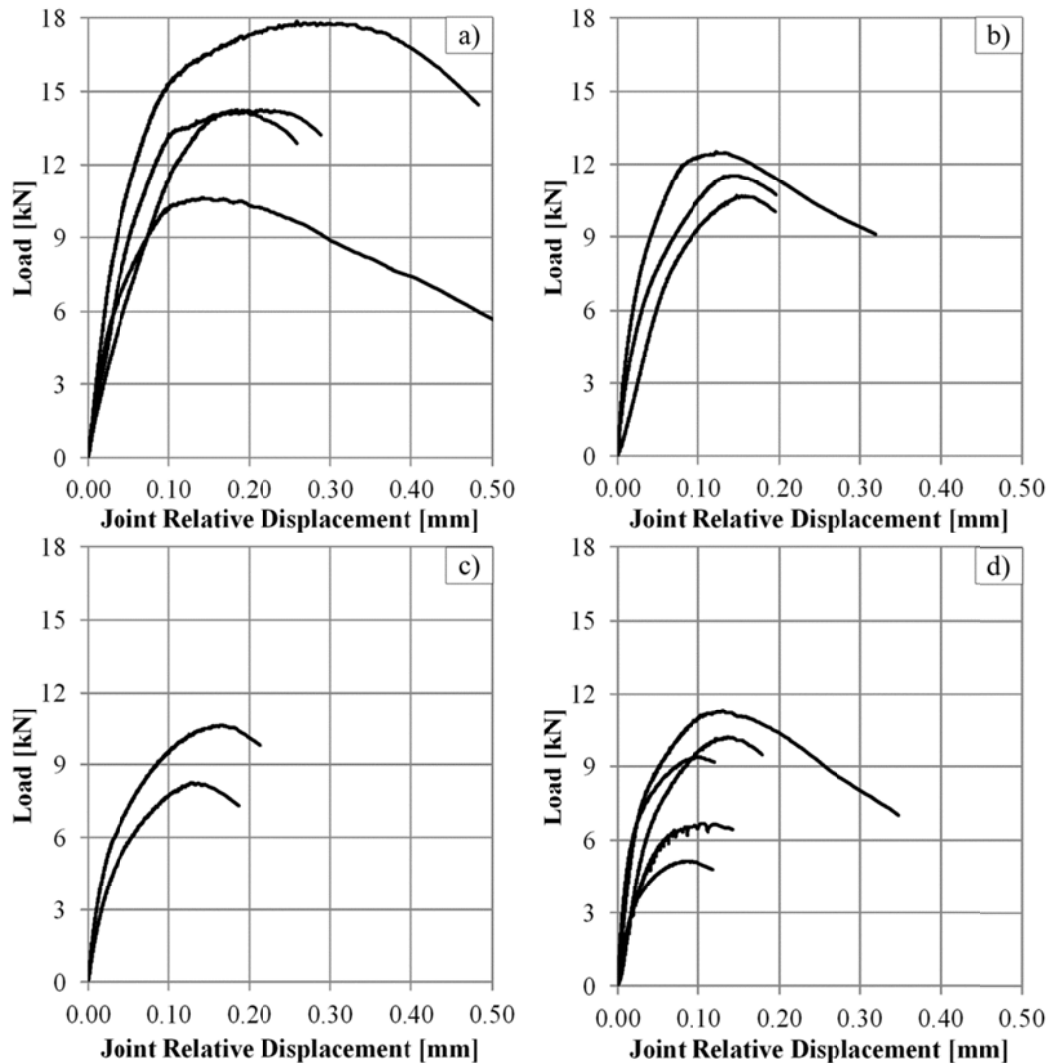

Figure 4.14 Brazilian tests on cores with inclined mortar joint: load vs. joint displacement curves for α=45° (a), 50° (b), 55° (c), 60° (d).

The stress state in the mortar joint at failure of the sample, according to Refs. (Benedetti & Pelà 2012; Pelà et al. 2012; Pelà et al. 2015; Marastoni et al. 2016), can be evaluated by means of Equations 4.2a,b:

$$\sigma_{max} = \frac{F_{max}}{A} \cdot \cos(\alpha) \; ; \quad \tau_{max} = \frac{F_{max}}{A} \cdot \sin(\alpha) \qquad\qquad (4.2a,b)$$

where σ_{max} is the normal compression in the joint, τ_{max} is the tangential shear stress in the joint, F_{max} is the maximum experimental load, A is the area of the mean section of the mortar joint (i.e. product between the diameter and length of the core sample) and α is the angle of inclination of the mortar joint with respect to the horizontal direction (Figure 4.15).
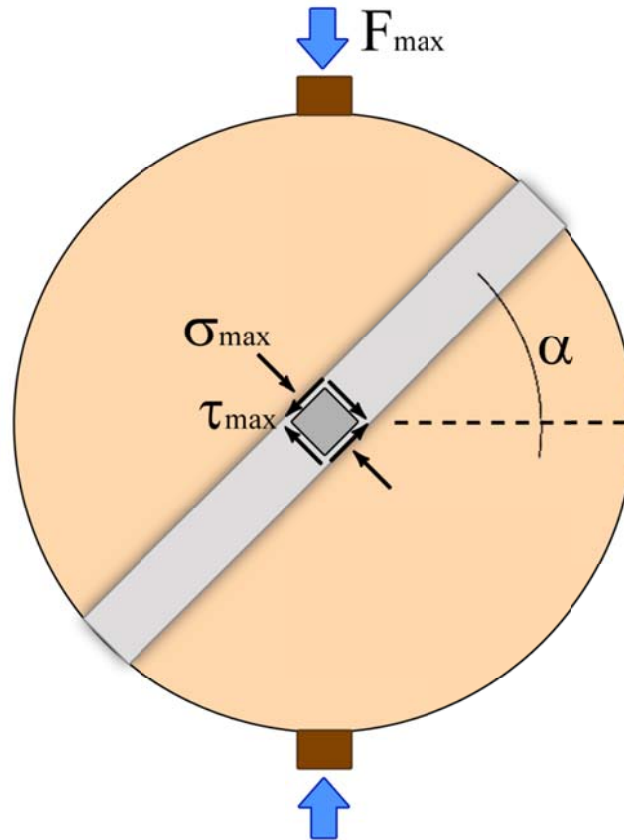

Figure 4.15 Brazilian tests on cores with inclined mortar joint: state of stress at failure.

Table 4.4 presents the summary of the experimental values at failure that were obtained from all the BTs for different inclinations of the diametral mortar joint. The average values of the failure loads show a descending trend with the increase of the angle α, in accordance with previous studies (Pelà et al. 2015; Pelà et al. 2012). For instance, the average failure load decreases from 14.23 kN for α=45° to 8.54 kN for α=60°. This is due to the increasing ratio between the tangential shear and normal stresses acting on the mortar joint as α increases.

Table 4.4 Experimental results of Brazilian tests on masonry cores with inclined mortar joint.

Sample	α [°]	F_{max} [kN]	σ_{max} [MPa]	τ_{max} [MPa]
1JC04	45	10.62	0.56	0.56
1JC11	45	14.19	0.76	0.76
1JC14	45	17.87	0.95	0.95
1JC19	45	14.26	0.76	0.76
1JC02	50	12.50	0.58	0.69
1JC06	50	11.53	0.55	0.66
1JC07	50	10.68	0.52	0.61
1JC09	55	10.63	0.46	0.66
1JC16	55	8.25	0.36	0.51
1JC05	60	5.12	0.19	0.33
1JC10	60	9.39	0.35	0.61
1JC13	60	11.32	0.42	0.73
1JC18	60	10.20	0.39	0.67
1JC21	60	6.69	0.26	0.45
Average *CV*	*45*	*14.23* *21%*	*0.76* *21%*	*0.76* *21%*
Average *CV*	*50*	*11.57* *8%*	*0.55* *6%*	*0.66* *6%*
Average *CV*	*55*	*9.44* *18%*	*0.41* *18%*	*0.58* *18%*
Average *CV*	*60*	*8.54* *30%*	*0.32* *30%*	*0.56* *30%*

4.2.2. Double Punch Tests on Mortar Joints

The DPT is a promising MDT technique that revealed to be suitable for the mechanical characterisation of mortar in existing masonry structures (Pelà et al. 2012; Benedetti & Pelà 2012). It consists in a local compression test performed on roughly 50×50 mm^2 mortar layers using two special punching devices with a contact surface diameter of 20 mm (Figure 4.16a). Being mortar a heterogeneous material and being the DPT executed on a small portion of the mortar layer, the experimental results usually present high scatter. In addition, the upper and lower faces of the mortar joint, once detached from the bricks during sampling, appear normally irregular. This drawback adds a further complexity to the DPT. However, DPT can provide useful information about the strength of mortar and is actually the only possible laboratory test that can be carried out on mortar samples extracted from existing masonry structures.

The DPTs were conducted following the DIN 18555-9:1999 standard (DIN 18555-9:1999 1999) and relevant references (Pelà et al. 2012; Benedetti & Pelà 2012; Henzel & Karl 1987), using a compression machine equipped with a force controlled 10 kN load cell.
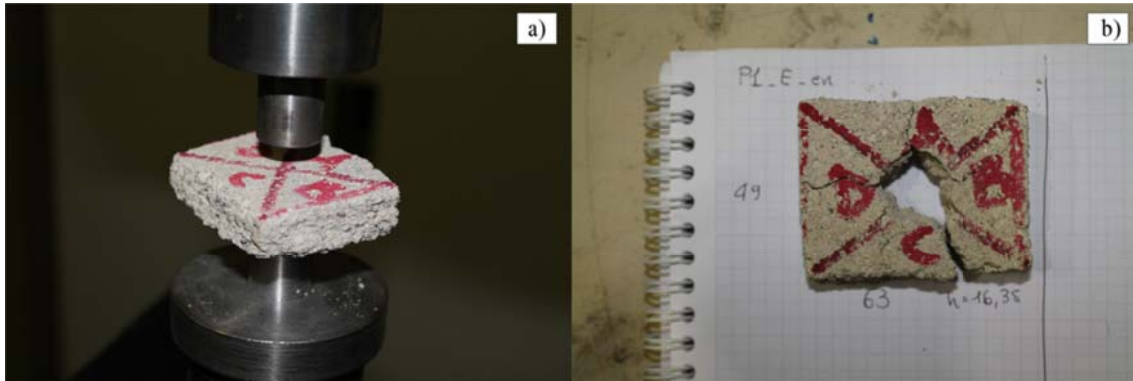

Figure 4.16 Double punch test of mortar joints before (a) and after failure (b).

The compressive strength from DPT is calculated by Equation 4.3:

$$\sigma_{max} = \frac{F_{max}}{\pi r^2}$$
(4.3)

where F_{max} is the maximum experimental load and r=10 mm is the radius of the tested surface. The DPT can hardly be considered as a simple uniaxial compression stress test. In fact, the sample is highly confined due to its small thickness, the friction with the punches and the presence of external material surrounding the loaded area. The stress state induced by DPT on the specimen seems to be actually triaxial axisymmetric. This phenomenon is confirmed also by the failure mode of the specimen (Figure 4.16b), where the surrounding material exhibits radial cracks arising from the area under the punches. These cracks are due to the confinement exerted by mortar surrounding the loading area. A discussion about the interpretation of the experimental data from DPT is included in the next section. Table 4.5 shows a summary of the results obtained from this experimental program.

Table 4.5 Experimental results of double punch tests on mortar joints.

Sample	σ_{max} [MPa]
P1_E	2.29
P2_E	2.91
P3_E	2.29
P4_E	3.41
P5_E	3.04
P2_E_2	2.60
P3_E_2	2.38
P4_E_2	3.40
P5_E_2	2.10
Average	*2.71*
CV	*18%*

4.3.   Interpretation of the Experimental Results

This section presents the comprehensive discussion and interpretation of the results from the BTs on masonry cores with inclined diametral mortar joint and the DPTs on mortar joints. The tests considered in this experimental program are analysed in depth to estimate the properties of mortar.

4.3.1. Brazilian Tests on Cores with Inclined Diametral Mortar Joint

The mechanical interpretation of the experimental results from BTs is carried out firstly using continuum mechanics theory. The mortar joint is not considered as an interface but as a continuum subject to a triaxial state of stress during the execution of the BT. This kind of interpretative approach was called *Continuum Model* in (Pelà et al. 2015) and was firstly proposed in (Pelà et al. 2012; Benedetti & Pelà 2012; Benedetti et al. 2008). Further improvements to the model are presented in this study together with its validation by comparison with experimental results obtained in the laboratory.

According to the Continuum Model, the state of stress in the mortar joint during the BT can be represented graphically in the σ-τ Mohr's plane by means of Mohr's circles. The circles representing the mortar's stress state at failure are tangent to the failure envelope. (Pelà et al. 2015) considered a Mohr-Coulomb criterion represented by a straight line. The parameters c and ϕ of the criterion, denoting the material's cohesion and friction angle, were determined using a least square method in order to best fit the experimental data set.

This research presents an improvement to the aforementioned approach, since it considers a more realistic nonlinear Mohr's criterion as failure envelope for the Mohr's circles of the BTs at failure (Pelà et al. 2012). In fact, the linear Mohr-Coulomb criterion is widely used for numerical modelling of a masonry element, since the prediction on its shear behaviour returns values in good agreement with the experimental results. On the other hand, dealing with historical masonry, it usually overestimate the tensile strength and the multiaxial compressive strength. Several authors suggested modified version of this criterion, introducing some limits in tensile and compressive strength (Pluijm et al. 2000; Lourenço et al. 1995). The nonlinear model proposed in (Pelà et al. 2012) allows to introduce a tensile limit without increasing the necessary parameters.

In addition, this work considers a more precise graphical representation of the stress state by Mohr's circles based on the representation of the complex triaxial state of stress actually experienced by the mortar during the BT and triplets tests. Figure 4.17 shows the comparison between the Mohr's circle representation of a generic BT as done in previous works (Pelà et al. 2015; Pelà et al. 2012; Benedetti & Pelà 2012; Benedetti et al. 2008) and in the present one. The former is drawn using a light grey line, whereas the second is drawn in dark grey. The stress state inside the mortar joint at failure is also presented, referring to Figure 4.15 and Equations 4.2a,b. As shown, the previous researches considered, as an approximation, zero confinement in the direction parallel to the joint. This hypothesis is reinterpreted here by including also the confinement effect σ_H in the Mohr's representation. This confinement is exerted by the stiffer circular segments of brick that limit the expansion of the softer diametral mortar joint during the execution of the BT. The graphical representation of this effect implies the construction of a smaller Mohr's circle than in the case of zero confinement (see Figure 4.17). Notice that compression stresses are considered positive in Figure 4.17 and also in the following ones.
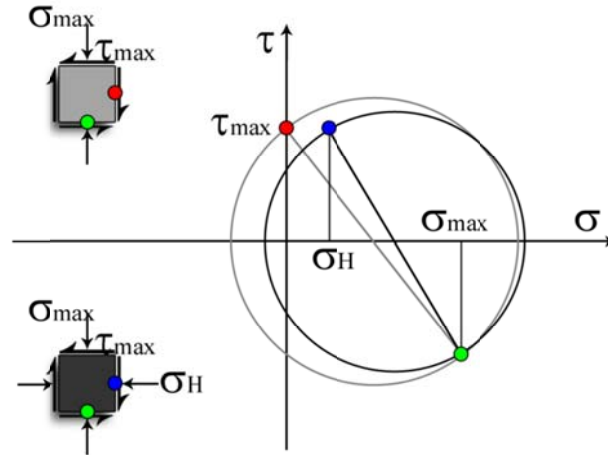
Figure 4.17 Continuum model. Mohr's circle representations of the failure stress state in the mortar joint during the Brazilian test: unconfined (grey, (Benedetti et al. 2008; Benedetti & Pelà 2012; Pelà et al. 2012; Marastoni et al. 2016)) vs. confined conditions (black).

Hilsdorf's theory about masonry in compression (Hilsdorf 1969) is considered to estimate the magnitude of the confinement stress σ_H. Hilsdorf's assumption of elastic behaviour of material's components prior to failure leads to a compatibility condition providing the confinement ratio K_H (Equation 4.4):

$$K_H = \frac{\sigma_H}{\sigma_{max}} = \frac{v_m - \frac{E_m}{E_b} \cdot v_b}{1 - v_m + (1 - v_b) \cdot \frac{E_m}{E_b} \cdot \frac{h_m}{h_b}} \qquad (4.4)$$

where v_m and v_b are the Poisson's coefficients of mortar and bricks, E_m and E_b the Young's moduli of mortar and bricks, h_m and h_b the thicknesses of the mortar joint and the bricks.

The confinement effect obtained from this theory requires the knowledge of numerous parameters of the material components, such as Young's moduli and Poisson's ratios of mortar and units. Those parameters are often difficult to estimate, thus it is important to establish how they influence the evaluation of the confinement ratio.

Considering the elastic properties of the materials of historical masonry, units are characterised by higher stiffness with respect to the mortar (i.e. Young's modulus), usually more than one order of magnitude (Binda et al. 1994; Filardi et al. 1996). Moreover, the thickness of the joints in ordinary brickworks ranges between 10 mm and 20 mm, while the units standard dimensions are usually more than 40 mm. Using these values in the Equation 4.4, the terms containing the Poisson's ratio of units become

negligible. This means implicitly that the units act as a constraint for the expansion of the mortar due to their high stiffness. Thus, it is possible to simplify the Equation 4.4 as follows.

$$K_H \cong \frac{v_m}{1-v_m}$$

(4.5)

The confinement ratio for BT using Equation 4.4 resulted $K_{H,B}$=0.415, having assumed in calculations the following average parameters: E_m=400 MPa, E_b=9792 MPa, v_m=0.30, v_b=0.17, h_m=15 mm and h_b=77 mm. Considering the simplified expression reported in Equation 4.5 the confinement ratio resulted $K_{H,B}$=0.429, only 3% higher than the previous evaluation. This result confirms that a good estimation of the confinement effect can be given by considering only the Poisson's ratio of the mortar.

The material's parameters that were not directly assessed by the experimental tests presented in the previous section were assumed on the base of reference values available in the literature. For instance, E_m and v_b are realistic values in good agreement with those provided in (Baronio et al. 1995; Binda et al. 1994; Vermeltfoort & Pluijm 1991) for lime mortar and bricks. The value of v_m was derived using the theory of elasticity with the assumed value of E_m and the experimental value G_m=154 MPa.

Hilsdorf's theory is based on the micromechanical analysis of a representative cell composed of one unit and one mortar joint. Since the core sample contains one layer of mortar and two half cylindrical pieces of unit, the thickness of the brick to be used in the equations are those in Figure 4.18.
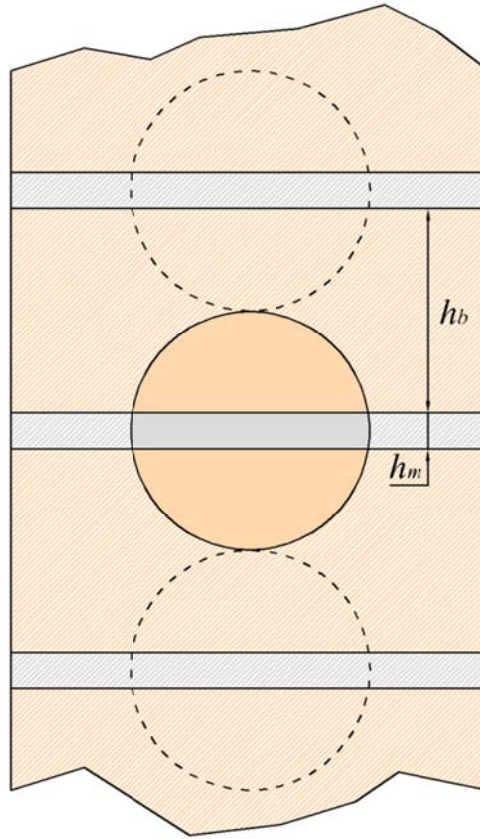
Figure 4.18 Magnitudes used for the evaluation of the Hilsdorf's confinement ratio.

The complete stress state in the mortar joint at failure is eventually defined using the following Equations 4.6a,b,c instead of those given in Equations 4.2a,b that did not consider the confinement effect (Pelà et al. 2015; Pelà et al. 2012; Benedetti & Pelà 2012).

$$\sigma_{max} = \frac{F_{max}}{A} \cdot \cos(\alpha) ; \quad \sigma_H = K_{H,B} \cdot \sigma_{max} ; \quad \tau_{max} = \frac{F_{max}}{A} \cdot \sin(\alpha) \quad\quad (4.6\text{a,b,c})$$

Table 4.6 presents the estimated values of the confinement stresses σ_H for each BT and thus complements the experimental results presented in Table 4.4 for their post-processing and interpretation.

Table 4.6 Estimation of the confinement stress $\sigma_{H,B}$ for the mechanical interpretation of the Brazilian tests.

Sample	α [°]	σ_H [MPa]
1JC04	45	0.23
1JC11	45	0.32
1JC14	45	0.40
1JC19	45	0.32
1JC02	50	0.24
1JC06	50	0.23
1JC07	50	0.21
1JC09	55	0.19
1JC16	55	0.15
1JC05	60	0.08
1JC10	60	0.14
1JC13	60	0.17
1JC18	60	0.16
1JC21	60	0.11

An alternative interpretative approach to the BTs was proposed in (Pelà et al. 2015) and called *Interface model*. In this second model, the mortar joint is analysed as a zero-thickness diametral interface that separates the core sample in two halves (Braga et al. 1992). The state of stress in the interface is described by only two components, i.e. the normal and tangential stresses σ and τ, see Figure 4.19. Failure of mortar is understood as shear sliding on this joint interface. The stress state at failure of each BT is represented by a point in the σ-τ plane whose coordinates are provided by Equations 4.2a,b. Due to the modelling of the mortar joint as an interface instead of a continuum, this model does not account for the triaxial stress state in the mortar joint at failure.
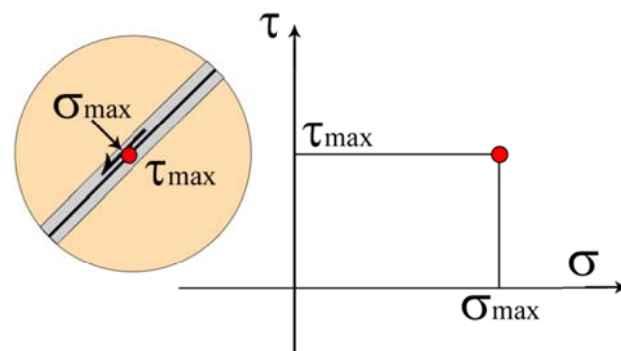
Figure 4.19 Interface model: mortar's stress state at failure from the Brazilian test.

For instance, the *Interface model* is the interpretation theory used in (EN 1052-3:2002 2002) for the triplets shear test.

The experimental setup used in this research for BTs allowed to develop a possible method for the estimation of another mechanical parameter of mortar, i.e. the tangential elastic modulus G_m. By measuring the relative displacement between the brick circular segments, which is due to the shear deformation of the mortar joint, it was possible to estimate G_m. Considering the initial elastic response of mortar, the tangential modulus can be calculated as the ratio between the tangential stress τ and the shear strain γ. The estimation of G_m depends on the stress/strain level at which it is calculated. Technical recommendations available in the literature do not provide any suggestion for the assessment of G_m. For this reason, it was found interesting to measure the variability of G_m values for different elastic stress levels. The tangential stress can be defined like in Equation 4.2b but for a load level lower than that at failure, i.e. still within the elastic range of mortar. The load level to be considered for the evaluation of G_m can be expressed as a percentage of the maximum failure load according to $\beta \cdot F_{max}$, where $0<\beta<1$. The shear strain is the deformation over the thickness of the joint. The tangential modulus is finally determined by Equation 4.7 as:

$$G_m = \frac{\beta \cdot \tau_{max}}{\gamma} = \frac{\beta \cdot F_{max}}{A} \cdot \sin(\alpha) \cdot \frac{t}{\delta} \tag{4.7}$$

where t is the thickness of the mortar layer and δ is the relative displacement measured between the two circular segments of brick at the load $\beta \cdot F_{max}$.
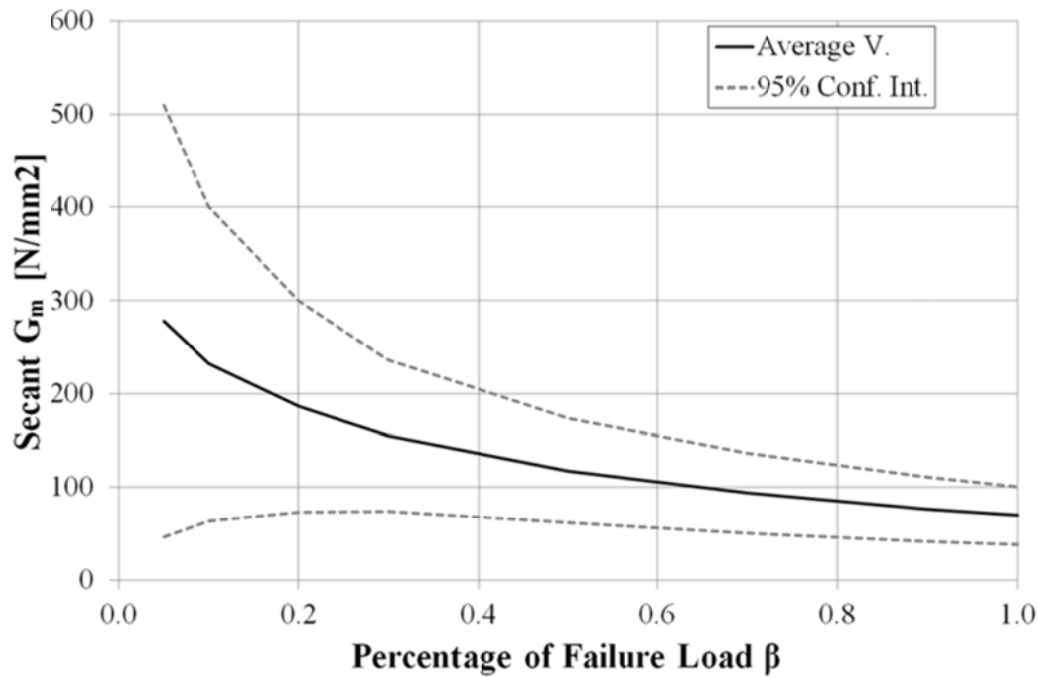
Figure 4.20 Secant tangential elastic modulus vs. elastic stress level.

Figure 4.20 shows the experimental law of variation of the mean secant G_m for different elastic stress levels. The mean values of secant G_m were obtained by averaging all the results from BTs on cores with different inclinations of the mortar joint. The continuous line indicates the mean values of the secant G_m corresponding to different values of β parameter, i.e. to different elastic stress levels before the maximum experimental load ($\beta=1$, $F=F_{max}$). The dotted lines define the 95% confidence interval considering a normal distribution (Gaussian). As shown, the experimental scatter around the mean secant tangential modulus is rather large for low values of β. This is due to the initial settlement of mortar in the core samples at the beginning of the loading test. After $\beta = 0.3$ the scattering reduces remarkably (CV is around 25%) and maintains a narrow variation until the failure load. Therefore, this study shows that the tangential elastic modulus G_m shall be estimated at least at the 30% of the maximum experimental load in order to obtain reliable results. The post-processing of experimental data from this research provided a tangential elastic modulus of mortar G_m=154 MPa. This method is based on a previous work found in literature (Pluijm 1993), where the shear modulus was directly obtained from a revisited version of the shear tests reported in (EN 1052-3:2002 2002).

It is important to underline that the deformation measured by the LVDTs is composed by both elastic deformation and shear slip that occurs in the brick-mortar interface. This

method provide an estimation of the elastic shear modulus useful for FEM applications, where localized discontinuity are not allowed and thus the total displacement is due to the elastic deformation only.

The evaluation of the responses of the BT specimens after the maximum load presents some difficulties. Once the specimen reaches the maximum value in the force-displacement curve, the crack grows in the mortar joint reducing sharply the capacity of the sample. When the crack splits the specimen into two parts, the weight of the upper part might exceed the residual friction on the mortar-unit interface producing the collapse of the specimen. Even using a rather high acquisition rate of 50 Hz, after the crack's appearance the load vs. displacement curve cannot be recorder due to this instantaneous snap.

In order to have an estimation of the lost data, a quadratic function was used to interpolate the data lost during the acquisition. Using a quadratic interpolation it was possible to link the last acquired data with those occurring after the snap in order to obtain a full definition of the material's softening response. The interpolating parabola is defined so that the continuity of the softening function and its derivative is ensured when the snap occurs. After reaching the vertex of the interpolating parabola, a constant value of residual force is maintained in order to connect with the last branch of the recorded data (see red line in Figure 4.21a). In some cases the crack propagation produced a rather short snap (see red line in Figure 4.21b) and thus the parabola was modified forcing it to go through the extreme points of the data loss (see blue line in Figure 4.21b).
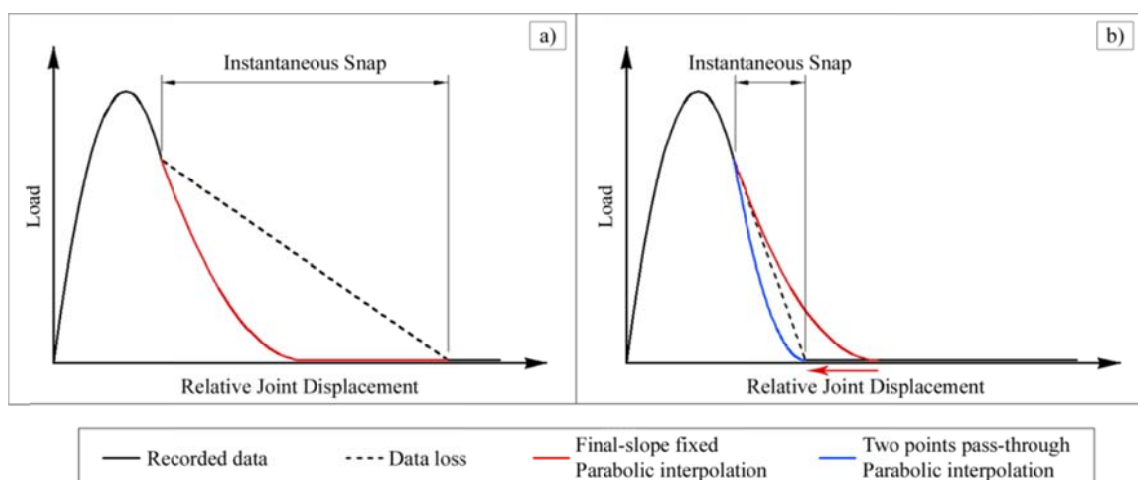
Figure 4.21 Parabolic interpolation of the post-peak branch fixing the slope of the last data acquired (a) and forcing the parabola to go through the extreme points of the data loss (b)

The method was employed in order to obtain a full evaluation of the softening behaviours of all the specimens, as reported in Figure 4.22.
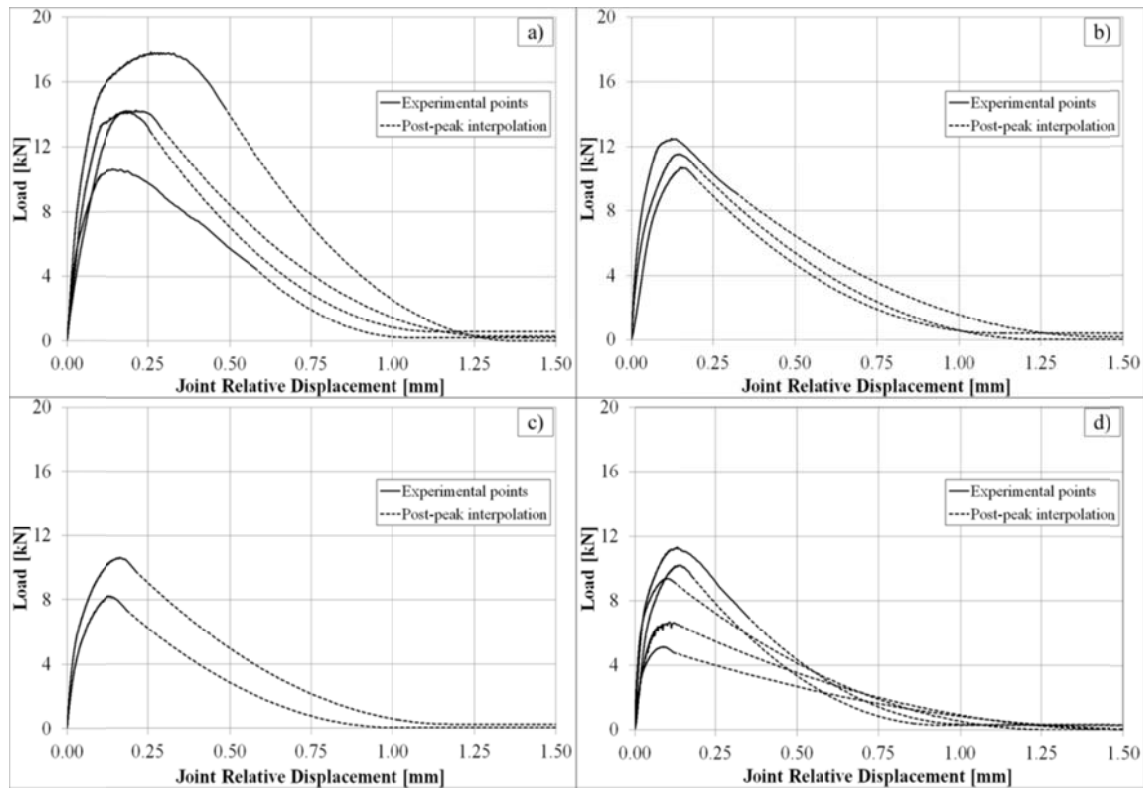
Figure 4.22 Experimental results with softening branch interpolated for inclinations of the joint of 45° (a), 50° (b), 55° (c) and 60° (d).

4.3.2. Triplet Shear Tests

The same considerations reported above in Section 4.3.1 about the BT interpretation can be used for the triplet shear tests. Dealing with the *Continuum model*, the interaction between brick and mortar acts at the same way of the BT. For this reason, the Hilsdorf's theory can be applied varying the parameters used in Equation 4.4. The confinement ratio resulted $K_{H,T}$=0.413, having assumed in calculations the following average parameters: E_m=400 MPa, E_b=9792 MPa, v_m=0.30, v_b=0.17, h_m=12 mm and h_b=45 mm. The material's parameters were chosen compliantly with the BT analysis shown in Section 4.3.1.

The complete stress state in the mortar joint at failure is reported in Table 4.7 and is defined using the following Equations 4.9a,b,c instead of those given in Equations 4.1a,b provided by the EN 1052-3:2002 (EN 1052-3:2002 2002).

$$\sigma_{max} = \frac{F_H}{A}; \quad \sigma_H = K_{H,T} \cdot \sigma_{max}; \quad \tau_{max} = \frac{F_{max}}{2 \cdot A} \tag{4.9a,b,c}$$

Table 4.7 Estimation of the confinement stress $\sigma_{H,T}$ for the mechanical interpretation of the triplet shear tests.

Sample	σ_{max} [MPa]	σ_H [MPa]
T1-NHL	0.99	0.41
T10-NHL	0.99	0.41
T13-NHL	0.99	0.41
T3-NHL	0.59	0.25
T7-NHL	0.59	0.25
T12-NHL	0.59	0.25
T2-NHL	0.20	0.08
T5-NHL	0.20	0.08
T11-NHL	0.20	0.08

4.3.3. Double Punch Test

A precise interpretation of the DPT results requires the estimation of the transversal confinement exerted by the loading punches on the flat sample of mortar. This is necessary in order to obtain a more precise graphical presentation by Mohr's circles of the stress states in DPTs. The Hilsdorf's theory (Hilsdorf 1969) is not suitable for DPT, since the hypothesis of constant horizontal stresses along the joint depth is not valid due to the fact that the dimensions of the metal punches are comparable to the thickness of the mortar specimen.

The analysis of the transversal confinement in the mortar sample was carried out by means of a numerical simulation of the DPT using a Finite Element Model (FEM). The 2D axisymmetric FEM was elastic and its only purpose was to evaluate the amount of horizontal confinement to which the mortar joint sample is subject during the DPT. The mesh was composed of 12000 nodes and 36601 eight-node plane elements (Figure 4.23a). Due to the axial symmetry of the problem, the mesh discretized only one-fourth of the real DPT, including both the 20 mm diameter punches and the mortar sample. Due to the irregular shapes of the specimens during the DPTs, only the inscribed cylinder to the sample was discretized as an approximation. Its outer dimension was 60 mm and its thickness was 15 mm. The mortar's Young's modulus was E_m=400 MPa and the Poisson's ratio was v_m=0.30. The Young's modulus of metallic punches was

E_s=200000 MPa and the Poisson's ratio was v_s=0.25. The values for mortar were estimated on the basis of the experimental results, while typical values were adopted for the steel. Figure 4.23b shows the evolution of the ratio between the horizontal and vertical stresses (σ_H/σ_{max}) obtained by the FEM analysis. The graphs show the laws of variation of the confinement ratio between the punches along different sections. As shown, the horizontal stress in the central section of the mortar sample can be estimated as 5% of the vertical pressure.
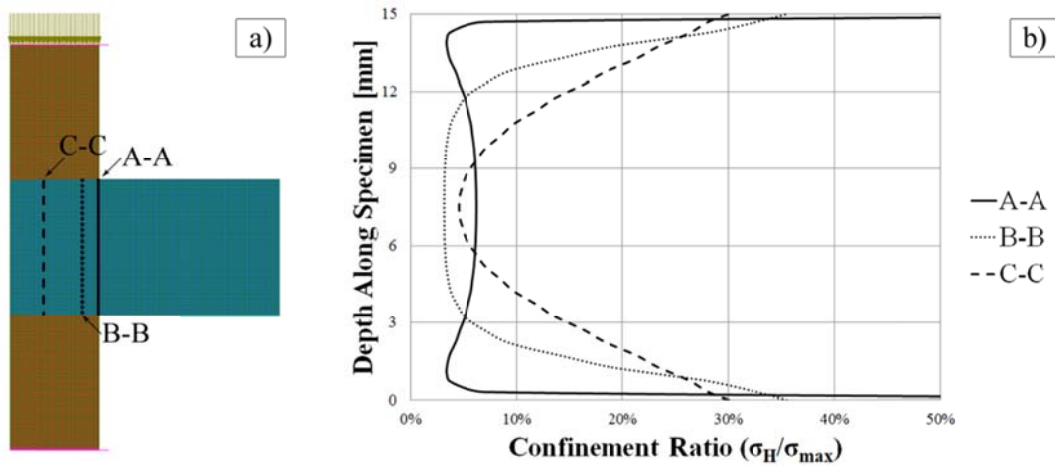
Figure 4.23 2D axisymmetric FEM model of DPT (a) to evaluate the confinement ratio between the punches (b).

After the FEM analysis, it was possible to draw with precision the Mohr's circle representing the stress state at failure of the mortar sample in the DPT. Instead of considering a uniaxial compression stress state, graphically represented by a Mohr's circle tangent to the vertical τ axis, this research proposes to consider also the effect of the confinement and thus the Mohr's circle is shifted away from the τ axis (Figure 4.24). The stress state representative of the failure of a mortar joint sample during DPT is finally estimated by means of the following equations:

$$\sigma_{max} = \frac{F_{max}}{A}; \quad \sigma_H = 0.05 \cdot \sigma_{max}; \quad \tau = 0 \qquad\qquad\qquad (4.10\text{a,b,c})$$
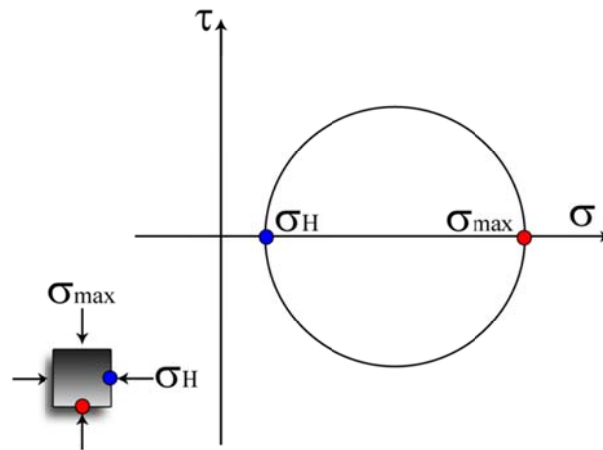
Figure 4.24 DPT confined stress state and Mohr's circle.

Table 4.8 presents the estimation of the horizontal confinement stress σ_H for each DPT of this experimental program, under the hypothesis assumed in Equations 4.10a,b,c.

Table 4.8 Estimation of the confinement stress $\sigma_{H,DPT}$ in double punch tests on mortar joints.

Sample	$\sigma_H \, [MPa]$
P1_E	0.12
P2_E	0.15
P3_E	0.11
P4_E	0.17
P5_E	0.15
P2_E_2	0.13
P3_E_2	0.12
P4_E_2	0.17
P5_E_2	0.11

4.3.4. Standard Tests

As reported in previous Section 4.1.2, the standard tests performed on mortar and units' specimens were interpreted following the reference standards or, if not available, adapted standards originally deployed for other materials.

Concerning the compressive and tensile tests, the state of stress in the sample can be assumed as uniaxial. In terms of graphical representation, this simple state of stress leads to a circle on the Mohr's plane that is tangent to the τ axis, as shown in Figure 4.25.
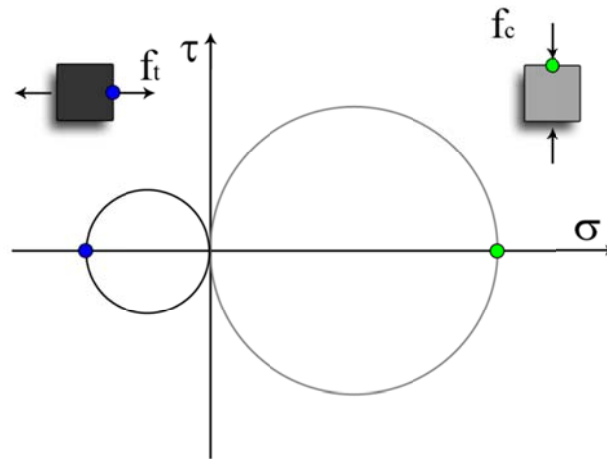
Figure 4.25 Tensile and compressive strength associated Mohr's circles.

The ultimate stress obtained by compression test both for mortar and units can be assumed as the compressive strength according to the relative standard (EN 772-1:2011 2011). On the contrary, flexural tensile strength can be hardly assumed as the pure tensile strength of the material. Several standards (fib 2013; EN 1992-1-1:2005 2005; D.M. 14/01/2008 2008) provide different rules for the conversion from flexural to tensile strength. Due to the empirical nature of these formulas, the results obtained for the characterisation of units are very different, spacing between an average value of $f_{tb,MC10}$=1.61 MPa provided by the Model Code 2010 (fib 2013) and $f_{tb,DM08}$=3.03 MPa obtained using the correction factor of the Italian Standard (D.M. 14/01/2008 2008). The comparison of the results obtained by the empirical formulas is reported in Table 4.9.

Table 4.9 Comparison of the conversions from flexural to tensile strength according to Model Code 2010 (MC10), Eurocode 2 (EC2) and Italian Standard (DM08).

Reference Standard	Average Value
$f_{tb,f}$ [MPa]	3.63
$f_{tb,MC10}$ [MPa]	1.61
$f_{tb,EC2}$ [MPa]	2.33
$f_{tb,DM08}$ [MPa]	3.03

The Eurocode 2 formula returns a value ($f_{tb,EC2}$=2.33 MPa) between the two aforementioned ones. For this reason, it was chosen as a possible reference for the

conversion from flexural to tensile strength. The conversion formula takes into account the possible non-standard dimensions of the specimens as reported in Equation 4.11.

$$f_{tb,EC2} = \frac{f_{tb,f}}{1.6-(h/1000)} \qquad\qquad (4.11)$$

Where $f_{tb,f}$ is the flexural strength calculated according to the three-point bending test (EN 772-6:2011 2011) and h is the height of the specimen.

Concerning the compression tests, the actual standard for units refers only to the whole unit compression (EN 772-1:2011 2011). This test was hardly executable on the bricks used in the reference experimental campaign due to their aspect ratio. In fact, the thickness of the units compared to their transversal dimensions was largely lower than the minimum requested from the standard.

For this reason the compressive strength was determined using the standard for mortar as reference (EN 1015-11:2007 2007). The compressive strength for the units was assumed as f_{cb}=18.40 MPa.

4.4.   Integrated Methodology of Micro-Mechanical Interpretation

An integrated method is proposed to post-process the experimental results from BTs and DPTs and to evaluate the properties of mortar. The *Continuum model* presented in Section 4.3.1 represents graphically the mortar's state of stress at failure by Mohr's circles in the σ-τ Mohr's plane (Figure 4.17). The failure criterion can be represented by the envelope of all the Mohr's circles. On the other hand, the *Interface model* (see Section 4.3.1) considers only a plane state of stress on the theoretical failure surface, identified as the mid-section of the mortar joint. The state of stress of one specimen is then represented as a point on the Mohr's plane (Figure 4.19).

The experimental results are usually scattered due to unavoidable heterogeneities in the mortar joints. For this reason, the failure envelope must be assessed by adopting a statistical approach leading to the determination of the best fit over the group of results in both models.

The data elaboration was carried out by means of a software developed in this research using Matlab (MathWorks 2013). The program was designed to process entirely the raw data coming from a laboratory test report, leaving to the user the possibility to select

different option for the interpretation method from the user-friendly interface. Moreover, it was studied to provide the necessary parameters for a numerical FE software developed by the Technical University of Catalonia and called COMET (CIMNE 2002). This software allows to compute nonlinear analysis with sophisticated constitutive models such as continuum damage model.

4.4.1. *Theoretical Development for Continuum Model*

A recent study (Pelà et al. 2015) proposed the adoption of a Mohr-Coulomb straight-line using the least squares method to minimize the sum of square distances between the line and ultimate Mohr's circles of all tested specimens. In a previous work of the same author (Pelà et al. 2012) also used a least squares analysis on the distances between the Mohr's circles and the failure surface, but it assumed a Mohr's parabolic failure envelope. This criterion can be defined by two positive constants, σ_0 and τ_0 in Equation 4.12, which indicate the intersections between the σ-τ axes and the parabola:

$$\left(\frac{\tau}{\tau_0}\right)^2 - \frac{\sigma}{\sigma_0} = 1 \tag{4.12}$$

The use of a Mohr's curved criterion like the parabolic one seems the most accurate to approximate the experimental set of data, as will be shown in the following. A numerical program was developed to automatize the least squares method and calculate the failure envelope. The input is the set of raw data obtained from the BTs and DPTs tests, such as dimensions of samples and failure loads. Starting from these input data the program associates a specific stress state to each sample, according to the hypotheses formulated in Section 4.3.1, Section 4.3.2 and Section 4.3.3 and it calculates the relevant Mohr's circles. Then, the software evaluates the minimum distances between the centres of the Mohr's circles and the parabolic failure criterion. This distance must be carefully evaluated, by considering the minimum one among all the possible lines that pass through the centres of the Mohr's circles and are perpendicular to the parabola. In particular, when the centre of a Mohr's circle lays between the vertex $(-\sigma_0,0)$ and a certain threshold $(\sigma_{crit},0)$ described in Equation 4.13 the minimum distance is the horizontal one, i.e. the point of tangency of the Mohr's circle is the vertex of the parabola (Figure 4.26).

$$\sigma_{crit} = \frac{\tau_0^2}{2 \cdot \sigma_0} - \sigma_0 \tag{4.13}$$
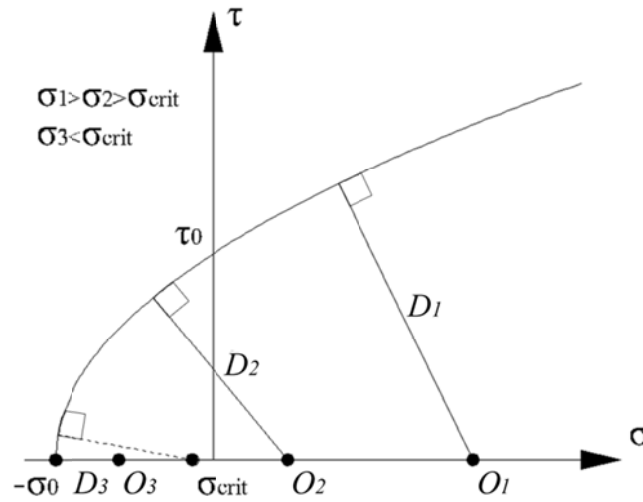
Figure 4.26 Calculation of minimum distances between the centres of the Mohr's circles and the parabolic failure criterion.

The distance D_i between the centre of the i-th Mohr's circle O_i and the parabola can be calculated depending on its position with respect to the threshold σ_{crit}. Notice that compression stresses are considered positive both in Figure 4.26 and in the following Equation 4.14 and Equation 4.15. The distance can be calculated using the following equations:

$$D_i = O_i + \sigma_0 \qquad\qquad If\ O_i \le \sigma_{crit} \tag{4.14}$$

$$D_i = \sqrt{\frac{O_i + \sigma_0 - \frac{\tau_0^2}{2 \cdot \sigma_0}}{\sigma_0} \cdot \tau_0^2 + \frac{\tau_0^4}{4 \cdot \sigma_0^2}} \qquad\qquad If\ O_i > \sigma_{crit} \tag{4.15}$$

The numerical algorithm then calculates the σ_0 value as the modulus of the mean principal tensile stress of the BTs with 60° inclination diametral mortar joint. This choice is motivated by a good agreement between the values of the mean principal tensile stress of the BTs with 60° inclination and the tensile strength provided by the flexural tests done on mortar samples, as will be remarked in the following. Such agreement indicates a plausible estimation of the tensile "cut-off" for the parabolic failure criterion. The flexural tests are not included in the proposal because it is based only on results obtained from nonstandard tests. Finally, a least square analysis is carried out on the remaining circles to minimize the sum of the squared residuals v_i

obtained as the difference between the *i*-th distance D_i and the *i*-th Mohr's circle radius R_i, as shown in Equation 4.16 and Equation 4.17, allowing to estimate the remaining parabola's parameter τ_0 (Figure 4.27).

$$v_i = D_i - R_i \qquad\qquad\qquad\qquad (4.16)$$
$$\sum v_i^2 = min \rightarrow \tau_0 \qquad\qquad\qquad\qquad (4.17)$$
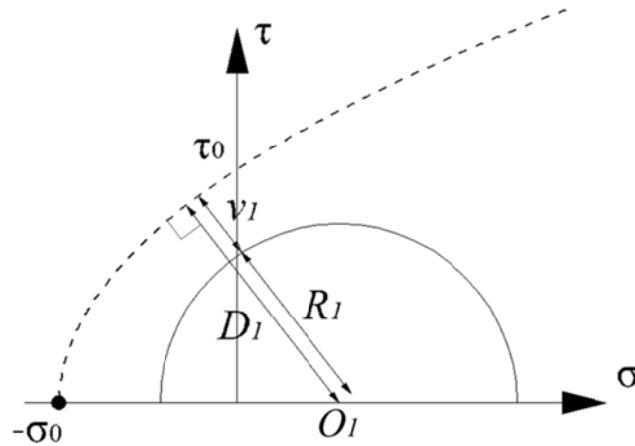
Figure 4.27 Least squares analysis used in the continuum interpretative model to evaluate the parabolic failure envelope.

While the tensile zone of the failure criterion is slightly nonlinear, the compressive one shows an almost linear trend. For this reason, it is interesting to compare the parabolic domain proposed in this research with the Mohr-Coulomb straight one suggested by (Pelà et al. 2015). In addition, the linear domain proposed by (Pelà et al. 2015) is here enriched by a tension cut-off inspired by the parabolic domain proposed in this work. The flowchart relative to the *Continuum model* implemented in the Interpretation Program is reported in Figure 4.28

INPUT

FLEX	TRIPLET	BRASIL_α	PUNCH	CMP_CUBE

Mohr's Circles Parameters

FLEX:
$\sigma_1 = -f_{fm}$
$\sigma_2 = 0$
$\tau = 0$
$R = [(\sigma_1-\sigma_2)^2/4 + \tau^2]^{1/2}$
$O = (\sigma_1+\sigma_2)/2$

TRIPLET:
$\sigma_1 = \sigma_{max}$
$\sigma_2 = K_{H,T}*\sigma_{max}$
$\tau = \tau_{max}$
$R = [(\sigma_1-\sigma_2)^2/4 + \tau^2]^{1/2}$
$O = (\sigma_1+\sigma_2)/2$

BRASIL_α:
$\sigma_1 = \sigma_{max}$
$\sigma_2 = K_{H,B}*\sigma_{max}$
$\tau = \tau_{max}$
$R = [(\sigma_1-\sigma_2)^2/4 + \tau^2]^{1/2}$
$O = (\sigma_1+\sigma_2)/2$

PUNCH:
$\sigma_1 = \sigma_{max}$
$\sigma_2 = K_{H,DPT}*\sigma_{max}$
$\tau = 0$
$R = [(\sigma_1-\sigma_2)^2/4 + \tau^2]^{1/2}$
$O = (\sigma_1+\sigma_2)/2$

CMP_CUBE:
$\sigma_1 = f_{cm}$
$\sigma_2 = 0$
$\tau = 0$
$R = [(\sigma_1-\sigma_2)^2/4 + \tau^2]^{1/2}$
$O = (\sigma_1+\sigma_2)/2$

yes $\alpha \geq 60$?   *no*

Principal Stresses
$\sigma_I = O - R$
$\sigma_{II} = O + R$
$\{\sigma_{tens}\} = [\overline{\sigma_I; \sigma_{II}}]$

Principal Stresses
$\sigma_I = O - R$
$\sigma_{II} = O + R$
$\{\sigma_{tan}\} = [\overline{\sigma_I; \sigma_{II}}]$

1st step
$\tau_0 = \tau_0^*$

Parabola Tensile Limit
$\sigma_0 = E[min(\sigma_{tens})]$

Parabola Singularity
$\sigma_{crit} = \tau_0^2/2\sigma_0 - \sigma_0$

yes   *for i-th test* $O_i > \sigma_{crit}$?   *no*

Orto-Distance Centre-Parabola
$D_i = [(O_i - \sigma_{crit})*\tau_0^2/\sigma_0 + \sigma_{crit}^2]^{1/2}$

Orto-Distance Centre-Parabola
$D_i = O_i + \sigma_0$

Calculation of Residual and Correction
$v_i = D_i - R_i$
$\Delta\tau_0 = -\partial_{\tau_0}(\Sigma v_i^2)/\partial_{\tau_0}^2(\Sigma v_i^2)$
$\tau_0 = \tau_0 + \Delta\tau_0$

no   *tolerance* $\Delta\tau_0/\tau_0 < \varepsilon$?   *yes*

MC Linear Cut-Off: solve for Φ
$c = \tau_0$
$R_{DPT} = O_{DPT}*\sin(\varphi) + c*\cos(\varphi)$

DPT Equivalent σ_{max}: solve for σ_{max}
$R_{DPT} = \sigma_{max}*(1 - K_{H,DPT})/2$
$O_{DPT} = \sigma_{max}*(1 + K_{H,DPT})/2$
$R_{DPT} = [(O_{DPT} - \sigma_{crit})*\tau_0^2/\sigma_0 + \sigma_{crit}^2]^{1/2}$

Mortar Strength Parameters for MC Linear
c, φ, f_{tm}
$f_{cm} = 2*c*\cos(\varphi)/[1 - \sin(\varphi)]$

Mortar Strength Parameters for Parabola
σ_0, τ_0
$f_{cm} = \tau_0^2/\sigma_0 + 2*\tau_0$
$f_{tm} = -\sigma_0$

Figure 4.28 Flowchart for the Continuum model interpretation.

Figure 4.29 shows both the parabolic and the linear failure domains. The parameters obtained for the Mohr's parabolic criterion and the Mohr-Coulomb linear domain with cut-off are shown in Table 4.10, with reference to the experimental results from BTs and DPTs.

Table 4.10 Parameters of the failure domains obtained from DPTs and BTs.

Parabolic domain		*Linear domain with cut-off*	
σ_0 [MPa]	0.34	c [MPa]	0.62
τ_0 [MPa]	0.62	φ [°]	33.11
		$f_{tm,CUT}$ [MPa]	0.34
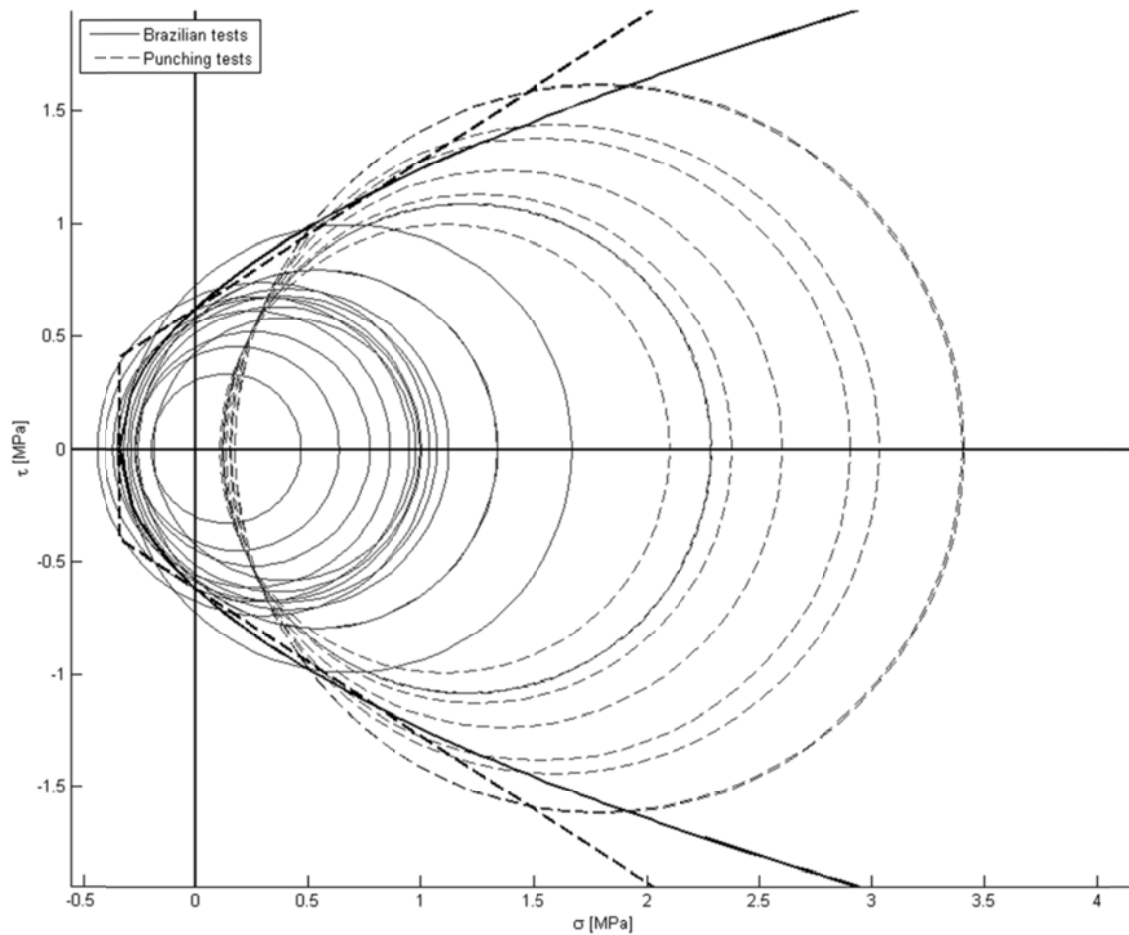
Figure 4.29 Estimated parabolic Mohr's and linear Mohr-Coulomb domains obtained from DPTs and BTs.

As for the evaluation of the Mohr-Coulomb linear domain, the cohesion c was assumed equal to the τ_0 parabola's parameter whereas the friction angle φ was estimated as the best-fit to the compressive part of the parabolic domain.

The *Continuum model* was then applied on the triplet shear tests using the state of stress defined by Equations 4.9a,b,c. The Mohr's circles reproducing the state of stress in triplets indicate a similar values of the principal tensile stress for all pre-compression levels, suggesting to calculate the σ_0 value as the average principal tensile stress of all the tests. It is important to underline that (according to EN 1052-3:2002 (EN 1052-

3:2002 2002)) the failure of the specimen involves simultaneously the two mortar layers. In the former campaign, for the lowest value of normal pre-compression (0.2 MPa) the specimens exhibited a small slip along the loading plates, sufficient to induce the premature cracking of one mortar joint before the other one. This problem brought to a lower value of the ultimate shear for 0.2 MPa pre-compression. Figure 4.30 reports the curve with the average displacement measured by the LVDTs in abscissa versus the load recorded by the load cell. Two peaks can be clearly noticed, relative to the failure of each mortar joint. This caused a premature loss of cohesion in one joint while the other was still not loaded. As a result, the shear capacity of the element appeared lower than the expected value.
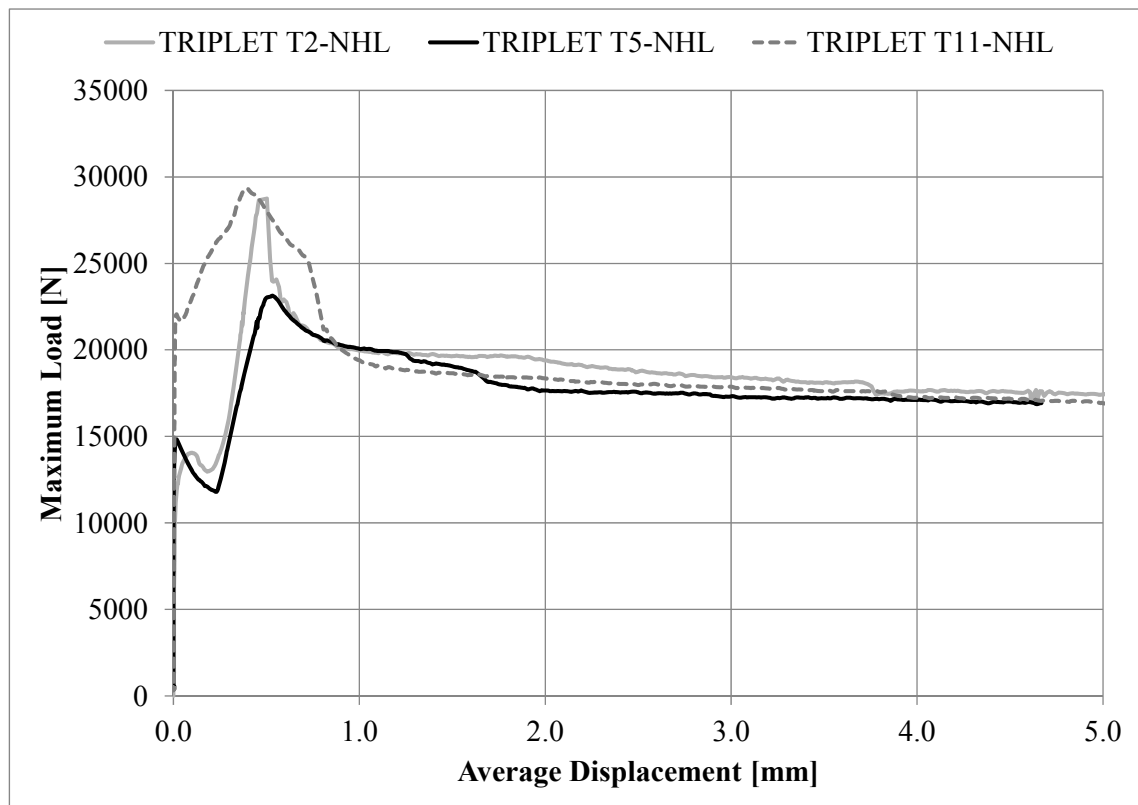
Figure 4.30 Force-Displacement curve of the triplet tests performed with 0.2 MPa of pre-compression.

Considering the results of the 0.2 MPa pre-compression triplets, the evaluation of the failure envelope of mortar leads to the underestimation of the mechanical parameters (Figure 4.31a). On the other hand, if the results of 0.2 MPa pre-compression triplets are discarded, the envelope is in remarkable agreement with the one obtained with the BTs (Figure 4.31b). The parameters obtained by the two interpretations are reported in Table 4.11 and Table 4.12.

Table 4.11 Parameters of the failure domains obtained from DPTs and triplets.

Parabolic domain		Linear domain with cut-off	
σ_0 [MPa]	0.28	c [MPa]	0.59
τ_0 [MPa]	0.59	φ [°]	35.43
		$f_{tm,CUT}$ [MPa]	0.28

Table 4.12 Parameters of the failure domains obtained from DPTs and triplets (0.2 MPa step excluded).

Parabolic domain		Linear domain with cut-off	
σ_0 [MPa]	0.34	c [MPa]	0.63
τ_0 [MPa]	0.63	φ [°]	33.18
		$f_{tm,CUT}$ [MPa]	0.34
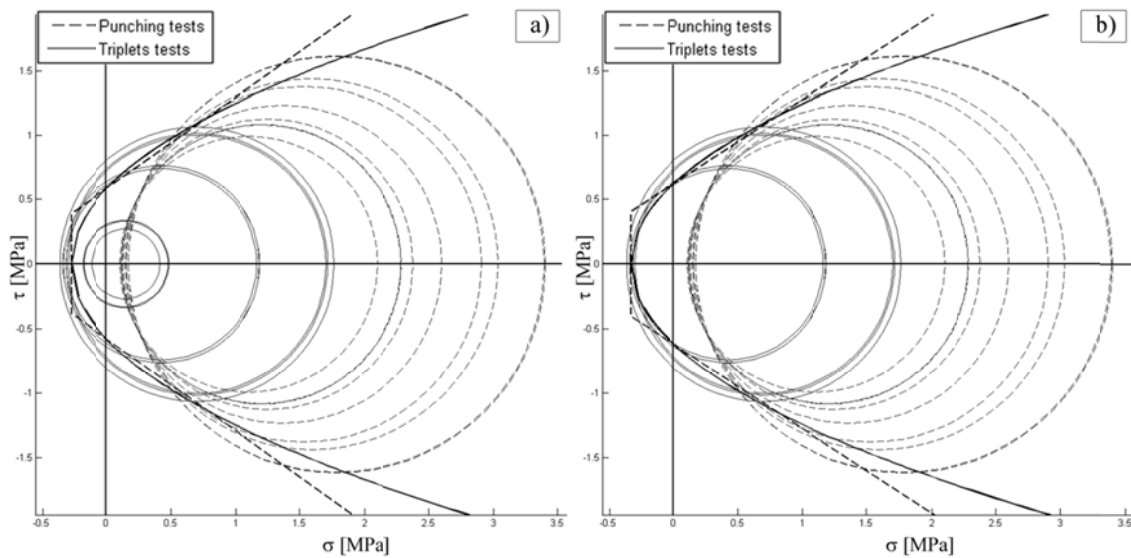
Figure 4.31 Estimated parabolic Mohr's and linear Mohr-Coulomb domains obtained from DPTs and triplets (a) and discarding the 0.2 MPa pre-compressed tests (b).

The proposed procedure showed its capability to allow the combination of different testing methods (BT, triplets and DPT) to evaluate the failure envelope of mortar. Execution and comparison of different testing techniques is highly advisable during the mechanical characterisation of existing materials (Pelà et al. 2015; Pelà et al. 2012; Benedetti & Pelà 2012). The proposed approach was then compared with the set of experimental results from the standard tests (flexure and compression tests on prismatic specimens and triplet shear tests). The comparison of the tests results has shown that BTs and triplets induce similar state of stresses on the mortar tested, allowing to use BT (performed on existing masonry) instead of triplet shear test. Moreover, the Mohr's circles corresponding to the flexural tests are tangent to the vertical axis of the σ-τ

Mohr's plane, since the only stress considered is the tensile one. Concerning the compressive standard tests according to the referenced standard (EN 1015-11:2007 2007), the result obtained from the test can be assumed as the compressive strength, i.e. the uniaxial ultimate state of stress. As for the triplet tests, these kind of standard tests actually could not be carried out in practical studies on existing and historical structures, being possible only the extraction of core samples for BT and mortar joint layers for DPT. However, it is interesting to note that the proposed interpretative approach is rather flexible and it allows us to include the outcomes from different testing techniques. The results of flexural tensile strength found in Section 4.1.2 are about 10% higher than the tensile strength estimation derived from the integrated model. Furthermore, the compressive strength prediction appears conservative of about 6% on the value obtained from the standard test. This means that a remarkable agreement is found between the mechanical parameters obtained from standard laboratory tests and those derived from the proposed MDT techniques. This fact confirms that combining BTs and DPTs is a reliable method to evaluate the mechanical properties of existing mortar in historical construction.

The continuum interpretative model allows us also to estimate the compression strength of mortar using Equation 4.18, derived from Mohr-Coulomb theory:

$$f_{cm} = \frac{2 \cdot c \cdot \cos(\varphi)}{1 - \sin(\varphi)} \qquad (4.18)$$

On the other hand, the tensile strength is defined by the cut-off value σ_0. The mortar's compressive and tensile strengths are f_{cm}=2.30 MPa and $f_{tm,CUT}$=0.34 MPa for the proposed methodology including BTs and DPTs only. Notice that the estimated compressive strength is only slightly lower than that directly obtained from standard compression strength on prisms (f_{cm}=2.45 MPa).

4.4.2. Theoretical Development for Interface Model

The second method proposed in (Pelà et al. 2015) to interpret the results from BTs on masonry cores with inclined diametral mortar joint and the triplets tests is the *Interface model*, already mentioned in Section 4.3.1 and Section 4.3.2. This method analyses the mortar joint as a plane interface, not explicitly accounting for the triaxial stress

interaction between bricks and mortar joint. For this reason, as discussed in (Pelà et al. 2015), this model seems more appropriate to describe the response of the mortar joints showing pure sliding along the brick-mortar interface (Figure 2.12b) instead of the parasymmetric failure (Figure 2.12a). Concerning the triplet tests the observed cracks after the failure were mainly located on the mortar-brick interface (Figure 4.32), suggesting the *Interface model* to be more appropriate for this kind of test.
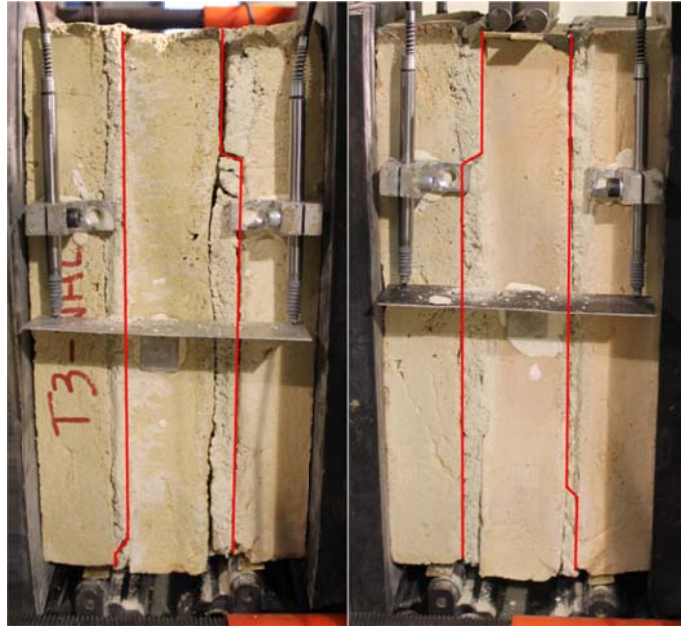
Figure 4.32 Typical failure of a triplet specimen after the test.

The interface model can consider only the results from the BTs or the triplets to evaluate the failure envelope parameters. In fact, other kinds of tests, like the DPT, cannot be included in this approach. However, the resulting model is simpler and is presented herein for the sake of comparison with the *Continuum model*.

Each test result is represented by a point on the Mohr's plane instead of a circle (Figure 4.19). The failure envelope is determined by a linear regression of the failure points to obtain a Mohr-Coulomb criterion characterised by two parameters, the friction angle Φ and the cohesion C. The *Interface model* relative flowchart of the Interpretation Program developed is reported in Figure 4.33.
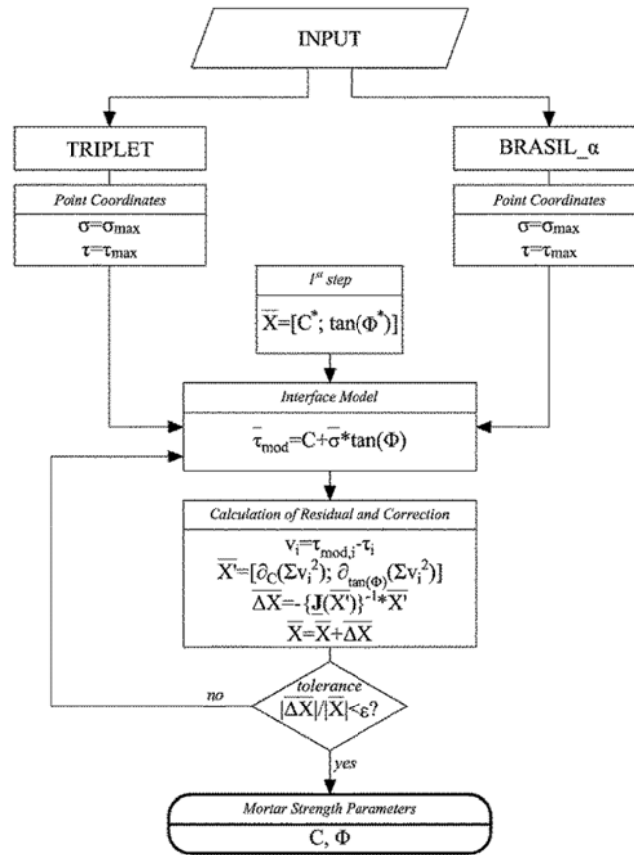
Figure 4.33 Flowchart for the Interface model interpretation.

Figure 4.34 shows the failure envelope obtained from the experimental program considered in this research. The interface model provides a friction angle $\Phi =32.32°$, while the cohesion is $C=0.32$ MPa.

The interface model does not allow to estimate the compression and tensile strengths of mortar. Equation 4.18 cannot be used to calculate f_{cm} because in this approach the parameters Φ and C have a different theoretical meaning.
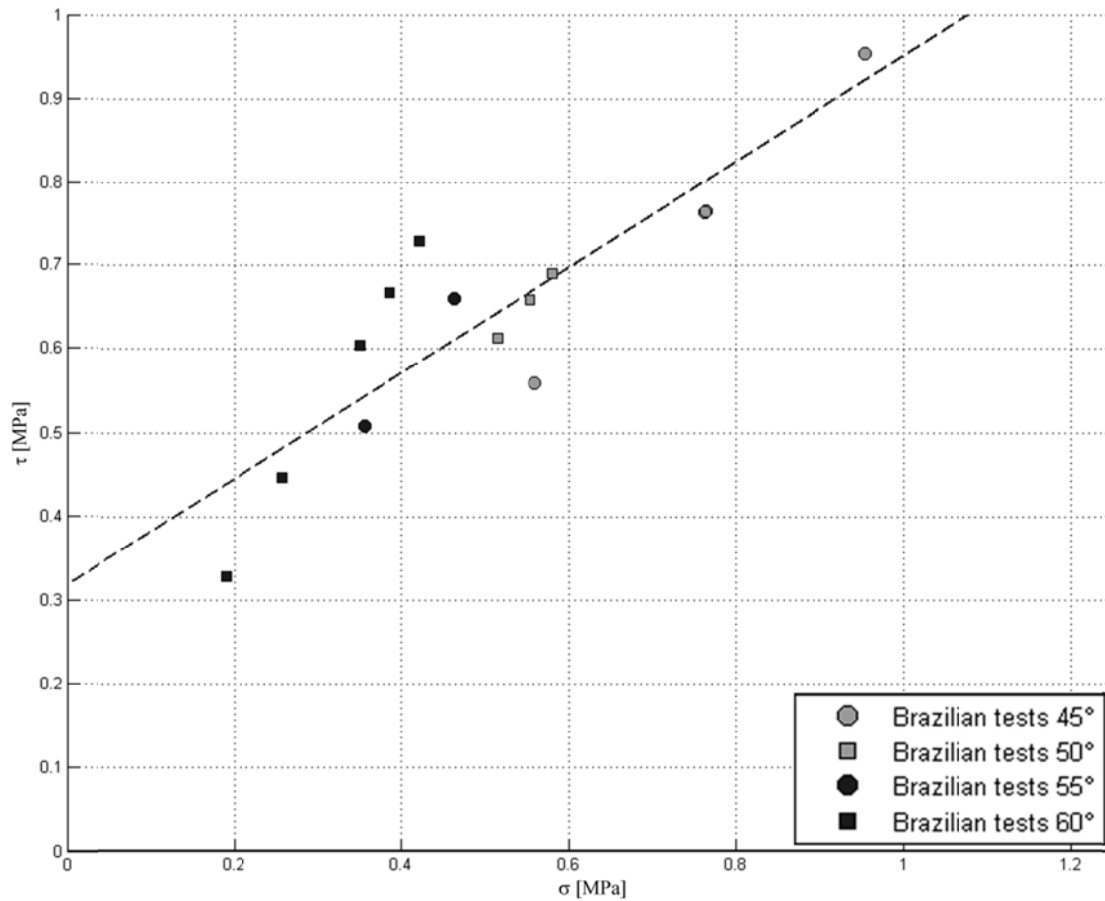
Figure 4.34 Estimated linear Mohr-Coulomb domain obtained with the interface model applied to BTs.

The same procedures were repeated for the triplets, taking into account the fact that the 0.2 MPa pre-compression triplets returned unreliable values. The comparison between the whole dataset and excluding the lowest pre-compression step is in agreement with the considerations made in Section 4.4.1. The parameters obtained considering the whole dataset are slightly lower than those obtained using the BT (see Figure 4.35a). Moreover, discarding the uncertain results discussed above the envelope's parameters become very close to the BT results (Figure 4.35b), with a friction angle Φ =32.61° and a cohesion C=0.36 MPa.
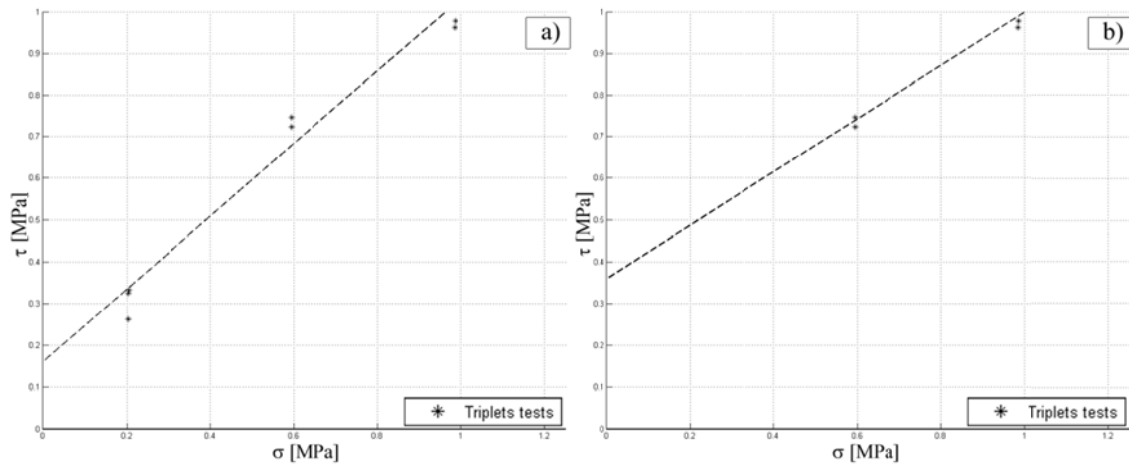
Figure 4.35 Estimated linear Mohr-Coulomb domain obtained with the interface model applied to triplets (a) and discarding the 0.2 MPa pre-compressed tests (b).

In line with the previous comments, the BTs can be considered as a possible alternative whenever the tests on triplets are not possible to be executed, like in existing historical structures.

4.4.3. Experimental Data Processing Software

The first screen of the experimental data processing software (Figure 4.36) shows the plots of the *Continuum model* graphs (such as Figure 4.29 and Figure 4.31a,b), and 4 sub-panels containing the input data and the outcomes of the process.
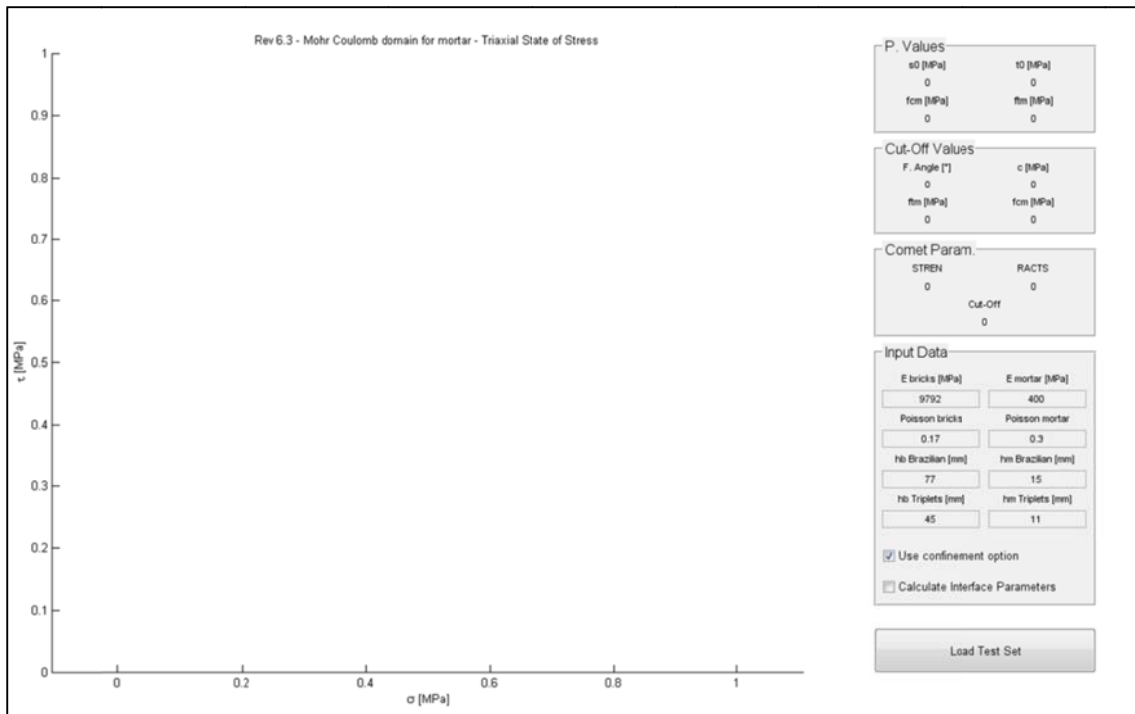
Figure 4.36 Initial screen of the experimental data processing software.

The *Input Data* panel contains all the geometric and elastic mechanical parameters, such as elastic modulus, Poisson's ratio and thickness of the components for BTs and triplet tests (brick and mortar). Under these tabs there are two check-boxes: the first activates or deactivates the confinement options for BTs and triplets (given by Equation 4.6b and Equation 4.9b) and for DPTs (given by Equation 4.10b); the second includes or excludes the *Interface model* from the interpretation. If the interface model option is checked, a new window emerges with the relevant graph plotted (such as Figure 4.34 and Figure 4.35a,b).

Once the parameters and the options are selected, by clicking the *Load Test Set* button it is possible to load the input file containing the raw data provided by the tests. This input file requires a precise format to be elaborated. Figure 4.37 shows an example of input datasheet.

TEST	NAME	D1 [mm]	D2 [mm]	LOAD [N]	D3 [mm]	H_LOAD [N]
BRASIL_50	1JC07	145.0	92.0	10685.641	16.0	0
BRASIL_60	1JC21	141.0	92.0	6688.000	16.0	0
BRASIL_45	1JC22	144.0	93.0	16018.483	19.0	0
PUNCH	P1_E	16.5	20.0	1589.646	55.0	0
PUNCH	P2_E	21.2	20.0	817.442	56.0	0
PUNCH	P3_E	20.0	20.0	747.636	52.1	0
FLEX	NHL_1_F	100.0	40.0	171.17	40.0	0
FLEX	NHL_2_F	100.0	40.0	151.06	40.0	0
FLEX	NHL_3_F	100.0	40.0	152.32	40.0	0
CMP_CUBE	NHL_1A_C	40.0	40.0	3839.400	40.0	0
CMP_CUBE	NHL_1B_C	40.0	40.0	3993.800	40.0	0
CMP_CUBE	NHL_2A_C	40.0	40.0	3835.100	40.0	0
TRIPLET	T1-NHL	145.0	305.0	86438.638	160.0	43568.110
TRIPLET	T2-NHL	145.0	305.0	28767.750	158.0	8981.621
TRIPLET	T3-NHL	145.0	305.0	66012.692	154.0	26264.556

Figure 4.37 Input file datasheet for the experimental data processing software.

The program can compute different kinds of tests, marked with the tags shown in the first column of Figure 4.37. In particular, these tests are possible:

- *Brazilian Tests on Cores with Inclined Diametral Mortar Joint* (tag: BRASIL_XX): the possible inclinations are from 30° to 60° every 5°.
- *Triplet Shear Tests* (tag: TRIPLET): every load step of pre-compression is allowed.
- *Double Punching Tests* (tag: PUNCH): required for the *Continuum model* interpretation.
- *Three Point Flexure Tests* (tag: FLEX): standard flexure test provided by EN 772-1:2011 (EN 772-1:2011 2011).
- *Compression Tests* (tag: CMP_CUBE): standard compression test provided by EN 772-1:2011 (EN 772-1:2011 2011).

The integrated methodology presented only works with multiple kinds of tests, and in particular it is necessary to carry out at least DPTs, and in addition BTs and/or triplet tests. The necessary information contained in the other columns are summarized in Table 4.13 and shown in Figure 4.38.

Table 4.13 Instructions for Input file formatting.

TEST	D1 [mm]	D2 [mm]	LOAD [N]	D3 [mm]	H_LOAD [N]
BRASIL_XX	Length	Diameter	Failure load	Joint thickness	-
TRIPLET	Small side	Long side	Failure load	Total height	Pre-Compression Load
PUNCH	Thickness	Punch diameter	Failure load	Average external side	-
FLEX	Flexural length	Height	Failure load	Base side	-
CMP_CUBE	Base side 1	Base side 2	Failure load	Height	-
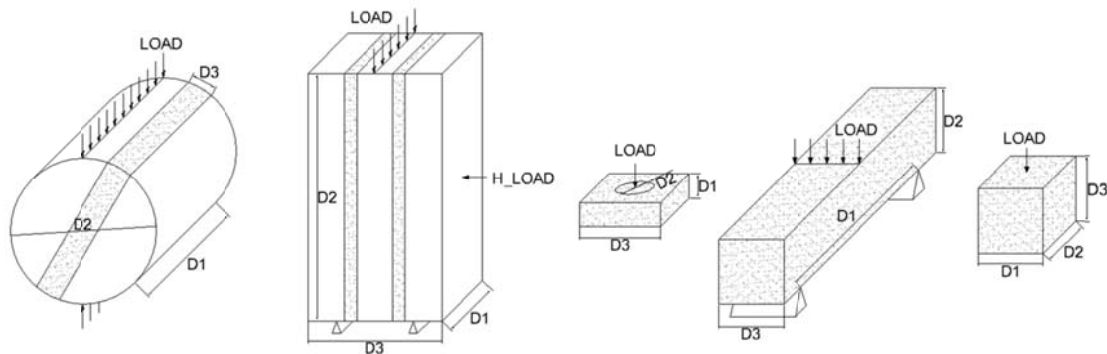
Figure 4.38 Input data for BT, triplet, DPT, flexure and compression standard tests.

The algorithm then separates all the tests on the basis of the tag, associating the relative state of stress according to the relative instructions reported in this chapter.

The other three panels reports the outcomes of the analysis. The first one tagged as "*P. Values*" reports the results of the parabolic Mohr-Coulomb failure criterion, such as the σ_0 and τ_0 parameters and the resulting compressive and tensile strength for the mortar investigated. The second panel ("*Cut-Off Values*") gives the parameters for the linearized version of the parabolic criterion, such as the friction angle φ, the cohesion c and the resulting compressive and tensile strengths. The latter panel reports the three parameters required by the finite element software COMET (CIMNE 2002) that will be used in Chapter 5 to perform the numerical analyses. In particular, *STREN* is the tensile strength expressed in Pa required by the Mohr-Coulomb criterion, *RACTS* the ratio between compressive and theoretical tensile strength of the Mohr-Coulomb criterion, *Cut-Off* is the value of the tension cut-off.

Chapter 5. Numerical Validation of Laboratory Experimental Tests

This chapter presents the numerical validation of the laboratory experimental tests described in Chapter 4. The analyses are aimed at supporting the hypotheses at the basis of the interpretative methodology proposed in Section 4.4.

First, linear analyses were performed to validate the hypotheses on the analytical evaluation of the state of stress in the cylindrical specimens subject to BT. Second, the parameters obtained in Section 4.4 were used in FE nonlinear analysis to test the reliability of the methodology by means of a software developed at the International Center for Numerical Method in Engineering (CIMNE) of the Technical University of Catalonia of Barcelona (Spain). Several models were performed to simulate the behaviour of mortar during the Brazilian test of masonry cores with rotated diametral mortar joint. Since the analytical interpretative methodology presented in Chapter 4 considers a triaxial state of stress in mortar, a plane stress analysis would not represent correctly the mechanical response of the material. Plane strain 2D and full 3D models can consider a more correct three-dimensional state of stress in mortar. The 3D analysis requires higher computational time than the 2D plane strain model. The latter considers the adoption of approximate but yet acceptable hypotheses that reduce the number of degrees of freedom and thus the computation time. However, some hypotheses of the plain-strain 2D model could lead to an erroneous estimation of the expected behaviour. The 3D and 2D plain strain analyses were carefully compared for the numerical simulation of both BTs and shear tests on triplets.

5.1.   Linear Analyses of Brazilian Tests

As reported in Section 4.2, the typical failure mode of the specimens with low strength mortar subjected to BT is the "parasymmetric" mode (Figure 2.12a and Figure 4.13). The stress state of the mortar during the BT adopted in the analytical interpretation of the test presented in Section 4.3.1 was evaluated by considering values of normal and tangential stresses averaged over the mid-section of the mortar joint (see Equations 4.6a,b,c). This hypothesis was widely accepted in other researches (Braga et al. 1992; Binda et al. 1994; Benedetti et al. 2008; Pelà et al. 2012; Mazzotti et al. 2014; Marastoni et al. 2016) and in this work it was also improved by adding the confinement effect due to the interaction of bricks and mortar derived from the Hilsdorf's theory (Hilsdorf 1969).

Despite the hypothesis of constant stress distribution over the mid-section of the joint, the experimental fracture starts spreading from opposite brick-mortar interfaces. In the most of cases, the fracture assumes a parasymmetric shape, propagating through the joint in the centre of the sample (as seen in Figure 4.13), as also seen in several previous studies (Marastoni et al. 2016; Pelà et al. 2015; Braga et al. 1992). Thus, the state of stress on the actual fracture plane can be compared with the one over the mid-section in order to validate the aforementioned hypothesis for the analytical interpretation of the test.

The comparison of the stress distributions between boundary and mid-section was carried out using two elastic 2D FEM analyses (Figure 5.1a) representing the BT with inclined mortar joint at 45° and 60°. The models were composed of 48576 triangular elements, for a total amount of 24489 nodes. The outer diameter of the modelled specimen is 100 mm including a mortar joint of 15 mm thickness. Since each model was calculated under plane strain condition, the analysis considers a unitary width of the specimen. The load was applied on an area of 6.5 mm^2/m to simulate the wooden supports used in the tests.

Table 5.1 summarises the values obtained in the experimental campaign concerning the elastic properties required by the Hilsdorf's theory.

Table 5.1 Mechanical parameters used in the linear analyses

Mortar Parameters			Units Parameters		
E_m	400	MPa	E_b	9792	MPa
v_m	0.30	-	v_b	0.17	-
h_m	15	mm	h_b	85	mm
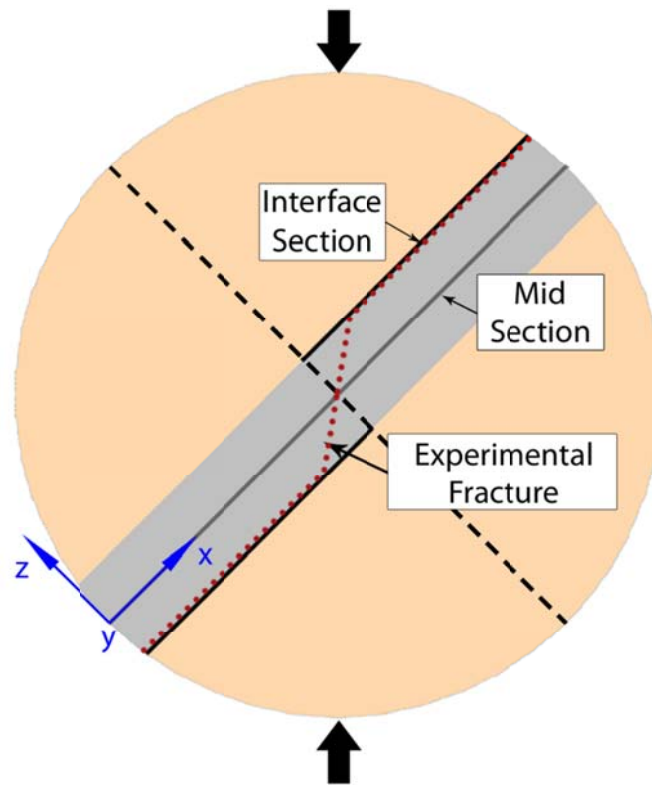
Figure 5.1 Elastic FE model mesh with section lines used for the stress plots: interface section (black line), mid-section (grey line) and experimental fracture (red dotted line).

Taking advantage of the parasymmetric geometry of the crack, the stresses are represented only on half part of the mortar joint for both the interface section and the mid-section. In order to simplify the stress calculations, the plots are reported on the interface section (black line in Figure 5.1). The red dotted line in Figure 5.1 depicts the position of the crack observed experimentally. The stresses are calculated following the local coordinates system reported in blue in Figure 5.1, with x-axis parallel to the mortar joint, z-axis orthogonal and y-axis normal to the model's plane. This reference system for the plot of stresses is centred on the external bound of the specimen.

Since the analyses were carried out in elastic conditions, the stress distributions are linearly dependent on the magnitude of the total force applied. For this reason, the comparison was achieved by representing adimensional normal and tangential stresses

$\hat{\sigma}$ and $\hat{\tau}$ respectively. The expressions of the aforementioned normalised stresses are reported in Equations 5.1a,b,c,d.

$$\hat{\sigma}_{zz,FE} = \frac{\sigma_{zz}}{F_{max}/A} \quad ; \hat{\tau}_{xz,FE} = \frac{\tau_{xz}}{F_{max}/A} \quad ; \hat{\sigma}_{xx,FE} = \frac{\sigma_{xx}}{F_{max}/A} \quad ; \hat{\sigma}_{yy,FE} = \frac{\sigma_{yy}}{F_{max}/A} \quad (5.1a,b,c,d)$$

Where σ and τ are the normal and tangential stresses relative to the local planes x-y-z obtained in the FE analyses, F_{max} is the total load applied on the specimen and A is the area of the mid-section of the mortar joint.
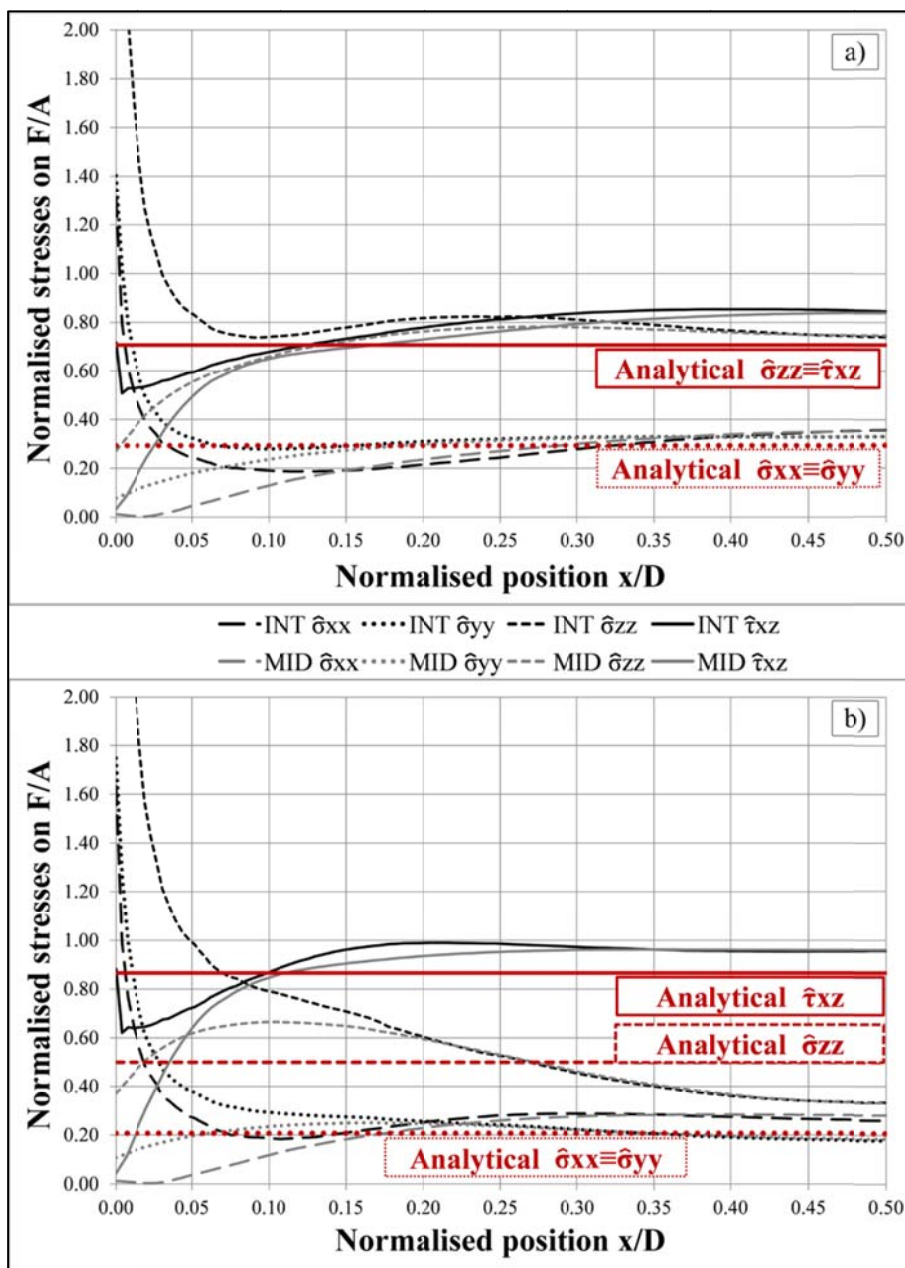
Figure 5.2 Normalised stress distributions comparison between mid-section, interface section and analytical solutions for 45° (a) and 60° (b).

Figure 5.2 reports the plots of the aforementioned analyses performed on specimens with diametral mortar joint inclined of 45° (Figure 5.2a) and 60° (Figure 5.2b) with respect to the horizontal. In both graphs, the abscissa reports the adimensional position x/D, where x is the position from the external bound of the specimen and D is the diameter of the sample. The ordinate axis reports the adimensional stresses $\hat{\sigma}$ and $\hat{\tau}$ according to Equations 5.1. According to the interpretation of the BT proposed in Section 4.3.1, the analytical state of stress is also reported as adimensional values as follow.

$$\hat{\sigma}_{zz,A} = \cos(\alpha) \quad ; \hat{\tau}_{xz,A} = \sin(\alpha) \quad ; \hat{\sigma}_{xx,A} = \hat{\sigma}_{yy,A} = K_H \cdot \cos(\alpha) \qquad (5.2a,b,c)$$

The interface stress distribution (Figure 5.2) reports small differences with the ones measured in the mid-section. For $x/D \leq 0.05$ the stresses are affected by a strong boundary effect due to the high discontinuity in the interface section. For this reason, the results for this small portion of the sample can be disregarded in the comparison. Considering the results for $x/D > 0.05$ the stress distributions of the two sections are in remarkable agreement each other.

Table 5.2 reports the average value of each stress measured on the boundary section and on the mid-section.

Table 5.2 Comparison between interface section and mid-section average adimensional stress plots.

	$\widehat{\sigma}_{zz,FE}$		$\widehat{\tau}_{xz,FE}$		$\widehat{\sigma}_{xx,FE}$		$\widehat{\sigma}_{yy,FE}$	
Num-45° INT	0.776	-	0.787	-	0.271	-	0.314	-
Num-45° MID	0.737	-5%	0.767	-2%	0.273	1%	0.303	-4%
Num-60° INT	0.538	-	0.935	-	0.252	-	0.237	-
Num-60° MID	0.473	-12%	0.927	-1%	0.237	-6%	0.213	-10%

The comparison of the average values of the stresses obtained by the FE analyses and those obtained with the analytical formulation reported in Equations 5.2a,b,c (red lines in Figure 5.2) shows good agreement (Table 5.3). The differences are sufficiently small to consider the constant stress distribution over the mid-section of the mortar joint as an acceptable approximation. Moreover, the Hilsdorf's theory provides a good estimation of the confinement effect on the mortar, thus validating the assumption made in the interpretation theory developed in Chapter 4.

Table 5.3 Comparison between average mid-section and analytical adimensional stress plots.

	$\hat{\sigma}_{zz}$		$\hat{\tau}_{xz}$		$\hat{\sigma}_{xx}$		$\hat{\sigma}_{yy}$	
Num-45° MID	0.737	-	0.767	-	0.273	-	0.303	-
Analytical-45°	0.707	-4%	0.707	-8%	0.294	7%	0.294	-3%
Num-60° MID	0.473	-	0.927	-	0.237	-	0.213	-
Analytic-60°	0.500	6%	0.866	-7%	0.208	-12%	0.208	-3%

5.2.   Isotropic Damage Model for Nonlinear Analyses

This section presents the constitutive model adopted in the nonlinear FEM analyses. An isotropic continuum damage model with only one scalar internal variable is adopted to monitor the local damage in the material (Simo & Ju 1987; Cervera 2003). This choice provides a simple constitutive model which, nevertheless, is able to reproduce the overall nonlinear behaviour including stiffness degradation and strain-hardening/softening response under tensile and shear stresses. The combination with a Mohr-Coulomb criterion with tension cut-off leads to the proper description of the frictional failure of the material.

5.2.1. Constitutive Model and Failure Criterion

The constitutive model considered is based on the concept of effective stress tensor, introduced in connection with the hypothesis of strain equivalence (Lemaitre & Chaboche 1978). The effective stress tensor $\bar{\sigma}$ can be computed in terms of the total strain tensor ε, as:

$$\bar{\sigma} = C : \varepsilon \tag{5.3}$$

Where C represents the (fourth-order) isotropic linear-elastic constitutive tensor and $(:)$ is the tensor product. The damage is modelled using a single scalar parameter, the so-called damage index d, which varies between 0 when the material is elastic and 1 when it is completely damaged. The constitutive equation relating effective and total stress tensors can be written as:

$$\boldsymbol{\sigma} = (1 - d)\bar{\boldsymbol{\sigma}} = (1 - d)\,\boldsymbol{C} : \boldsymbol{\varepsilon} \tag{5.4}$$

For the particular purpose of this research, the use of a single damage variable with an isotropic constitutive law is justified by the nature of the tests represented which only involve tensile and shear stress states (Saloustros et al. 2015).

In compliance with the formulation postulated by Simo and Ju (Simo & Ju 1987), a scalar positive quantity, termed as equivalent stress Σ, is defined in order to identify 'loading', 'unloading' or 'reloading' situations for a general 3D stress state. The equivalent stress can assume several forms, depending on the damage threshold criterion assumed. The present work considers the Mohr–Coulomb criterion with tension cut-off, which can be expressed in the following form:

$$\Sigma = \max\left\{\frac{K+1}{2\cdot K}\cdot\max\begin{bmatrix}|\bar{\sigma}_1 - \bar{\sigma}_2| + \rho(\bar{\sigma}_1 + \bar{\sigma}_2)\\|\bar{\sigma}_1 - \bar{\sigma}_3| + \rho(\bar{\sigma}_1 + \bar{\sigma}_3)\\|\bar{\sigma}_2 - \bar{\sigma}_3| + \rho(\bar{\sigma}_2 + \bar{\sigma}_3)\end{bmatrix}; \frac{f_t}{f_{t,CUT}}\cdot\bar{\sigma}_1\right\} \tag{5.5}$$

Where $\bar{\sigma}_1 > \bar{\sigma}_2 > \bar{\sigma}_3$ are the effective principal stresses, K is the compression/tension ratio (according to the Mohr-Coulomb failure surface) expressed as $K = f_c/f_t$ and $\rho = \frac{K-1}{K+1}$ is an adimensional coefficient. The term $f_{t,CUT}$ is the cut-off tensile strength. Tensile stresses are intended as positive.

The damage criterion is defined in the effective stress space as:

$$\phi(\Sigma, r) = \Sigma - r \leq 0 \tag{5.6}$$

Where r is an internal stress-like variable representing the current damage threshold, which drives the monotonical expansion of the damage surface. The initial value of the damage threshold is $r_0 = f_t$. The expansion of the damage surface for loading, unloading and reloading conditions follows the Kuhn-Tucker relations and the damage consistency condition, which are

$$\dot{r} \geq 0; \quad \phi(\Sigma, r) \leq 0; \quad \dot{r}\cdot\phi(\Sigma, r) = 0 \tag{5.7}$$

$$if \ \phi(\Sigma, r) = 0 \quad then \quad \dot{r}\cdot\phi(\Sigma, r) = 0 \tag{5.8}$$

The Kuhn-Tucker relations lead to the explicit definition of the current values of the internal variable r (Cervera 2003):

$$r = \max[r_0, \max(\Sigma)] \tag{5.9}$$

Note that Equation 5.9 allows to compute the current values for r in terms of the current value of Σ, which depends explicitly on the current total strains.

The internal damage variable $d = d(r)$ is explicitly defined in terms of the current value of the damage thresholds, so that it is a monotonically increasing function such that $0 \leq d \leq 1$. In the present work, the damage variables are computed according to the exponential softening law proposed by Cervera et al. (Cervera et al. 2010):

$$d(r) = 1 - \frac{r_0}{r} \exp\left\{2H_d\left(\frac{r_0-r}{r_0}\right)\right\} \quad with \quad r_0 \leq r \tag{5.10}$$

Where $H_d \geq 0$ is the discrete softening parameter. In order to ensure mesh-size objective results, the specific dissipated energy g_f is adjusted for each damaged finite element so that the equation (Bažant & Oh 1983; Oliver 1989).

$$g_f \cdot l_{ch} = G_f \tag{5.11}$$

Where l_{ch} is the characteristic width of the crack in the discrete problem and G_f is the material's tensile fracture energy. For the isotropic damage model with exponential softening, the specific energy dissipated is

$$g_f = \left(1 + \frac{1}{H_d}\right)\frac{(f_t)^2}{2E} \tag{5.12}$$

The discrete softening parameter H_d can be obtained by using Equations 5.11 and 5.12, as follows.

$$H_d = \frac{l_{ch}}{l_{mat}-l_{ch}} \tag{5.13}$$

Where the material characteristic length $l_{mat} = 1/H_{mat}$, with $H_{mat} = (f_t)^2/(2EG_f)$, depends only on the material properties (Cervera et al. 2010).

5.2.2. Characteristic Length for the Discrete Models

The fracture mechanics represent a crack like a discontinuity in the deformation field. The energy is dissipated over the cracked surface A and is called fracture energy G_f (see Figure 5.3a). On the other hand, in continuum mechanics this discontinuous phenomenon cannot be represented. For this reason, the crack is smeared over a volume with characteristic length l_{ch} (see Figure 5.3b). Therefore, the total energy W dissipated over the volume V must satisfy the following condition:

$$G_f = \frac{W}{A} = \frac{W}{V} \cdot l_{ch} = g_f \cdot l_{ch} \tag{5.14}$$
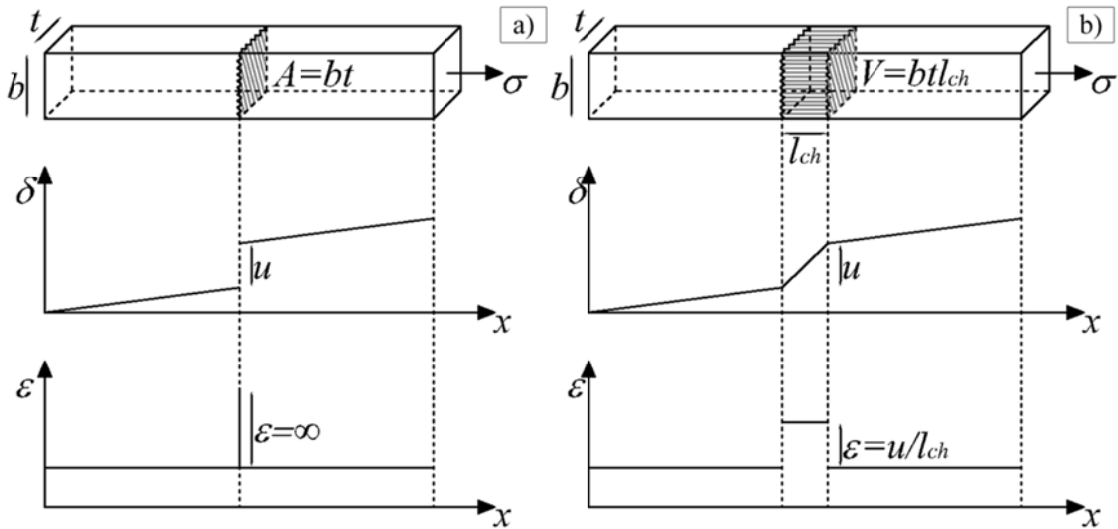
Figure 5.3 Comparison between displacement and deformation fields in Fracture Mechanics (a) and Continuum Damage Mechanics (b).

When moving to the discrete FEM problem, the characteristic length l_{ch} is used to regularise the softening behaviour according to Equation 5.14. This characteristic length depends on the size of the finite element (Bažant & Oh 1983; Oliver 1989), due to strain localization in a single row of finite elements after the formation of the discrete crack. Thus, the characteristic length l_{ch} expresses the discrete crack bandwidth in the FE model. The magnitude of the characteristic length l_{ch} depends on the type of finite

element. The definitions of the characteristic length for different types of finite elements
are summarized in Figure 5..
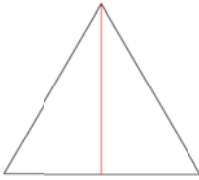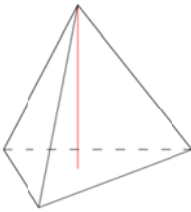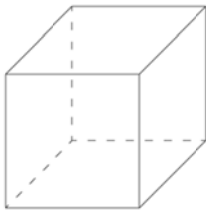
Figure 5.4 Characteristic lengths for different types of elements.

5.3.   3D Nonlinear Analyses of Brazilian Tests and Triplets

The BT was simulated using three-dimensional FE models. The nonlinear analyses were
carried out using the constitutive law presented in Section 5.2.1. Four models were
built, one for each angle of inclination of the mortar joint with respect to the horizontal
direction. The models were discretised using structured meshes of hexahedral elements.
This approach was used also for triplets, performing nonlinear analyses on 3D models.
Each model considered a different value of pre-compression according to the
corresponding experimental tests. For the sake of comparison, the triplet shear test with
zero normal confinement was also carried out.

The relative displacement of the mortar joint was carried out by means of two control
points for each specimen, named as P1 and P2. In order to have more realistic results,
the points were chosen on the external face of the specimens. The relative displacement
was measured in parallel direction with respect to the mortar joints both for BT and
triplet models.

Taking advantage of the symmetry of the BT specimens, only half of the depth was
represented, constraining the nodes of the central transversal section (see Figure 5.5).

The dimensions of the models are reported in Table 5.4. The average values of the characteristic length l_{ch} of the discrete crack bandwidth are also reported.
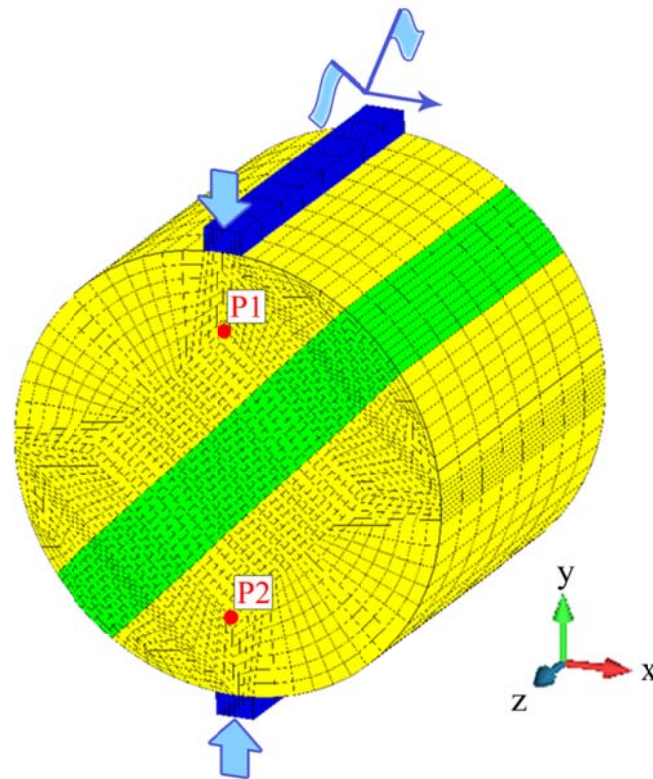
Figure 5.5 3D model of Brazilian Tests with control points and symmetry plane.

Table 5.4 Characteristics of 3D numerical models of Brazilian Tests.

Model	Type of Elements	N. Points	N. Elements	$l_{ch,m}$ [m]	$l_{ch,b}$ [m]
1JC45M_3D	hexahedral	15381	13248	0.0021	0.0019
1JC50M_3D	hexahedral	15381	13248	0.0022	0.0019
1JC55M_3D	hexahedral	14958	12880	0.0021	0.0019
1JC60M_3D	hexahedral	16650	14352	0.0020	0.0015

Due to the symmetry of the triplet specimens, only a quarter of the sample was modelled cutting it over the two symmetry planes (i.e. *xy* and *yz*) and providing the proper constrain conditions (see Figure 5.6). The characteristics of the triplet models are summarised in Table 5.5.
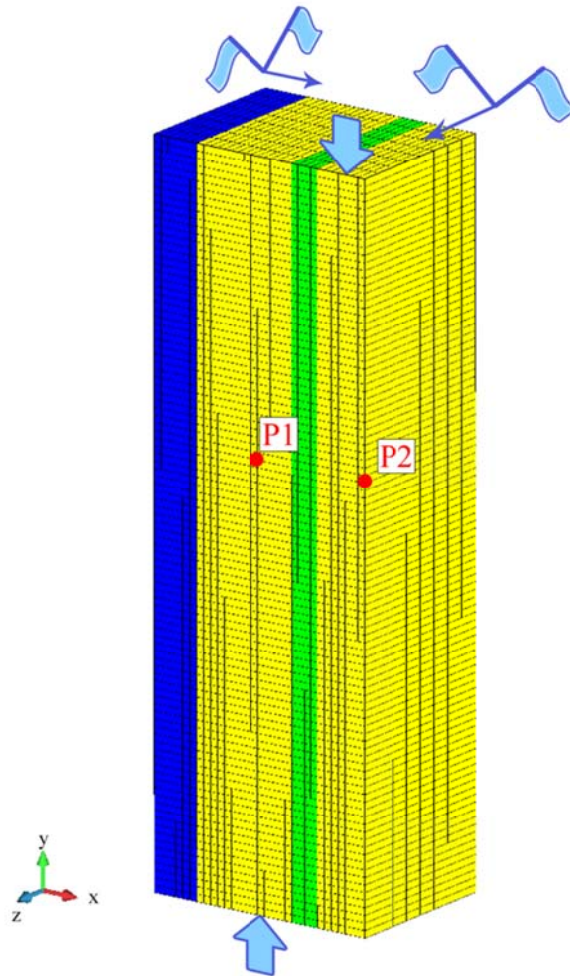
Figure 5.6 3D model of triplets with control points and symmetry planes.

Table 5.5 Characteristics of 3D numerical models of triplets.

Model	Type of Elements	N. Points	N. Elements	$l_{ch,m}$ [m]	$l_{ch,b}$ [m]
TX-NHL-1.0_3D	hexahedral	29088	24800	0.0030	0.0033
TX-NHL-0.6_3D	hexahedral	29088	24800	0.0030	0.0033
TX-NHL-0.2_3D	hexahedral	29088	24800	0.0030	0.0033
TX-NHL-0.0_3D	hexahedral	29088	24800	0.0030	0.0033

The numerical analyses were carried out under vertical displacement control, measuring the shear deformation of the joint for BT and measuring the relative displacement of two reference points on the units for the triplets. For BT models, the vertical loading was applied to the model of the core sample using elastic high-stiffened elements. The base supports and the loading plates in the triplets were not modelled, but their effect was taken into account by constraining the corresponding nodes in the model. The steel plates used for the pre-compression of the specimens were also included in the model, using elastic high-stiffened elements.

The mechanical parameters used for the analyses were obtained from the material characterisation discussed in Section 4.4.1 and are reported in Table 5.6. The parameters not directly obtained from the experimental campaign were assumed on the basis of reference values found in literature. As for the fracture energy, some authors (Lourenço 1996; Pluijm 1993) showed that realistic values of the fracture energy for shear behaviour of mortar can be chosen in the range of 10 to 250 J/m². Moreover, the same authors provided values between 60 and 130 J/m² for solid clay units characterised by tensile strength ranging from 1.50 MPa to 3.50 MPa. For this reason, the fracture energy for mortar and units was set to $G_{f,m}$=100 J/m² and $G_{f,b}$=100 J/m² respectively.

Table 5.6 Mechanical properties used in the nonlinear analyses.

Mortar properties		Brick properties	
E_m [MPa]	400	E_b [MPa]	9792
v_m [MPa]	0.30	v_b [MPa]	0.17
$G_{f,m}$ [J/m²]	100	$G_{f,b}$ [J/m²]	100
c_m [MPa]	0.62	f_{tb} [MPa]	2.33
φ_m [°]	33.11	f_{cb} [MPa]	18.40
$f_{tm,CUT}$ [MPa]	0.34		

Where E is the Young's modulus, v the Poisson's modulus, G_f the fracture energy, c is the cohesion, φ is the internal friction angle, $f_{tm,CUT}$ the cut-off tensile strength for mortar, f_{tb} and f_{cb} are the Mohr-Coulomb tensile and compressive strength for units. The m and b subscripts are used for mortar and bricks respectively.

The models were carried out on a workstation equipped with an Intel Xeon E5-1620 clocked at 3.6 GHz and 16 GB of RAM. Each analysis took about 9 hours, depending on the type of the elements and on the dimension of the mesh.

5.4.   2D Plain Strain Nonlinear Analyses of Brazilian Tests and Triplets

Figure 5.7 reports the models developed using 2D elements under plane strain conditions in order to represent the longitudinal confinement stress on the mortar. The dimensions of the 2D models are reported in Table 5.7. The same mechanical parameters shown in Table 5.6 were used for the two-dimensional models.
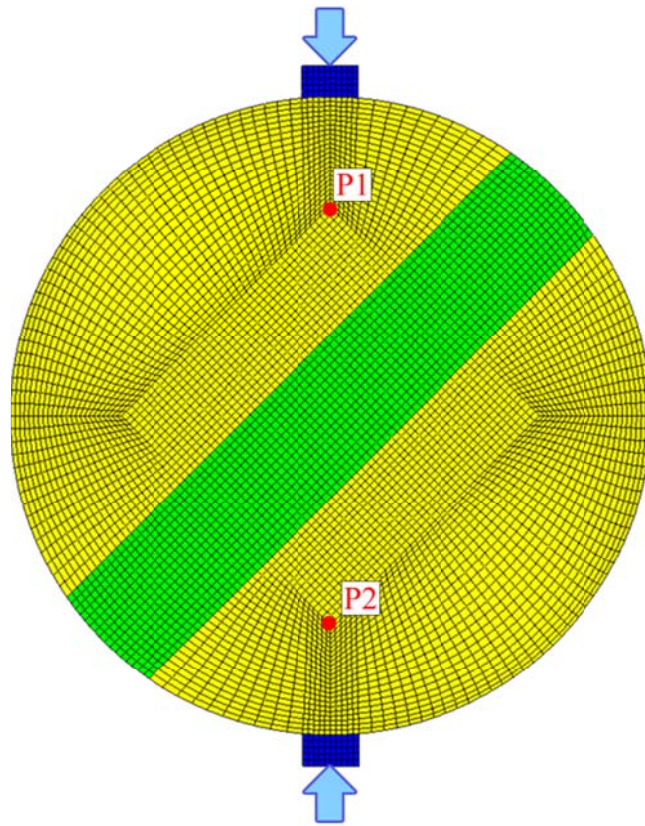
Figure 5.7 2D models of Brazilian Tests with control points.

Table 5.7 Characteristics of 2D numerical models of Brazilian Tests.

Model	Type of Elements	N. Points	N. Elements	$l_{ch,m}$ [m]	$l_{ch,b}$ [m]
1JC45M_2D	quadrilateral	6355	6256	0.0010	0.0010
1JC50M_2D	quadrilateral	6355	6256	0.0010	0.0010
1JC55M_2D	quadrilateral	7083	6976	0.0010	0.0010
1JC60M_2D	quadrilateral	6153	6056	0.0010	0.0010

Triplets' models were discretized taking advantage of the symmetry to reduce the dimension of the meshes. The meshes used are reported in Figure 5.8 and their dimensions are presented in Table 5.8.
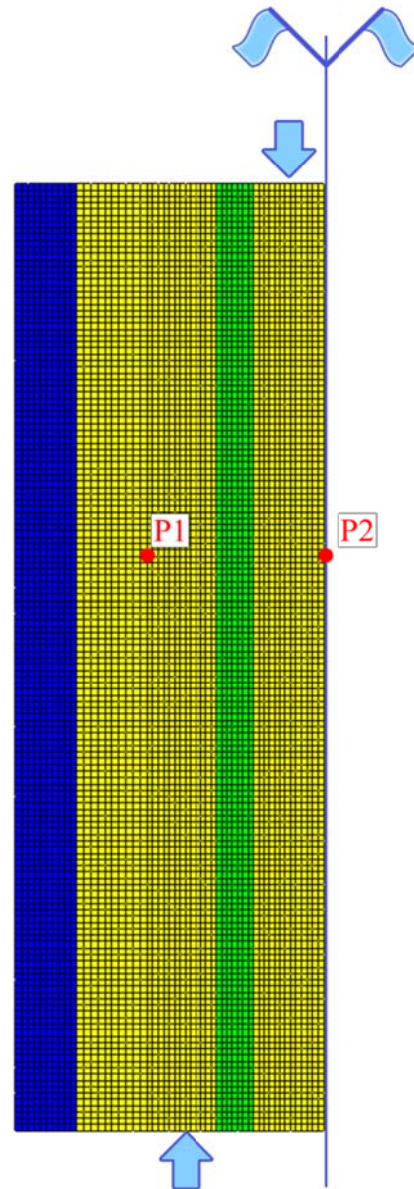
Figure 5.8 2D models of triplets with control points.

Table 5.8 Characteristics of 2D numerical models of triplets.

Model	Type of Elements	N. Points	N. Elements	$l_{ch,m}$ [m]	$l_{ch,b}$ [m]
TX-NHL-1.0_2D	quadrilateral	6868	6700	0.0020	0.0020
TX-NHL-0.6_2D	quadrilateral	6868	6700	0.0020	0.0020
TX-NHL-0.2_2D	quadrilateral	6868	6700	0.0020	0.0020
TX-NHL-0.0_2D	quadrilateral	6868	6700	0.0020	0.0020

The plane strain analysis on the same workstation described in previous section took about 5 minutes.

5.5.   Discussion and Comparison of the Numerical Results

This section presents the results of the numerical analyses for both BTs and triplets. The outcomes of these models are necessary to validate the accuracy of the integrated methodology applied to the *Continuum model* discussed in Section 4.4.2 for the analytical interpretation of the experimental laboratory tests.

5.5.1. *Brazilian Test on Cores with Inclined Diametral Mortar Joint*

The analyses ran on BT with both 2D and 3D models showed good agreement with the experimental failure observed.

The parasymmetric configuration of the BT is responsible of the initiation of damage in two opposite positions located on the mortar-brick interfaces, as discussed in the previous section. The increasing deformation given in the numerical simulation enlarges at each step the area subjected to damage, localized in a single layer of elements.

The nature of the problem suggests that the cracks arise from two opposite points over the brick-mortar interfaces, propagating parasymmetrically in the surrounding areas with a certain angle of inclination. Thus, two cracks grow parallel one respect to the other. Depending on the magnitude of the stresses involved, these cracks can connect each other in the centre of the mortar layer (Figure 5.9) or split the damage flow maintaining two parallel paths (Figure 5.11b).
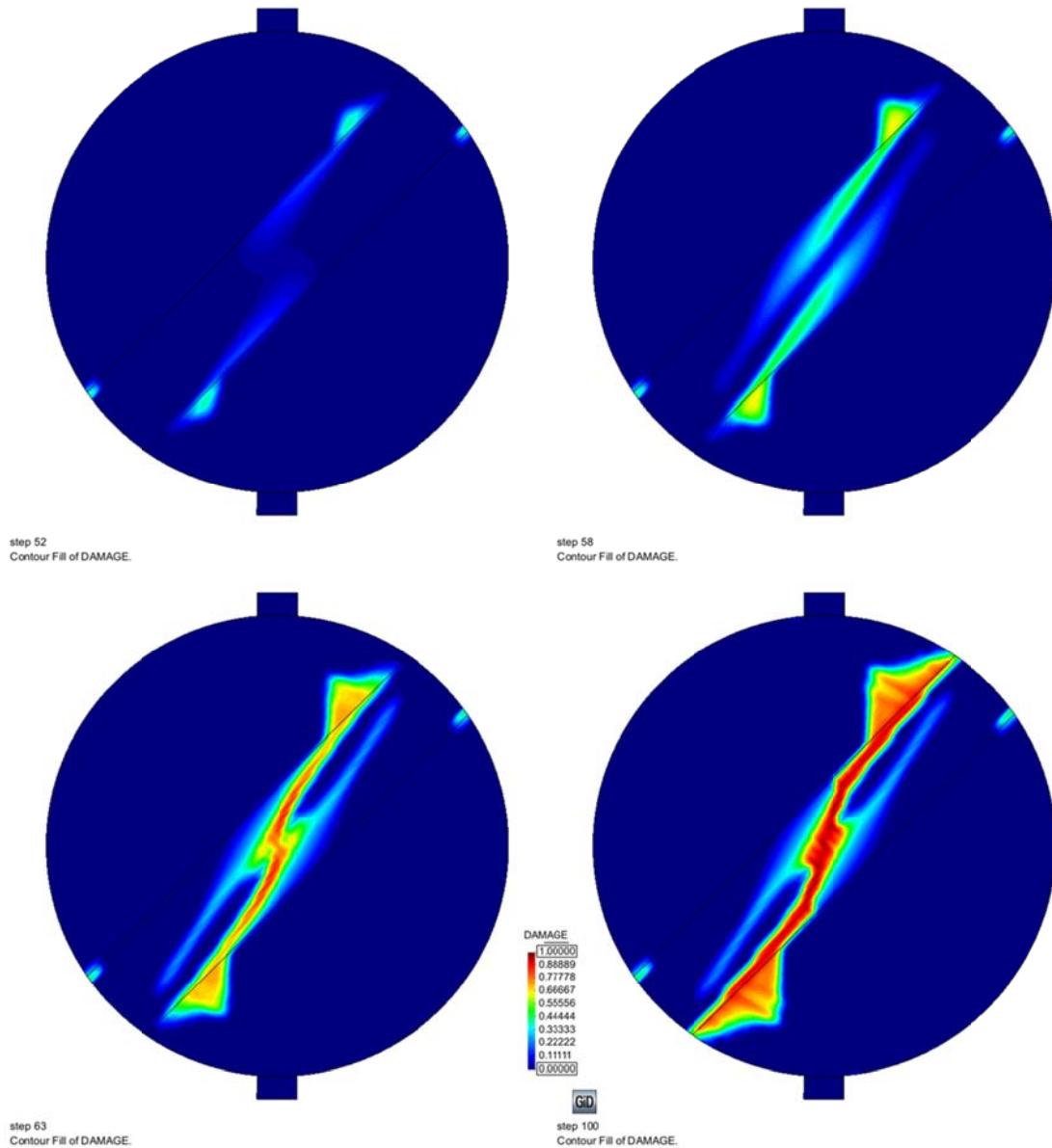
Figure 5.9 Damage contour of 1JC45M_2D model (step 4).

As noticeable in Figure 5.9, for low angles of inclination of the mortar joints, the damage starts in the units close to the mortar-units interfaces. The position can be identified approximately by connecting the loading support with the mortar layer in the orthogonal direction, as reported in Figure 5.10.
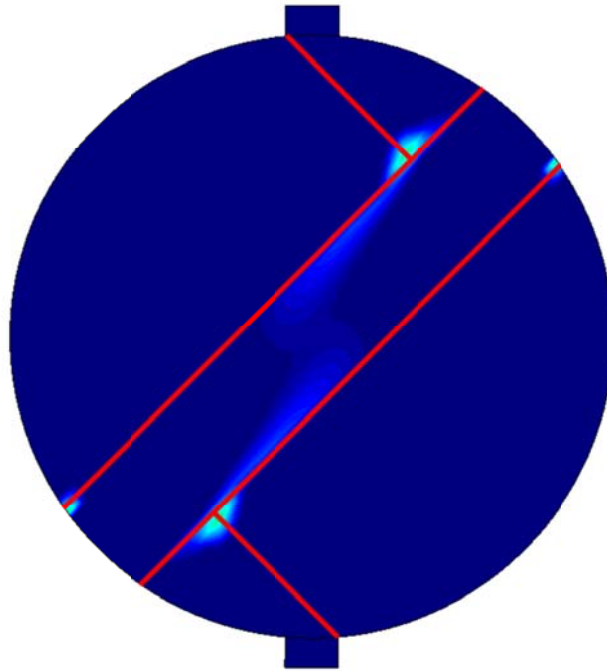
Figure 5.10 Damage initiation position for 1JC45M_2D (step 52).

On the other hand, for high angles of inclination of the mortar joint (e.g. 60º), the damage starts in the mortar very close to the specimen's centre (see Figure 5.11a). However, after few steps the cracks crosses the mortar joint connecting the opposite interfaces and reaching the same points obtained previously by connecting perpendicularly the loading support with the mortar layer (see Figure 5.11b).
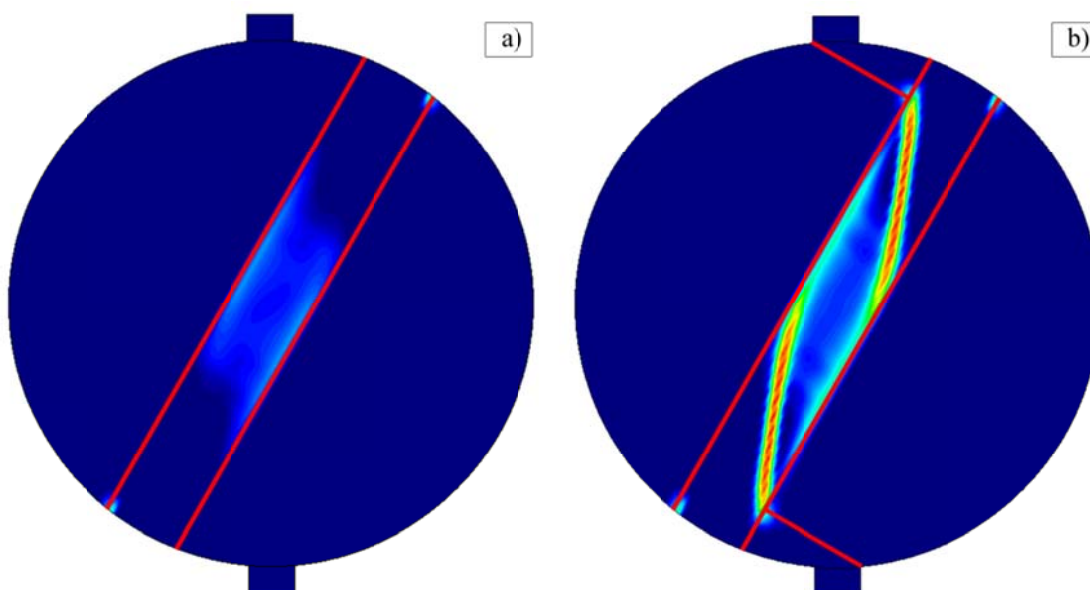
Figure 5.11 Damage initiation position for 1JC60M_2D (step 34) (a) and crack propagation in the units (step 41) (b).

The two opposite positions of damage in the interface are due to a concentration of tensile stresses in the units. The mutual interaction between mortar and units leads to a concentration of tensile stresses in these points. This phenomenon is justified by the Hilsdorf's theory (Hilsdorf 1969) reported in previous Chapter 4. In fact, those tensile stresses are related to the normal compressive stresses acting on the mortar joint.

For low angle of inclination of the mortar joint (e.g. 45º), the magnitude of the compression is rather high, and thus the tensile stress in the units. For this reason, the first elements that exhibited damage were located on the bricks. On the contrary, the failure of the units for high angle of inclinations appeared after the mortar.

The experimental results confirmed this mechanism, where for several specimens subjected to BT with mortar joint inclined at 45° the crack involved also an external unit's wedge as shown in Figure 5.12.

Figure 5.12 Experimental failure for BT with mortar joint inclined at 45°: unit's wedge separation.

As reported in Figure 5.12 and Figure 5.13, in the experimental tests the crack showed a particular shape, curved internally to the specimen. This phenomenon is due to a non-

constant state of stress over the third dimension that cannot be considered using 2D analyses.

Figure 5.13 Experimental failure for BT with mortar joint inclined at 55°: internal crack pattern.

In a FE model, the cracks can be identified by considering the tensile principal strain contour or the total displacement contour. In the three-dimensional models the physical representation of the third dimension allowed to evaluate the internal stress variation along the longitudinal axis of the core sample. For the most of the models the differences are barely visible comparing the external faces (Figure 5.14a) and the central cross-sections (Figure 5.14b), where the cross-fracture changes its inclination.
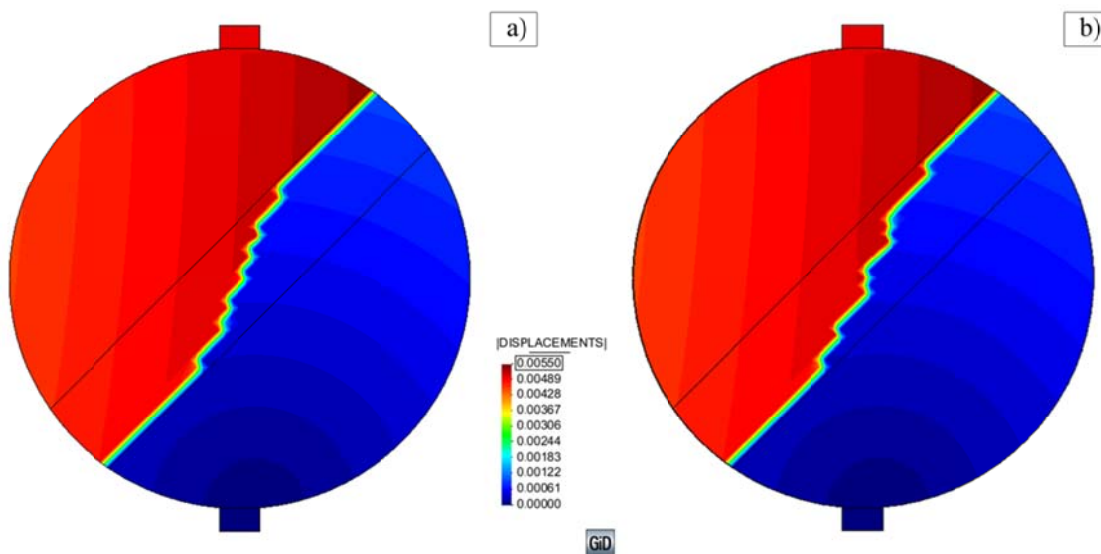
Figure 5.14 Displacement on 1JC45M_3D model: external face (a) and central cross-section (b).

On the contrary, 60° inclined models exhibited different locations of the crack in the external face (Figure 5.15a) and in the central cross-section (Figure 5.15b).
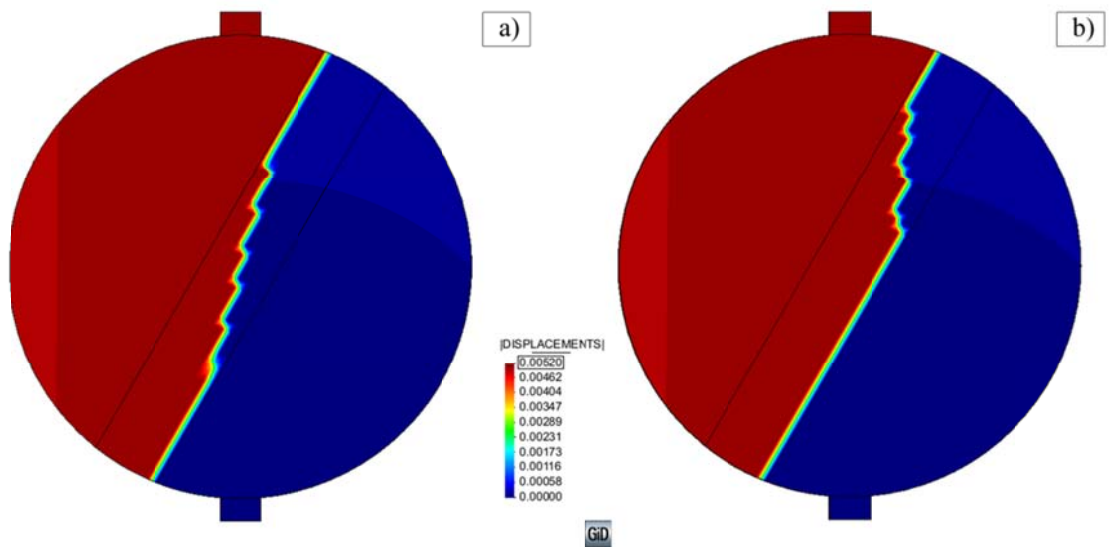
Figure 5.15 Displacements on 1JC60M_3D model: external face (a) and central cross-section (b).

Figure 5.16a shows the damage contour over the mid-section of the mortar joint. The two crack patterns join in longitudinal direction producing a characteristic Y shaped damage field. During the analysis, one of the two damage paths prevails on the other, increasing the strain locally in a single row of elements (see Figure 5.16b). Evaluating the contour of total displacements on the specimen, the fracture is clearly visible as a clear jump located in a row of elements (Figure 5.16c). The crack shape is consistent with the experimental one observed in Figure 5.13.
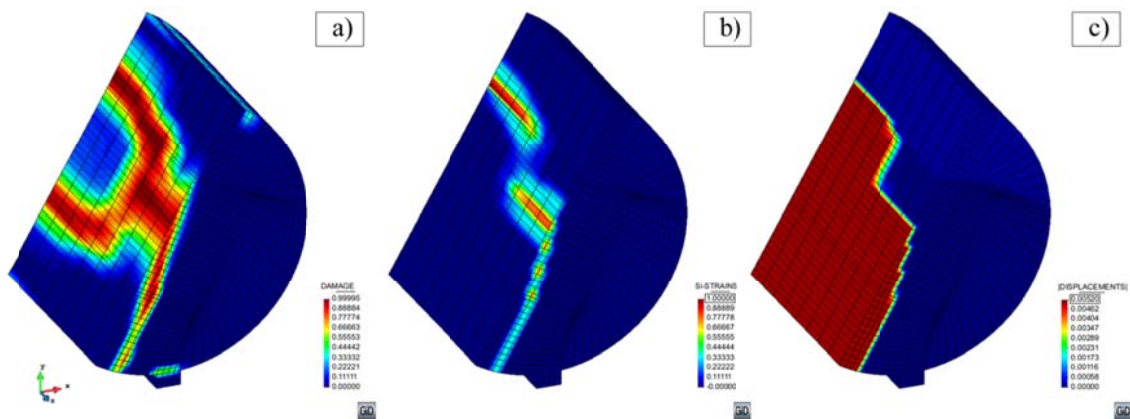
Figure 5.16 1JC60M_3D model mid-section of the mortar joint cut: damage distribution (a) principal tensile strain ε_I (b) and total displacements (c).

Concerning the 2D analyses, the results obtained are in good agreement with the 3D models. According with the models' boundary conditions, the crack patterns of the central cross sections for the 3D models agree with those obtained using plane strain models (Figure 5.17).

The only difference between 2D and 3D models can be noticed in the BT with mortar joint inclined at 60°. In fact, the crack in the 2D model occurred in a different location, if compared with the 3D model. As discussed above, the parasymmetry of the specimens could theoretically allow the formation of two distinct damage paths. However, one crack arises before the other in the numerical analysis and thus only one of the two possible cracks can be displayed by the model.
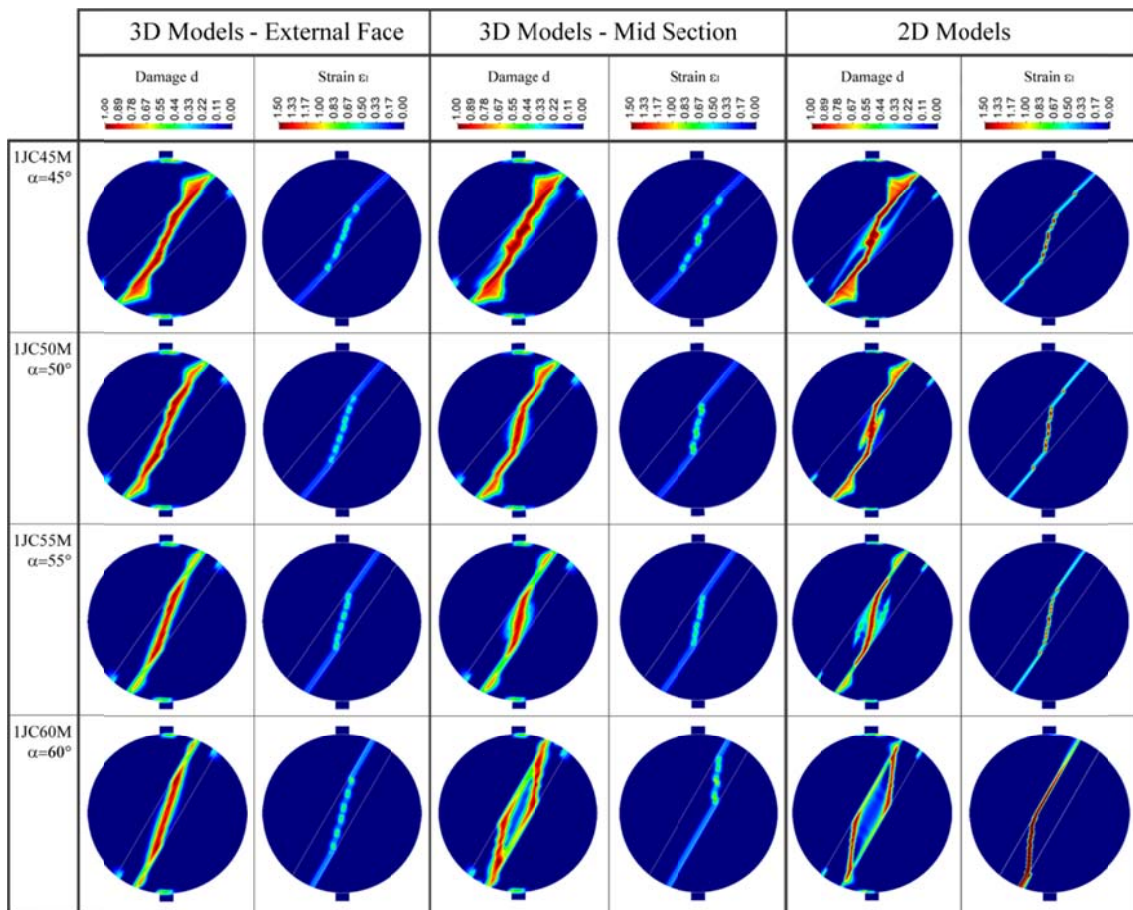
Figure 5.17 Numerical analyses results for 3D and 2D models for BT: damage and principal tensile strain ε_I contours.

The numerical analyses returned conservative values for the failure load in the range of -6÷-16% of the experimental one. It is important to underline that the higher differences observed were relative to the tests performed at inclinations of the mortar joint that

exhibited high scattered values (i.e. 45° and 60°). For 50° and 55° of mortar joint inclination the differences settles in a more appropriate range, confirming the good agreement of the interpretation methodology. The comparison between experimental and numerical results is reported in Table 5.9.

Table 5.9 Experimental and numerical ultimate load for BT with inclined diametral mortar joint.

α [°]	$F_{max,EXP}$ [kN]	$F_{max,2D}$ [kN]	% error	$F_{max,3D}$ [kN]	% error
45	14.23	12.60	-12%	11.92	-16%
50	11.57	10.78	-7%	10.38	-10%
55	9.44	8.84	-6%	8.73	-7%
60	8.54	7.56	-12%	7.50	-12%

Figure 5.18 shows the comparison of the load vs. relative displacement of the mortar joint obtained by the FE models and the corresponding experimental envelopes.
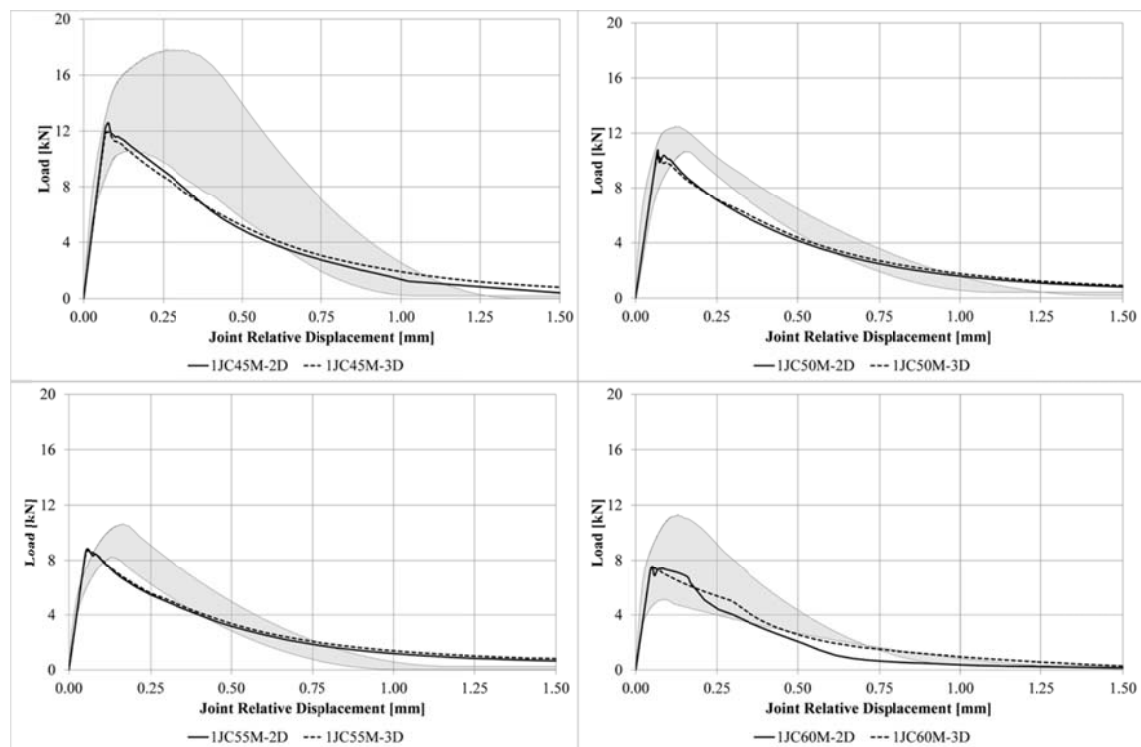
Figure 5.18 Load vs. joint relative displacement comparison between numerical analyses and experimental envelopes for BT with α=45° (a), α=50° (b), α=55° (c) and α=60° (d).

The estimation of the shear elastic modulus reported in Section 4.3.1 shows its reliability in the elastic part of the loading curves, where numerical and experimental results are almost superposed. However, the constitutive model chosen considers a

linear elastic behaviour for the material until failure, leading to an underestimation of the displacement at the peak load. Considering a nonlinear behaviour of the material also in the elastic branch by means of a hardening behaviour could grant a more correct estimation of the deformation of the joint at the peak load.

5.5.2. Triplet Shear Tests

Concerning the failure mode on triplets, it is possible to observe similar aspect of the BT failures. The cracks arise from the extreme parts of the mortar layer (i.e. close to the loading plates and base supports) and cross the joints propagating along the opposite interface (Figure 5.19). These intersections appeared very close to the loading areas, where the local force concentration led to a composite state of stress.

Figure 5.19 Experimental failure for triplets shear tests: internal crack formation.

The results of the numerical simulations are in good agreement with the experimental failures, as observed in the BT models. Contrary to the BT models, the damage is entirely located into the mortar joint for all the pre-compression levels, without affecting the units.

Figure 5.20 shows the damage contour progression during the analysis for the TX-NHL-1.0-2D model. The damage starts close to the loading area in the mortar-brick interface (step 38). After few steps (step 48), also the lower part of the mortar joint starts cracking with the same inclination of the first one. Step 53 represents the moment of the maximum bearing capacity of the specimen, after which both cracks spread on the mortar-unit interfaces (step 54). In the following steps, the two damage contours grow in opposite direction, involving at each step a larger amount of elements located on the two interfaces. The specimen exhibited a load capacity drop between steps 122 and 123. The elements of one interface are all involved by damage at step 123.
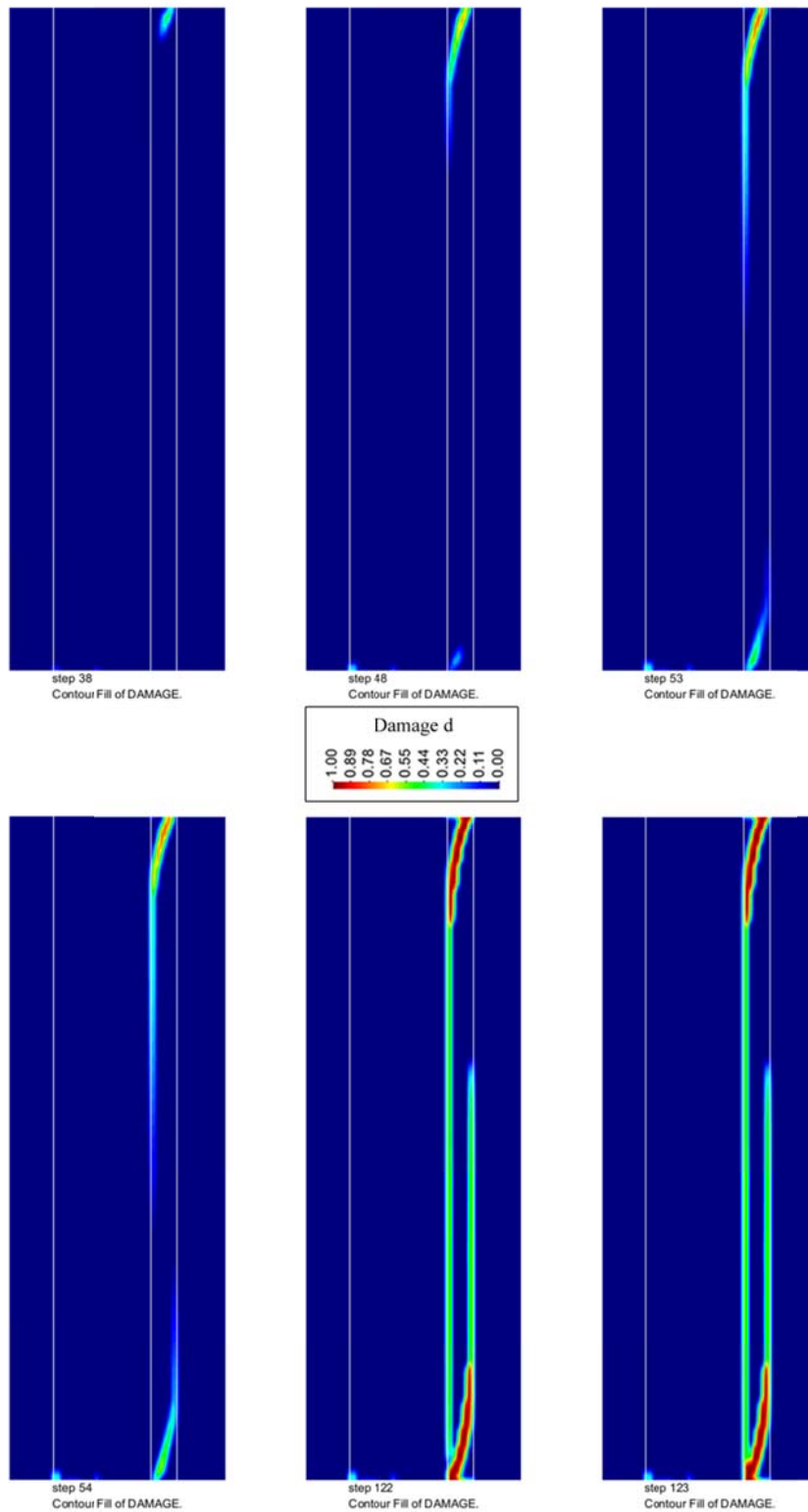
Figure 5.20 Damage contour for TX-NHL-1.0-2D at different steps.

The three-dimensional models were discretized using larger elements in order to reduce the computational costs. In the specific case of the triplet specimen without any pre-compression, this led to a different crack shape. The two damage patterns evolving on

the mortar-unit interfaces joined in the centre of the mortar joint, producing a further crossing crack in the model. However, the crack patterns of the 3D models resulted in remarkable agreement with those obtained in plane strain analyses. Figure 5.21 shows the comparison between 2D and 3D numerical results for damage and principal tensile strain contours.
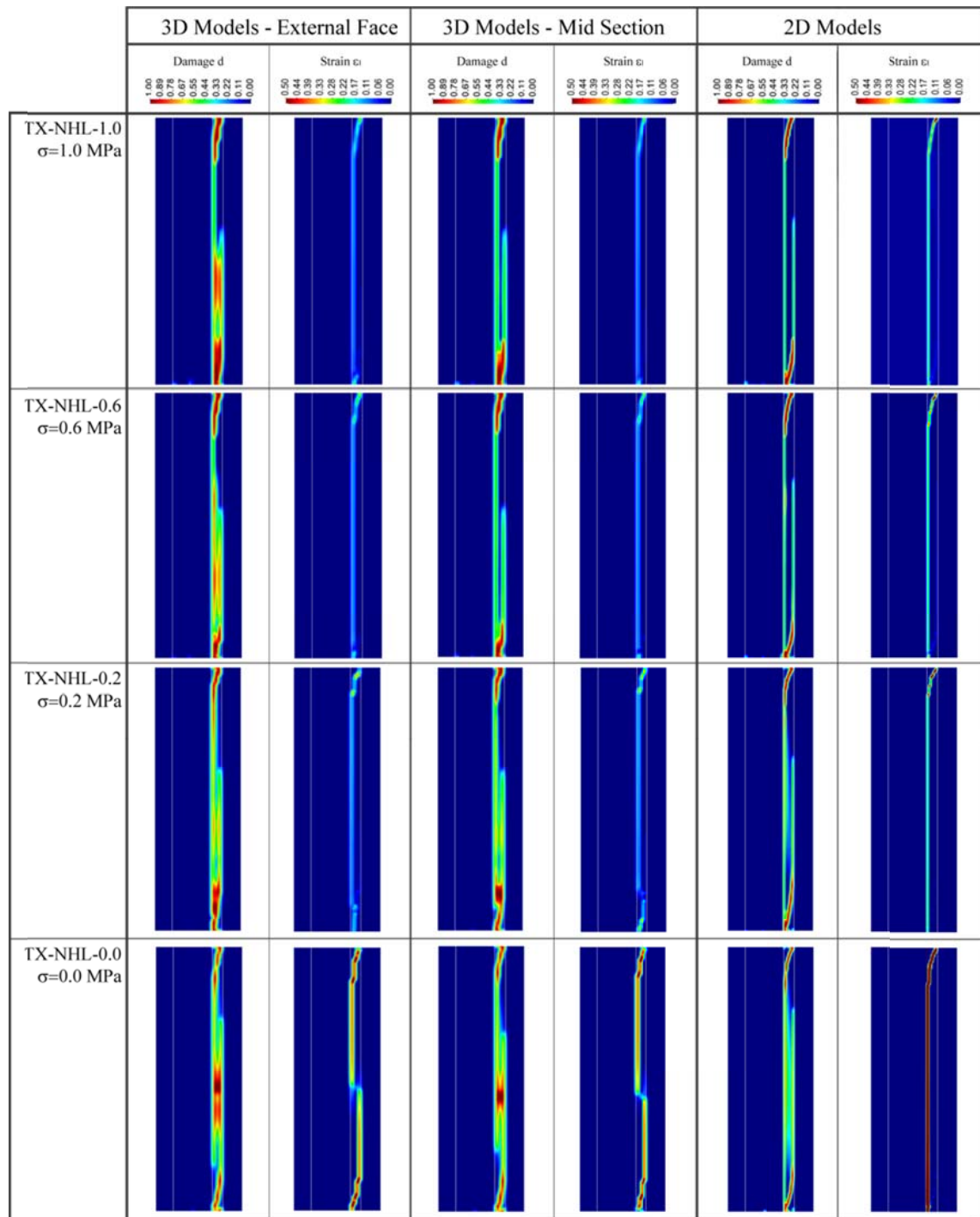
Figure 5.21 Numerical analyses results for 3D and 2D models of triplets: damage and principal tensile strain ε_I contours.

The numerical analyses returned different values of ultimate loads depending on the pre-compression levels. For 1.0 MPa, the numerical models underestimate the ultimate loads by around 15%. On the contrary, for 0.6 MPa the ultimate forces obtained from the models are completely in agreement with the experimental results. The experimental results for 0.2 MPa displayed non-simultaneous cracking of the two mortar layers as (Figure 4.30), returning lower values of maximum loads than the expected ones. The corresponding numerical models reported higher values of the ultimate shear load, confirming the problems already discussed in Section 4 about the experimental setup for 0.2 MPa of pre-compression. The maximum loads of experimental and numerical tests are reported in Table 5.10.

Table 5.10 Experimental and numerical ultimate loads for triplets tests.

σ_{max} [MPa]	$F_{max,EXP}$ [kN]	$F_{max,2D}$ [kN]	% error	$F_{max,3D}$ [kN]	% error
0.00	-	29.78	-	29.67	-
0.20	27.09	41.24	+52%	40.96	+51%
0.60	65.36	60.56	-7%	60.95	-7%
1.00	87.49	76.19	-13%	76.40	-13%

Figure 5.22 shows the comparison of the load vs. relative displacement of the mortar joint obtained by the FE models and the corresponding experimental envelopes.
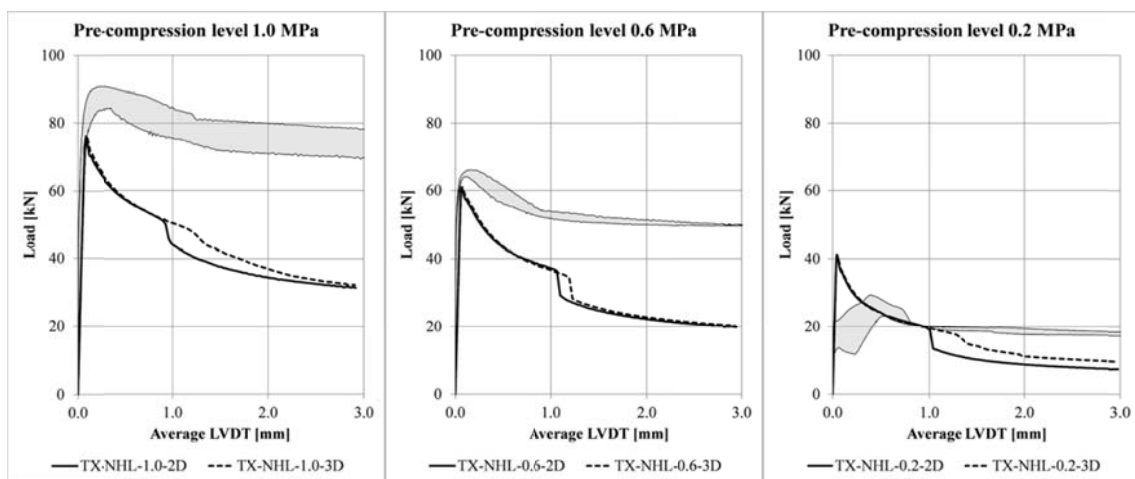
Figure 5.22 Numerical results compared to experimental tests for triplets.

While the numerical models yield with good approximation the estimation of the peak load, the softening branch cannot be represented correctly. The triplet test is characterised by a coupled frictional-cohesive behaviour until failure, where only

internal micro-cracks appear and thus the materials can be considered as continuous entities. In the numerical models, the onset of cracking was described correctly for all the pre-compression levels, confirming that the *Continuum Model* proposed in Section 4.4.1 provides reliable results in terms of ultimate strength capacity of the materials. Once the cracking phenomenon initiates with the appearance of macro-cracks, the residual mechanism is characterised experimentally by a pure frictional interface behaviour. The residual frictional angle is normally different than the initial friction angle used in the continuum damage model (Lourenço 1996). Due to the simple format of the nonlinear constitutive model adopted in the present research, the residual strength exhibited by the experiments cannot be reproduced by the numerical analyses. More sophisticated models should be necessary for a more precise description of the nonlinear behaviour of the triplet samples, that is governed by the residual frictional angle of the material.

Chapter 6. Conclusions

6.1. Summary

The preservation of existing masonry constructions, and in particular those pertaining to the built cultural heritage, is still a challenging task. The experimental characterisation of these buildings requires considerable knowledge about their structural health, but it is always necessary to minimize the damage during the inspection activities.

This research represents an original contribution to the investigation procedures aimed at the assessment of the existing masonry buildings. Both standard and non-standard minor destructive techniques have been analysed, providing further improvements concerning the execution of the tests and the post processing of the experimental results.

Chapter 1 has provided an introduction and the objectives of the research.

Chapter 2 has presented a brief overview of the current masonry standards in the European Union both for new masonry and for the assessment of historical masonry. Most of the available standards for masonry characterisation are addressed to new constructions. They usually refer to masonry structures composed of fired-clay units and cement/lime mortars produced according to strict guidelines concerning their composition and their manufacturing. The industrial production process of realisation leads to materials with standardised features and very small differences between elements' behaviours.

Structural members composed by different kinds of units and binders are very common in historical masonry, and they can be even deteriorated by environmental factors.

Hence, the mechanical characterisation of these materials should not be carried out referring to the standards for new constructions. The few standards related to the assessment of existing masonry provide different techniques for the mechanical investigation. The available testing techniques are classified depending on the amount of damage caused by the inspection, i.e. Destructive Testing (DT), Minor-Destructive Testing (MDT) and Non-Destructive Testing (NDT). The state-of-the-art on the available experimental approaches has focused on the emerging MDT techniques, such as the in-situ penetrometric test and the extraction of core samples to be tested in the laboratory. These methodologies has showed to be suitable for historical buildings, since they can provide reliable results while producing limited damages on the investigated part of the structure.

A state-of-the-art of available numerical analyses for the assessment of existing masonry has been also presented. Micro modelling is probably the most sophisticated tool to analyse the real behaviour of the material, particularly concerning its local response at the level of constituents. It leads to very accurate results, but it requires an intensive computational effort. For the particular purpose of this research, we have focused on micro-scale models for the investigation of the laboratory tests developed during this study. The constitutive law adopted in these models is based on *Continuum Damage Mechanics*, which provides a powerful and general framework for the derivation of consistent material models suitable for engineering applications.

Chapter 3 presents the development of a novel MDT instrumentation. The X-Drill system is based on the field vane test used for soils. It consists in a four-winged pin to be inserted in the material to investigate. A torque is then applied to the pin through a torque wrench, recording the maximum value at failure. A previous research on the X-Drill proposed a simple empirical calibration based on a simple linear regression between standard compressive strength of the mortar and the maximum torque measured. In this research, the original format of the system has been enriched making important improvements on its geometrical properties in order to reduce the uncertainties of the results. An analytical theory has been also developed based on the local stress in the contact area between the pin's wings and the mortar, leading to a linear correlation depending on the geometrical properties of the instrument and on the mechanical parameters of the material investigated. Finally, the instrument has been calibrated in the laboratory using a large set of mortar specimens with different compressive strengths. The correlation between maximum torque and compressive

strength using a linear regression has shown a high coefficient of determination, confirming the reliability of a linear correlation rule. Moreover, the resulting parameters of the linear regression compared to those found using the analytical model returned rather comparable values for realistic ranges of the mechanical properties of the mortar. Chapter 4 has presented a large experimental campaign carried out on core samples extracted from historical-like masonry walls. The experimental campaign has included also the analysis of standard specimens prepared according to the relevant standard for compression, flexural and shear tests. The extraction has been carried out using a novel dry coring technique. This novel technique has revealed to be more suitable than the water-cooled coring, since in historical structures the water used for the cooling of the bit can spoil the mortar joints usually constituted by poor material. The samples were core drilled from the walls to be subject to the Brazilian Test (BT) with inclined mortar joint. This kind of test induces a composite state of stress of compression-shear on the mortar joint. The cored walls were dismantled to extract mortar joint specimens for Double Punch Test (DPT). While the standard tests are not feasible in the case of the assessment of existing buildings, both the BT and DPT show to be suitable for real experimental campaigns on existing structures. The BT setup has been enhanced by introducing LVDTs on both circular faces, measuring the relative displacement of the two semi-cylindrical brick parts. This solution has provided further information about elastic and nonlinear properties of the mortar. The outcomes of the BT and the DPT have been combined using a three-dimensional state of stress representation (i.e. Mohr's Circles), resulting in a more precise estimation of the failure envelope. The resulting compressive, tensile and shear strengths obtained by the failure envelope have been compared with those from the standard tests, confirming the good agreement of the results.

Chapter 5 has presented the numerical validation of the results obtained in the previous Chapter 4. 2D and 3D FE analyses have been carried out, using a constitutive model based on Continuum Damage Mechanics. The constitutive law of isotropic continuum damage can represent the softening behaviour of the material through a single scalar parameter. The degradation of the material's capacity occurs for either compression, tension or shear actions. Since the tests modelled have involved mainly tension and shear failure in the mortar, the isotropic continuum damage model has been used. In particular, the samples tested have been modelled using micro-models, i.e. the units and

the mortar have been defined separately using the parameters obtained by the previous experimental activity.

6.2.   Main Contributions

6.2.1. Penetrometer for in-situ MDT

Concerning the novel penetrometer developed, the technical improvements are aimed at reducing the uncertainties in the measurements. The original version of the X-Drill (Christiansen 2011) has been improved in this research by means of further details on the shape of the pin, making the technique more appropriate for the analysis of existing historical mortars. The principal modifications introduced are:

- reduction of the diameter of the pin's cross section from 10 mm to 9 mm, allowing to insert it into thinner mortar joints;
- definition of the wings length L_w=15 mm, for a better standardisation of the penetration depth;
- reduction of the body's diameter from 10 mm to 6.5 mm, allowing the X-Drill to penetrate deeper into the mortar joint.

A theoretical model has been proposed to interpret the results of the novel penetrometric test. It is based on plane-stress assumption at the contact section between the instrument's wings and the mortar. The torque applied by the instrument induces the formation of tangential stresses along the failure surface (identified as the circumscribed circle at the pin's cross section), as well as normal stresses over the wing's contact section. Due to the material surrounding the loaded area, it is possible to assume a constrained condition of the mortar in the radial direction, producing a confinement effect on the investigated mortar. The resulting state of stress can be represented by a Mohr's circle on the σ-τ plane, allowing the evaluation of the corresponding Mohr-Coulomb failure surface.

The interpretation model has been validated by a wide experimental dataset. The analytical predictions have been compared with the experimental results obtained in the laboratory. Penetrometric and compressive tests were executed on cubic specimens built using different types of mortars. Each mortar was characterised by a different mixture

of components in order to obtain a rather wide range of compressive strengths. The results obtained can be summarised as follows:

- The proposed theoretical model is based on the local failure of the mortar located in the contact zone with the instrument's wings. The correlation rule between the measured torque and the compressive strength of the mortar is reduced to a linear law, where the slope depends on the geometric parameters of the instrument, the assumed Poisson's ratio of the mortar and the friction angle;

- the dependency of the correlation factor on the Poisson's modulus in a realistic range of values shows rather low sensitivity, reducing the bias introduced by the uncertain evaluation of the Poisson' modulus.

- concerning to the experimental results, a linear regression gives high value of the coefficient of determination (R^2=0.958), confirming the linear law as a reliable model to express the relationship between the compressive strength and the torque measured by the X-Drill test;

- The proposed interpretation model and the relative experimental results are in good agreement for realistic values of the Poisson's ratio. For v_m=0.30 the model shows high accuracy for mortars having f_c<2.0 MPa, and returns conservative values for higher resistance mortars. Reducing the Poisson's modulus, the model gets closer to the experimental strengths for higher resistance mortars and overestimates the strengths of lower resistance mortars.

- The proposed in-situ MDT technique has shown its suitability as a complementary test to laboratory destructive ones, in order to reduce invasive inspection activities on masonry historical buildings.

6.2.2. Laboratory Tests for MDT

The second part of this work has focused on the laboratory tests performed on extracted specimens. The proposed methodology of interpretation combines the outcomes of different tests (i.e. BT, DPT and triplets) into an integrated procedure for the definition of the failure criterion of the mortar. The following conclusions can be drawn on the basis of the results obtained from the aforementioned tests:

- The dry extraction performed in the experimental program has shown to be more suitable for historical masonry than the water-cooled drilling, since weak mortars are often present and the water may spoil the specimen. None of the specimens was

damaged during the dry core drilling of the walls. The novel dry extraction procedure seems a reliable option for sampling, even from the interior of existing buildings.

- The novel experimental setup developed for the BTs with inclined mortar joint has afforded an estimation of the mortar's shear elastic modulus, besides the strength parameters. This estimation has been made possible by the use of displacement control via the LVDTs placed on both faces of the specimens. An estimation of G_m=154 MPa has been obtained by considering the secant value at 30% of the maximum load.

- The vertical displacement control used for the Brazilian Tests combined with a high sampling rate of the acquisition control unit (50 Hz) has allowed recording part of the softening branch during the tests. However, the high fragility of the failure mechanism has caused a loss of data during the descending branch of the loading curves. An interpolation of the lost data has been carried out by means of a quadratic function, allowing having a full description of the softening behaviour of the mortar joint under shear actions.

- The Brazilian tests were performed at different inclinations of the diametral joint (45°, 50°, 55° and 60°), inducing different combinations of shear and compression to the mortar. The specimens exhibited a characteristic "parasymmetric" failure in most of the cases, with a fracture crossing the mortar joint and involving the two opposite brick-mortar interfaces. The results have shown that for $\alpha \geq 45°$ the crack starts in the mortar layer, sometimes involving small parts of the brick near the loading area, confirming previous results by the authors (Pelà et al. 2015).

- The triplets tests were performed at different pre-compression levels of 0.2 MPa, 0.6 MPa and 1.0 MPa, according to the reference standard (EN 1052-3:2002 2002). The specimens' failure was mainly located at the interface between mortar and unit, except for the external parts of the joints close to the loading area and to the supports, where the cracks cross the joint to the opposite interface. The results have shown that for 0.2 MPa of pre-compression the samples exhibited a non-simultaneous cracking of the two joints, returning non-reliable values of ultimate load. For this reason, these tests have been discarded from the analyses.

- The compressive strength obtained from the DPTs (2.71 MPa) resulted 10% higher than that obtained from standard compression tests on mortar prisms (2.45 MPa),

due to the confinement induced by the external material surrounding the loaded area and exerted by the punches over the flat specimen.

The interpretative theories proposed in (Pelà et al. 2015; Marastoni et al. 2016), i.e. *continuum model* and *interface model*, have been used to process the results from the experimental program and to provide realistic estimations of mortar's mechanical parameters. The main outcomes from the two models, as well as the main novelties introduced by the present study, are summarized below:

- The *continuum model* has been improved with a more refined micromechanical interpretation of the triaxial stress states in the samples at failure. This has allowed a more precise representation of the Mohr's circles of the experimental test on the σ-τ plane. As for the BT and triplets, the Hilsdorf's theory has been considered to estimate the horizontal confining stress in the mortar, providing a value around the 40% of the transversal compression. As for the DPT, the horizontal confining stress has been estimated using the FEM, providing a conventional value around the 5% of the vertical compression. The introduction of the confinement components has improved remarkably the definition of the Mohr's circles for BTs, triplets and DPTs. Another novel improvement to the *continuum model* has been the adoption of a Mohr's parabolic failure criterion. It has been adjusted using a least square method applied to the Mohr's circles obtained from the experimental tests. The parameters of the Mohr's parabolic failure envelope for BTs and DPTs resulted σ_0=0.34 MPa and τ_0=0.62 MPa in the present experimental campaign. The nonlinear envelope has been also simplified using a linear Mohr-Coulomb criterion with tension cut-off, whose constitutive parameters are c=0.62 MPa, φ=33.11° and $f_{tm,CUT}$=0.34 MPa. The compressive strength has been derived using the Mohr-Coulomb theory as f_{cm}=2.30 MPa.

- The integrated methodology applied to the triplets tests and DPTs has shown remarkable agreement with that calculated with BTs and DPTs. The resulting parabolic failure envelope is characterised by σ_0=0.34 MPa and τ_0=0.63 MPa , almost superposed to those obtained from BTs and DPTs. The linearization of the parabolic envelope has led to consistent results, being the constitutive parameters obtained c=0.63 MPa, φ=33.18° and $f_{tm,CUT}$=0.34 MPa.

- The *interface model* considers the mortar joint as a two-dimensional interface, with the thickness of the joint collapsed in its central section. The state of stress is represented as a point instead of a circle on the σ-τ plane, excluding the possibility of

integrating the DPTs results in the calculation of the failure envelope. Using the points from the sole BTs, a linear Mohr-Coulomb failure envelope has been calculated using a linear regression with C=0.32 MPa and Φ=32.32°.

- As for the triplets results, the *interface model* has reported similar results compared to those obtained by the BTs. The linear regression of the points representing the state of stress of the triplets at the failure moment has returned as parameters C=0.36 MPa and Φ=32.61°.

- The proposed MDT techniques and their interpretation theories have shown their suitability for the experimental activities of mechanical characterisation of historical masonry of the built cultural heritage. The proposed sampling technique can ensure limited invasivity to the existing structure. The novel integrated methodology for the processing of DPTs and BTs has shown good reliability and robustness.

6.2.3. *Numerical modelling of laboratory tests*

The validation of the integrated methodology has been carried out using linear and nonlinear analyses on 2D and 3D FE models. The constitutive law used for the nonlinear analyses is an isotropic damage model, based on the *Continuum Model* parameters obtained from the combination of BTs and DPTs.

The principal results derived from the numerical analyses of BTs are summarised below:

- The linear elastic analyses carried out on BT models have confirmed the good approximation of the state of stress on the mortar joint calculated with the analytical formulas adopted in previous works (Braga et al. 1992; Benedetti et al. 2008; Pelà et al. 2012). The estimation of the confinement stresses in the mortar joints by means of the Hilsdorf's theory (Hilsdorf 1969) have been also confirmed as a good estimation method, returning consistent results compared with the elastic FE models.

- The nonlinear analyses carried out on BT models have provided results in good agreement with the experimental ones, both in case of 2D and 3D models. The cracks' patterns and their evolutions at each step of the analyses fully agreed with the experimental fractures. The three-dimensional models have shown their capability to represent internal variations of the crack patterns, displaying realistic fracture's shapes in agreement with the experimental evidence. The 2D models have provided a good estimation of the cracking phenomena relatively to the central cross-section of the specimens.

- The load vs. displacement curves obtained by the 2D and 3D nonlinear analyses have resulted in agreement with the experimental ones. All the BT models have lost more than 95% of their bearing capacity in the first 1.50 mm of relative displacement of the joints like in the experimental case, with a comparable descending trend.

- The numerical failure loads of the BT with inclined mortar joint have returned slightly conservative values if compared with the experimental results, confirming the integrated methodology of interpretation of the laboratory tests as a reliable strategy for the evaluation of the mortar behaviour.

The outcomes from the numerical simulations of triplet tests are summarised below:

- The 2D and 3D nonlinear analyses have provided cracks' patterns in agreement with the experimental fractures. The larger finite elements used in the 3D mesh in order to limit the computation effort has led to different results in some specimens.

- The numerical failure loads of the triplet tests have returned slightly conservative values if compared with the experimental results, confirming the integrated methodology of interpretation of the laboratory tests as a reliable strategy for the evaluation of the mortar behaviour.

6.3.   Suggestions for future work

The penetrometric method proposed in this doctoral thesis gives room for possible developments of the experimental technique, as for the execution of the test and for the proposal of more sophisticated interpretation theories. The following aspects seem worthy of future work:

- The calibration of the proposed penetrometric method could be improved by considering a wider range of strengths for the tested mortars.

- Besides the comparison of the penetrometer readings with the compressive strengths derived from cube specimens, it could be interesting to investigate further comparisons between the penetrometric estimations and other types of laboratory tests, like DPT on mortar joints extracted from the same walls tested with the X-drill.

- New optimized shapes of the pin could be proposed in order to obtain more reliable results and reduce the experimental scattering. Also, torque wrench with digital display could be adopted to improve the precision of the reading.

- The analytical interpretation rule proposed in this work depends on the geometric properties of the penetrometer and on the elastic parameters of the mortar. Further experimental investigations should be necessary to get more precise correlation rules.

- Other possible models for the interpretation of the X-drill method could be proposed, using other theoretical frameworks like fracture mechanics, plasticity or limit analysis.

- Further experimental campaigns could be carried out in order to investigate the possible causes of the appearance of an initial bias M_0 on the reading of the torque during the test execution. Appropriate measures should be carried out in order to limit the effects of this phenomenon and to improve the precision of its evaluation.

The experimental campaign carried out on core samples and joint specimens extracted from the walls has provided promising results that could be further complemented with the following studies:

- More combinations of material components could be explored in the laboratory, in order to enlarge the experimental database for a better calibration of the MDT technique.

- Besides the comparison between BT on core samples and shear tests on triplets, it would be interesting a comparison with other experimental tests aimed at evaluating the shear behaviour of mortar, like shear tests on couplets or diagonal compression tests on wallets.

- It would be interesting to carry out a comparison between the results from BT of core samples and those from the in-situ shear-jack test.

- The evaluation of the tensile strength of mortar from flexure tests should be investigated better, since the available standards (fib 2013; EN 1992-1-1:2005 2005; D.M. 14/01/2008 2008) provide different empirical formulas yielding very different results.

As for the numerical simulation of the MDT experimental technique, the following suggestions for future work can be presented:

- Carrying out numerical analyses with improved constitutive laws, like those including the effect of both initial and residual friction behaviour of the material. This improvement would provide numerical results more realistic and more in agreement with those obtained from experimental tests on triplets.

- Comparing the numerical results obtained in this work with those derived from other micro-modelling strategies. For example, simplified micro-modelling could be used, i.e. replacing the whole mortar joint with an interface element. Another alternative could be the use of detailed micro-modelling, i.e. introducing the discretization of both the mortar joint by continuum elements and the brick-mortar discontinuity by interface elements.

References

ACI Committee 228, 2004. *Nondestructive Test Methods for Evaluation of Concrete in Structures*,

ASTM C1196, 1991. Standard Test Method for In Situ Compressive Stress Within Solid Unit Masonry Estimated Using Flatjack Measurement. *ASTM International*.

ASTM C1197, 1991. Standard Test Method for In Situ Measurement of Masonry Deformability Properties Using the Flatjack Method. *ASTM International*.

ASTM C803, 2010. Standard Test Method for Penetration Resistance of Hardened Concrete. *ASTM International*.

ASTM E837, 2008. Determining Residual Stresses by the Hole-Drilling Strain-Gage Method. *ASTM International*.

Baronio, G., Binda, L. & Saisi, A., 1995. Analisi di Malte Antiche e Comportamento di Malte Riprodotte in Laboratorio. In *7° Convegno Nazionale - L'ingegneria Sismica in Italia*. Siena, Italy, pp. 267–276.

Bažant, Z.P. & Oh, B.H., 1983. Crack band theory for fracture of concrete. *Matériaux et Constructions*, 16(3), pp.155–177. Available at: http://link.springer.com/10.1007/BF02486267.

Benedetti, A. & Pelà, L., 2012. Experimental Characterization of Mortar By Testing on Small Specimens. In *15th International Brick and Block Masonry Conference*. Florianópolis, Brazil.

Benedetti, A., Pelà, L. & Aprile, A., 2008. Masonry Properties Determination Via Splitting Tests on Cores With a Rotated Mortar Layer. In *8th International Seminar on Structural Masonry*. Instanbul, Turkey.

Bilello, C. et al., 2007. Experimental Tests and Theoretical Issues for the Identification of Existing Brickwork. In *10th North American Masonry Conference*. St. Louis, Missouri, USA, pp. 964–974.

Binda, L. et al., 1999. Investigation On Materials And Structures For The Reconstruction Of The Partially Collapsed Cathedral Of Noto (Sicily). In C. A. Brebbia & W. Jager, eds. *6th International Conference Structural Studies*. Dresden, Germany: WIT Press, pp. 323–332. Available at: http://www.witpress.com/elibrary/wit-transactions-on-the-built-environment/42/5622.

Binda, L. et al., 1994. Measuring Masonry Material Properties. In D. . Abrams & G. M. Calvi, eds. *U.S.-Italy Workshop on Guidelines for Seismic Evaluation and Rehabilitation of Unreinforced Masonry Buildings*. Pavia, Italy, pp. 326–347.

Binda, L. & Tiraboschi, C., 1999. Flat-Jack Test: A slightly destructive technique for the diagnosis of brick and stone masonry structures. *International Journal for Restoration of Buildings and Monuments*, 5(5), pp.449–472. Available at: http://www.stru.polimi.it/home/binda/lav246.PDF.

Binda, L., Tiraboschi, C. & Baronio, G., 2003. On-site investigation on the remains of the Cathedral of Noto. *Construction and Building Materials*, 17(8), pp.543–555. Available at: http://linkinghub.elsevier.com/retrieve/pii/S0950061803000576.

Borri, A. et al., 2011. Shear behavior of unreinforced and reinforced masonry panels subjected to in situ diagonal compression tests. *Construction and Building Materials*, 25(12), pp.4403–4414. Available at: http://dx.doi.org/10.1016/j.conbuildmat.2011.01.009.

Braga, F. et al., 1992. A test method to assess the shear strength of existing masonry structures - Theoretical basis and first experimental results. In *International Workshop CNR-GNDT "Effectiveness of Injection Techniques for Retrofitting of Stone and Brick Masonry Walls in Seismic Areas."* Milan, Italy, pp. 204–227.

Brencich, A., Corradi, C. & Sterpi, E., 2004. Experimental Approaches to the Compressive Response of Solid Clay Brick Masonry. In *13th International Brick and Block Conference*. Amsterdam, NL, pp. 1–10.

Brencich, A. & Sabia, D., 2008. Experimental identification of a multi-span masonry bridge: The Tanaro Bridge. *Construction and Building Materials*, 22(10), pp.2087–2099.

Brencich, A. & Sterpi, E., 2006. Compressive Strength of Solid Clay Brick Masonry :

Calibration of Experimental Tests and Theoretical Issues. In P. B. Lourenço et al., eds. *Structural Analysis of Historical Constructions*. New Delhi, India, pp. 757–766.

Brignola, A. et al., 2008. Identification of Shear Parameters of Masonry Panels Through the In-Situ Diagonal Compression Test. *International Journal of Architectural Heritage*, 3(1), pp.52–73. Available at: http://www.tandfonline.com/doi/abs/10.1080/15583050802138634.

Cervera, M. et al., 2010. A crack-tracking technique for localized damage in quasi-brittle materials. *Engineering Fracture Mechanics*, 77(13), pp.2431–2450. Available at: http://dx.doi.org/10.1016/j.engfracmech.2010.06.013.

Cervera, M., 2003. *Viscoelasticity and rate-dependent continuum damage models*, Barcelona, Spain. Available at: https://www.researchgate.net/profile/Miguel_Cervera/publication/270271792_Viscoelasticity_and_Rate-Dependent_Continuum_Damage_Models/links/54a3da1c0cf256bf8bb14203.pdf.

Chen, W.-F. & Han, D.-J., 1988. *Plasticity for Structural Engineers*, New York, USA: Springer-Verlag New Yotk Inc.

Christiansen, P.D.V., 2011. In Situ Determination of the Compressive Strength of Mortar Joints Using an X-Drill. *Masonry International*.

CIMNE, 2002. COMET: Coupled Mechanical and Thermal Analysis. , pp.1–182. Available at: http://www.cimne.com/comet.

Circolare 02/02/2009 n. 617, 2009. Istruzioni per l'applicazione delle "Norme tecniche per le costruzioni" di cui al D.M. 14 gennaio 2008.

Colla, C., 2009. Diagnosi di elementi strutturali lignei e murari mediante tomografia sonica: esempi applicativi per la valutazione dello stato di conservazione di beni storico-culturali. In *13° Congresso AIPnD, Conferenza nazionale sulle prove non distruttive monitoraggio diagnostica*. Rome, Italy, p. 11.

Colla, C. et al., 2011. Experimental Studies by Combined NDT fo Capillary Rise Monitoring in Masonry Specimens. In M. Krüger, ed. *European Workshop on Cultural Heritage Preservation EWCHP-2011*. Berlin, Germany: Fraunhofer IRB Verlag, pp. 131–139.

Colla, C., 2003. Non-Destructive Evaluation of Brick Masonry via Scanning Impact-Echo Testing. In *9th North American Masonry Conference*. Clemson, South Carolina, USA: The Masonry Society, pp. 954–965.

Colla, C. et al., 2008. Thermography investigations of roman archaeological masonry. In L. Binda, M. Di Prisco, & R. Felicetti, eds. *RILEM Symposium on On Site Assessment of Concrete, Masonry and Timber Structures*. Varenna, Italy: RILEM Publications S.A.R.L., pp. 923–932.

Corradi, M., Borri, A. & Vignoli, A., 2003. Experimental study on the determination of strength of masonry walls. *Construction and Building Materials*, 17(5), pp.325–337. Available at: http://linkinghub.elsevier.com/retrieve/pii/S0950061803000072.

D.M. 14/01/2008, 2008. Approvazione delle nuove norme tecniche per le costruzioni.

DIN 18555-9:1999, 1999. Testing of mortars containing mineral binders - Part 9: Hardened mortars. Determination of the mortar compressive strength in the bed joint.

Drdácký, M., 2011. Non-Standard Testing of Mechanical Characteristics of Historic Mortars. *International Journal of Architectural Heritage*, 5(4-5), pp.383–394. Available at: http://www.tandfonline.com/doi/abs/10.1080/15583051003717788.

EN 1015-1:1999, 2007. Methods of test for mortar for masonry - Part 1: Determination of particle size distribution (by sieve analysis).

EN 1015-11:2007, 2007. Methods of test for mortar for masonry - Part 11: Determination of flexural and compressive strength of hardened mortar.

EN 1052-3:2002, 2002. Methods of test for mortar masonry - Part 3: Determination of inicial shear strength.

EN 12390-13:2013, 2013. Testing hardened concrete - Part 13: Determination of secant modulus of elasticity in compression.

EN 12504-1:2009, 2009. Testing concrete in structures - Part 1: Cored specimens. Taking, examining and testing in compression.

EN 197-1:2011, 2011. Cement - Part 1: Composition, specifications and conformity criteria for common cements.

EN 1992-1-1:2005, 2005. Eurocode 2: Design of concrete structures - Part 1-1: General rules and rules for buildings.

EN 1996-1-1:2005, 2005. Eurocode 6: Design of masonry structures – Part 1-1: General rules for buildings – rules for reinforced and unreinforced masonry.

EN 459-1:2010, 2010. Building lime - Part 1: Definitions, specifications and conformity criteria.

EN 771-1:2011, 2011. Specification for Masonry Units - Part 1: Clay Masonry Units.

EN 771-6:2011, 2011. Specification for Masonry Units - Part 6: Natural stone masonry

units.

EN 772-1:2011, 2011. Methods of test for masonry units - Part 1: Determination of compressive strength.

EN 772-6:2011, 2011. Methods of test for masonry units - Part 6: Determination of bending tensile strength of aggregate concrete masonry units.

EN 998-2:2010, 2010. Specification for Mortar for Masonry - Part 2: Masonry Mortar.

Endo, Y. et al., 2015. Comparison of seismic analysis methods applied to a historical church struck by 2009 L'Aquila earthquake. *Bulletin of Earthquake Engineering*, 13(12), pp.3749–3778. Available at: http://link.springer.com/10.1007/s10518-015-9796-0.

Faria, R., Oliver, J. & Cervera, M., 1998. A strain-based plastic viscous-damage model for massive concrete structures. *International Journal of Solids and Structures*, 35(14), pp.1533–1558. Available at: http://linkinghub.elsevier.com/retrieve/pii/S0020768397001194.

Felicetti, R. & Gattesco, N., 2006. Le Prove Penetrometriche per la Stima della Risposta Meccanica delle Malte nelle Murature degli Edifici Storici. In *Sperimentazione su materiali e strutture*. Venice, Italy, pp. 224–232.

fib, 2013. *fib Model Code for Concrete Structures 2010*, Weinheim, Germany: Wiley-VCH Verlag GmbH & Co. KGaA. Available at: http://doi.wiley.com/10.1002/9783433604090.

Filardi, B. et al., 1996. Valutazione della Resistenza a Taglio di una Tipologia Muraria Tramite Prove su Pannelli, Carote e Triplette. In *La Meccanica delle Murature tra Teoria e Progetto*. Messina, Italy, pp. 75–84.

Gabrielli, E. & Colla, C., 2014. Monitoring of weathering effect evolution in porous masonry construction materials : NDT and mechanical tests. In *9th International Masonry Conference*. Guimarães, Portugal.

Galli, E. et al., 2014. Mechanical and Mineralogical Characterization of Mortar in Masonry Buildings Damaged by the 20-29th May Earthquake in Emilia A. Di Tommaso, G. Castellazzi, & C. Gentilini, eds. *Key Engineering Materials*, 624, pp.379–386. Available at: http://www.scientific.net/KEM.624.379.

Gambarotta, L. & Lagomarsino, S., 1997. Damage Models for the Seismic Response of Brick Masonry Shear Walls. Part I: The Mortar Joint Model and Its Applications. *Earthquake Engineering & Structural Dynamics*, 26(4), pp.423–439. Available at: http://onlinelibrary.wiley.com/doi/10.1002/(SICI)1096-

9845(199704)26:4<423::AID-EQE650>3.0.CO;2-#/abstract.

Gucci, N. & Barsotti, R., 1997. Determinazione in situ della capacità portante della malta. *Costruire in Laterizio*, 60/97, pp.454–459.

Henzel, J. & Karl, S., 1987. Determination of Strength of Mortar in the Joints of Masonry by Compression Tests on Small Specimens. *Darmstadt Concrete*, 2, pp.123–136.

Hilsdorf, H.K., 1969. *Investigation into the failure mechanism of brick masonry loaded in axial compression*, Gulf Publishing Company.

ISCARSAH, 2003a. Principles for the Analysis, Conservation and Structural Restoration of Architectural Heritage. *International Council on Monuments and Sites*.

ISCARSAH, 2003b. Recommendations for the analysis, conservation and structural restoration of Architectural Heritage. *International Council on Monuments and Sites*.

Kachanov, L., 1986. *Introduction to continuum damage mechanics*, Springer Science & Business Media. Available at: https://books.google.com/books?id=qB5JCAAAQBAJ&pgis=1.

Van Der Klugt, L.J.A.R., 1991. The pointing hardness tester - an instrument to meet a need. *Materials and Structures*, 24, pp.471–476.

Lemaitre, J. & Chaboche, J.L., 1978. Aspects phénoménologiques de la rupture par endommagement. *Journal de Mécanique Appliquée*, 2(3), pp.317–365. Available at: http://trid.trb.org/view.aspx?id=1048150.

Liberatore, D., Spera, G. & Cotugno, M., 2001. A New Penetrometer Test on Mortar Joints. In *Workshop on On-Site Control and Non-Destructive Evaluation of Masonry Structures*. Mantova, Italy, pp. 191–202.

Lombillo, I., Villegas, L. & Elices, J., 2010. Minor destructive techniques applied to the mechanical characterization of historical rubble stone masonry structures V. Peixoto de Freitas, ed. *Structural Survey*, 28(1), pp.53–70. Available at: http://www.emeraldinsight.com/doi/abs/10.1108/02630801011040860.

Lotfi, H.R. & Shing, P.B., 1994. Interface Model Applied to Fracture of Masonry Structures. *Journal of Structural Engineering*, 120(1), pp.63–80. Available at: http://ascelibrary.org/doi/10.1061/(ASCE)0733-9445(1994)120:1(63).

Lourenço, P.B., 1996. *Computational strategies for masonry structures*, Available at: http://www.narcis.nl/publication/RecordID/oai:tudelft.nl:uuid:4f5a2c6c-d5b7-

4043-9d06-8c0b7b9f1f6f.

Lourenço, P.B., Rots, J.G. & Blaauwendraad, J., 1995. Two approaches for the analysis of masonry structures - micro and macro-modeling. *Heron*, 40(4), pp.313–340. Available at: http://heronjournal.nl/40-4/3.pdf.

Lubliner, J. et al., 1989. A plastic-damage model for concrete. *International Journal of Solids and Structures*, 25(3), pp.299–326. Available at: http://linkinghub.elsevier.com/retrieve/pii/0020768389900504.

Marastoni, D. et al., 2016. Combining Brazilian tests on masonry cores and double punch tests for the mechanical characterization of historical mortars. *Construction and Building Materials*, 112, pp.112–127. Available at: http://linkinghub.elsevier.com/retrieve/pii/S0950061816302276.

MathWorks, 2013. MATLAB. Available at: http://it.mathworks.com/help/matlab/getting-started-with-matlab.html.

Mazars, J., 1986. A description of micro- and macroscale damage of concrete structures. *Engineering Fracture Mechanics*, 25(5-6), pp.729–737.

Mazzotti, C., Sassoni, E. & Pagliai, G., 2014. Determination of shear strength of historic masonries by moderately destructive testing of masonry cores. *Construction and Building Materials*, 54, pp.421–431. Available at: http://dx.doi.org/10.1016/j.conbuildmat.2013.12.039.

McCann, D.. & Forde, M.., 2001. Review of NDT methods in the assessment of concrete and masonry structures. *NDT & E International*, 34(2), pp.71–84. Available at: http://linkinghub.elsevier.com/retrieve/pii/S0963869500000323.

McCann, D.., Jackson, P.D. & Fenning, P.J., 1988. Comparison of the seismic and ground probing radar methods in geological surveying. In *IEE Proceedings*. IET, pp. 380–390.

Milosevic, J. et al., 2012. Experimental Tests on Rubble Masonry Specimens–Diagonal Compression, Triplet and Compression Tests. *15th World Conference on Earthquake Engineering*. Available at: http://peer.berkeley.edu/~aschell/15WCEE/pdf/WCEE2012_1191.pdf.

Montazerolghaem, M. & Jaeger, W., 2014. A Comparative Numerical Evaluation of Masonry Initial Shear Test Methods and Modifications Proposed for EN 1052-3. *International Masonry Conference 2014*, pp.1–10.

NIKER Project, 2010a. *D3.1: Inventory of earthquake-induced failure mechanisms related to construction types, structural elements, and materials.*,

NIKER Project, 2010b. *D4.1: Specification for laboratory specimens and testing strategies on walls.*,

NIKER Project, 2011. *D4.3: Technical report with the experimental results.*,

Oliver, J., 1989. A consistent characteristic length for smeared cracking models. *International Journal for Numerical Methods in Engineering*, 28(2), pp.461–474. Available at: http://doi.wiley.com/10.1002/nme.1620280214.

Oliver, J. et al., 1990. Isotropic damage models and smeared crack analysis of concrete. In *Computer Aided Analysis and Design of Concrete Structures; Proceedings 2nd International Conference*. pp. 945–958.

Page, A.W., 1981. The Biaxial Compressive Strength of Brick Masonry. *Proceedings of the Institution of Civil Engineers*, 71(3), pp.893–906. Available at: http://www.icevirtuallibrary.com/doi/abs/10.1680/iicep.1981.1825.

Pelà, L. et al., 2014. Analysis of the Effect of Provisional Ties on the Construction and Current Deformation of Mallorca Cathedral. *International Journal of Architectural Heritage*, (April 2015). Available at: http://www.tandfonline.com/doi/abs/10.1080/15583058.2014.996920#.VNzBry6E dps.

Pelà, L., 2009. *Continuum Damage Model for Nonlinear Analysis of Masonry Structures*. Technical University of Catalonia & University of Ferrara.

Pelà, L., Aprile, A. & Benedetti, A., 2009. Seismic assessment of masonry arch bridges. *Engineering Structures*, 31(8), pp.1777–1788. Available at: http://linkinghub.elsevier.com/retrieve/pii/S0141029609000716.

Pelà, L., Benedetti, A. & Marastoni, D., 2012. Interpretation of Experimental Tests on Small Specimens of Historical Mortars. In J. Jasieńko, ed. *Structural Analysis of Historical Constructions*. Wrocław, Poland: DWE, pp. 716–723.

Pelà, L., Cervera, M. & Roca, P., 2013. An orthotropic damage model for the analysis of masonry structures. *Construction and Building Materials*, 41, pp.957–967. Available at: http://linkinghub.elsevier.com/retrieve/pii/S0950061812004837.

Pelà, L., Cervera, M. & Roca, P., 2011a. Continuum damage model for orthotropic materials: Application to masonry. *Computer Methods in Applied Mechanics and Engineering*, 200(9-12), pp.917–930. Available at: http://linkinghub.elsevier.com/retrieve/pii/S0045782510003257.

Pelà, L., Cervera, M. & Roca, P., 2011b. Continuum model for inelastic behaviour of masonry. In *Congresso dell'Associazione Italiana di Meccanica Teorica e*

Applicata. pp. 1–10. Available at: http://upcommons.upc.edu/e-prints/handle/2117/14777.

Pelà, L., Roca, P. & Benedetti, A., 2015. Mechanical Characterization of Historical Masonry by Core Drilling and Testing of Cylindrical Samples. *International Journal of Architectural Heritage*. Available at: http://www.tandfonline.com/doi/full/10.1080/15583058.2015.1077906.

Petracca, M. et al., 2016. Regularization of first order computational homogenization for multiscale analysis of masonry structures. *Computational Mechanics*, 57(2), pp.257–276. Available at: "http://dx.doi.org/10.1007/s00466-015-1230-6.

Pluijm, R. Van Der, 1993. Shear Behaviour of Bed Joints. In *The Sixth North American Masonry Conference*. Philadelphia, Pennsylvania (US), pp. 125–136.

Pluijm, R. Van Der, Rutten, H. & Ceelen, M., 2000. Shear Behaviour of Bed Joints. In *12th International Brick/Block Masonry Conference2*. Madrid, Spain, pp. 1849–1862. Available at: http://www.hms.civil.uminho.pt/ibmac/2000/1849.pdf.

Quinteros, R.D., Oller, S. & Nallim, L.G., 2012. Nonlinear homogenization techniques to solve masonry structures problems. *Composite Structures*, 94(2), pp.724–730. Available at: http://dx.doi.org/10.1016/j.compstruct.2011.09.006.

Richards, A.F., 1988. *Vane shear strength testing in soils: Field and laboratory studies* 1014th ed. A. F. Richards, ed., Philadelphia, Pennsylvania (US): Astm International.

Roca, P. et al., 2013. Continuum FE models for the analysis of Mallorca Cathedral. *Engineering Structures*, 46, pp.653–670. Available at: http://linkinghub.elsevier.com/retrieve/pii/S014102961200404X.

Roca, P. et al., 2010. Structural Analysis of Masonry Historical Constructions. Classical and Advanced Approaches. *Archives of Computational Methods in Engineering*, 17(3), pp.299–325. Available at: http://link.springer.com/10.1007/s11831-010-9046-1.

Roca, P. et al., 2012. Viscoelasticity and Damage Model for Creep Behavior of Historical Masonry Structures. *The Open Civil Engineering Journal*, 6, pp.188–198.

Saisi, A. et al., 2000. Radar and sonic as complementary and/or alternative tests in the survey of structures. In *International Congress More than Two Thousand Years in the History of Architecture Safeguarding the Structure of our Architectural Heritage*. Bethlehem, Palestine, p. 6.

Saloustros, S. et al., 2014a. Assessment of structural damage in historical constructions using numerical models: the case of the church of the Poblet Monastery. *9th International Conference on Structural Analysis of Historical Constructions*. Available at: http://dx.doi.org/10.1016/j.engfailanal.2014.10.015.

Saloustros, S. et al., 2014b. Numerical analysis of structural damage in the church of the Poblet Monastery. *Engineering Failure Analysis*, 48, pp.41–61. Available at: http://linkinghub.elsevier.com/retrieve/pii/S135063071400315X.

Saloustros, S., Pelà, L. & Cervera, M., 2015. A crack-tracking technique for localized cohesive–frictional damage. *Engineering Fracture Mechanics*, 150, pp.96–114. Available at: http://dx.doi.org/10.1016/j.engfracmech.2015.10.039.

Sassoni, E., Franzoni, E. & Mazzotti, C., 2014. Influence of Sample Thickness and Capping on Characterization of Bedding Mortars from Historic Masonries by Double Punch Test (DPT). *Key Engineering Materials*, 624, pp.322–329. Available at: http://www.scientific.net/KEM.624.322.

Simo, J.C. & Ju, J.W., 1987. Strain- and stress-based continuum damage models-I. Formulation. *International Journal of Solids and Structures*, 23(7), pp.821–840.

Sinha, B.P., Gerstle, K.H. & Tulin, L.G., 1964. Stress-Strain Relations for Concrete Under Cyclic Loading. *Journal Proceedings*, 61(2), pp.195–212. Available at: https://www.concrete.org/publications/internationalconcreteabstractsportal.aspx?m=details&ID=7775.

UIC, 1995. Leaflet 778-3R: Recommedations for the inspection, assessment and maintainance of masonry arch bridges.

Válek, J. & Veiga, R., 2005. Characterisation of mechanical properties of historic mortars: testing of irregular samples. In C. A. Brebbia, ed. *Structural Studies, Repairs and Maintenance of Heritage Architecture IX*. WIT Press, pp. 365–374.

Vermeltfoort, A.T. & Pluijm, R. Van Der, 1991. Strength and Deformation Properties of Masonry to be Used in Computer Calculations. *9th International Brick and Block Masonry Conference*, pp.244–251. Available at: http://www.hms.civil.uminho.pt/ibmac/1991/244.pdf.

VSM Regione Toscana, 2003. Rilevamento della Vulnerabilità Sismica degli Edifici in Muratura - Manuale per la Compilazione della Scheda GNDT/CNR di II Livello.

Yaman, I.O. et al., 2001. Ultrasonic pulse velocity in concrete using direct and indirect transmission. *ACI Materials Journal*, 98(6), pp.450–457. Available at: http://digitalcommons.calpoly.edu/cenv_fac/195/.

Zucchini, A. & Lourenço, P.B., 2009. A micro-mechanical homogenisation model for masonry: Application to shear walls. *International Journal of Solids and Structures*, 46(3-4), pp.871–886. Available at: http://dx.doi.org/10.1016/j.ijsolstr.2008.09.034.

Zucchini, A. & Lourenço, P.B., 2002. A micro-mechanical model for the homogenisation of masonry. *International Journal of Solids and Structures*, 39(12), pp.3233–3255.

Figure Captions

Table Captions